



UNIVERSITÀ  
DEGLI STUDI  
FIRENZE

**Dottorato in Informatica, Sistemi e Telecomunicazioni**

Indirizzo: Dinamica Non Lineare e Sistemi Complessi

Ciclo XXVI

Coordinatore: Prof. Luigi Chisci

*Finite size effects in  
stochastic spatio-temporal models*

Settore Scientifico Disciplinare FIS/03

**Dottorando:**

Dott.ssa Claudia Cianci

**Tutore:**

Prof. Duccio Fanelli

**Co-Tutore:**

Dott.ssa Francesca Di Patti

**Referente**

Prof. Stefano Ruffo

Anni 2011/2013



# Contents

<b>Introduction</b>	<b>5</b>
<b>1 Biological applications: intracellular calcium oscillation model</b>	<b>9</b>
1.1 Biological context and existing literature . . . . .	10
1.2 Stochastic model and the master equation . . . . .	11
1.2.1 The role of finite size fluctuations . . . . .	16
1.2.2 Leading order: the mean field limit . . . . .	19
1.2.3 The next to leading approximation . . . . .	19
1.3 The power spectrum of fluctuations . . . . .	21
1.4 Conclusion . . . . .	24
<b>2 Validity of van Kampen expansion beyond Gaussian-approximations</b>	<b>25</b>
2.1 Analytical study of non Gaussian fluctuations . . . . .	25
2.1.1 The stochastic Kaneko model . . . . .	27
2.1.2 The master equation and its expansion . . . . .	28
2.1.3 The $N^{-1/2}$ terms . . . . .	29
2.1.4 The $N^{-1}$ corrections . . . . .	30
2.1.5 Analytical estimates of the fluctuations distribution moments . . . . .	31
2.1.6 Beyond the Gaussian approximation . . . . .	33
2.1.7 Non Gaussian corrections to the moments of the distribution . . . . .	36
2.1.8 The asymptotic evolution of the third moments . . . . .	38
2.2 Voter model . . . . .	42
2.3 WKB versus generalized van Kampen system size expansion . . . . .	47
2.3.1 Introduction . . . . .	47
2.3.2 Model . . . . .	48
2.3.3 The van Kampen system size expansion . . . . .	49
2.3.4 The WKB expansion . . . . .	51
2.3.5 Numerical simulations . . . . .	54
2.3.6 Details of van Kampen expansion . . . . .	56
2.3.7 Details of WKB approximation . . . . .	58
2.4 Conclusion . . . . .	59
<b>3 Spatial model: Stochastic Turing pattern formation</b>	<b>61</b>
3.1 Stochastic Turing Patterns for systems with one diffusing species . . . . .	61
3.2 Deterministic reaction-diffusion system with one diffusing species . . . . .	63
3.3 The Model and its Master Equation . . . . .	66
3.4 Equations for the mean-field and the fluctuations . . . . .	68

3.5	Power Spectrum of fluctuations . . . . .	69
3.6	A simple stochastic reaction–diffusion model . . . . .	77
3.7	Conclusion . . . . .	81
<b>4</b>	<b>The effect of crowding in Brussellator-type models</b>	<b>83</b>
4.1	Turing instabilities in reaction–diffusion systems with cross diffusion . . .	83
4.1.1	The Diffusion model . . . . .	84
4.1.2	The region of Turing order . . . . .	87
4.2	The modified Brussellator model . . . . .	93
4.2.1	The stochastic model and its master equation . . . . .	94
4.2.2	The mean field limit . . . . .	97
4.2.3	The Stochastic analysis: power spectrum of fluctuations . . . . .	104
4.2.4	Details of the van Kampen expansion . . . . .	108
4.2.5	Details of the power spectrum calculation . . . . .	109
4.3	Conclusion . . . . .	111
	<b>Conclusion</b>	<b>113</b>
	<b>A The Gillespie algorithm</b>	<b>115</b>
	<b>Bibliography</b>	<b>120</b>

# Introduction

A feature of many complex systems is the interaction between different types of individuals or agents. These agents could, for example, represent people in a model of disease-spreading, or molecules in a system of chemical reactions. The classical approach to study the dynamics of such models is based on the deterministic framework, commonly referred to as the mean-field limit, in which the evolution of the concentration of the species is described by coupled ordinary differential equations: the concentrations are assumed to be continuous variables, and they explicitly depend on time, and also on space in the case of spatially extended systems. These equations may include the presence of multiple fundamental interaction mechanisms, such as effects of competition and cooperation. However, this is an approximation that ignores the dynamics of a single individual, in favour of a global macroscopic view of the whole. The populations are in fact supposed infinite, a working hypothesis that can not capture crucial aspects related to the discreteness of the medium.

Alternatively to the deterministic approach, one can proceed with the stochastic modelling, retaining the descriptive level of the individual. The system is composed of a finite number of constituents, whose microscopic interactions are encoded by means of chemical reactions, having a determined success rate. A reaction between the agents is a stochastic event, and its probability depends on the relative concentrations of the reactants. In the limit of infinite size the two approaches coincide, while working with a finite number of elements the intrinsic noise can deeply influence the macroscopic dynamics of the system. Under certain conditions, the finite size effects can determine the emergence of spatio-temporal regular dynamics, revealing a degree of collective organization otherwise absent in the context of the deterministic formulation. These effects have been observed analytically and numerically in models such as predator-prey [1] and in other biomedical applications [2, 3, 4, 5]. Recently, a self-organized dynamics has also been detected in presence of autocatalytic reactions [3].

The two levels of description can be correlated through an analytical tool, known as the van Kampen method. This technique is a perturbative procedure in the inverse of the size of the system. This acts as a small parameter, that enables us to characterize the stochastic corrections to the mean-field equations.

The aim of the first two chapters of this thesis is twofold. First we will analyse numerically and analytically some stochastic models in order to highlight the role of fluctuations due to finite size effects. Secondly, we will show the limit of the classical use of van Kampen expansion and we will suggest how to improve the prediction.

In particular, in the first chapter, we will introduce a stochastic intracellular calcium oscillation model. We will demonstrate that the stochastic component of the dynamics, which is not considered in deterministic reference models, can show the emergence of

self-sustained oscillations, named quasi-cycles.

The second chapter is devoted to investigate the van Kampen expansion beyond the classical Gaussian approximation, commonly used in the literature. Indeed, when the system is characterized by a low number of individuals, the distribution of fluctuations is skewed and thus the Gaussian profile, obtained at the conventional order of approximation, is not appropriate, higher orders corrections can be in principle accounted for to reconcile theory and simulation. To investigate this probability we will introduce two different models: the first one is a auto-catalytic reaction scheme due to Kaneko [6], while the second one is the well-know voter model [7]. For both models we will derive the van Kampen expansion beyond the Gaussian order and we will find a generalized Fokker-Planck equation, that will enable us to write down the system for the moments of the fluctuations. Once solved numerically such a system, one can rebuild the profile of the distribution of fluctuations. In the last section of this chapter we will present another method of approximation, the Wentzel–Kramers–Brillouin (WKB) [8], and we will discuss its validity with respect to the van Kampen method.

The models considered so far do not explicitly account for an important aspect which proves essential in the dynamics of interacting particles: the space. Indeed, a wide field of investigation focuses on the study of spontaneous formation of inhomogeneous stationary states in spatially extended systems. Some of them are explained by means of a fundamental paradigm of the deterministic context: the Turing instability [9]. In analogy with the a-spatial models, also for this class of problems, under suitable conditions, the intrinsic noise can induce the formation of self-organized collective dynamics that are not predicted in the mean-field approximation [10]. Starting from this background, the purpose of the last two chapters is to elaborate on the role of the finite size effects showing that the stochastic system can be driven toward spatio-temporal organized configuration not predicted by the deterministic formulation.

In particular, in the third chapter, we will present a model in one spatial dimension that is used for studying pattern formation and wave propagation in individual based models of population dynamics. We will consider the problem of pattern formation in a generic two species reaction-diffusion model, under the hypothesis that only one species can diffuse [11]. For such system, the classical Turing instability cannot take place. At variance, by working in the generalized setting of a stochastic formulation, Turing like patterns can develop, seeded by finite size corrections. General conditions are given for the stochastic Turing patterns to occur. From the shape of the power spectrum, we categorize the patterns in two classes, waves or stationary Turing-like patterns.

Finally, in the fourth chapter, we will account explicitly for the finite carrying capacity of the hosting volume. Starting from a microscopic formulation of the Brusselator model, cross diffusive terms appear in the diffusion equation, when the competition for space is taken into consideration. Working in the context of the deterministic approach and due to the modified diffusion scheme we will show that the Turing instability can take place for some parameters not predicted by the standard approach. In particular we will see that the Turing instability can set in for all ratios of the main diffusivities, also when the (isolated) activator diffuses faster than the (isolated) inhibitor. Indeed, while in the classical approach it is necessary that one species diffuses much faster than the other, in our revisited diffusion scheme this mathematical constraint is no longer valid [12]. In the same chapter a stochastic variant of the Brusselator model is studied. The model accounts for a long range coupling among constituents [13]. The mean-field limit of the model is

studied, and the conditions for Turing and wave instability are obtained. A degenerate, cusp-like transition that separates the domains of Turing and wave order can take place. The point of transition is worked out analytically. Again, the region of Turing instability, as delimited by such transition point, can set in if the inhibitor diffuses slower than the activator. This is a consequence of the generalized diffusion scheme analyzed and which originates from having imposed an effect of spatial competition.





# Chapter 1

## Biological applications: intracellular calcium oscillation model

The effect of noise on non-linear dynamical systems has been studied for a long time and is now a well-defined field. Recent studies concern systems which fundamentally involve discrete entities, for example individuals in an ecological system. The populations is modelled stochastically, for example random births and deaths. In some cases it may be that the stochastic effects alter substantially the behaviour of non-linear system. It is possible to observe different properties of a given system in the presence or in the absence of noise. Examples can be found in a lot of different contexts such as population dynamics [1], evolutionary game theory [14], and epidemics [15]. In these cases we refer to the noise as intrinsic noise, coming from the system itself.

One of the most famous effects found in these systems regards the existence of a temporal oscillatory behaviour, as we have mentioned in the introduction. It was found that in some situations, the noise has an influence in demographic behaviour. The stochasticity of the system would be sufficient to perturb the stationary state, predicted by a deterministic or mean-field type analysis, and produce cyclic behaviour. This kind of oscillatory behaviours are referred to as quasi-cycles [1].

In particular, in this first chapter, we present a model of biological relevance that is characterized by quasi-cycles. This is a model for calcium intracellular oscillations that are important for the functioning of the cellular machinery. We have investigated the model, both numerically and theoretically. The classical models for calcium oscillation are deterministic and the intrinsic noise (due to individual based effects) is not considered. This noise is relevant at low concentrations, a regime of interest for intracellular calcium oscillations. Recently, Li and Hou [16] have published a microscopic version of the Goldbeter model [17, 18]. The Goldbeter model is a scheme for calcium dynamics, which assumes two species in mutual interaction. Working in such generalized stochastic context, it was shown numerically [16] that the intrinsic noise can yield stochastic oscillations. Motivated by this observation, we have developed an analytical study to explain the spontaneous emergence of quasi-cycles in the above stochastic  $Ca^{2+}$  model [16]. The analysis is performed under a linear noise approximation. We obtained a close prediction for the power spectrum of stochastic fluctuations. The presence of a peak at non-zero frequency in the profile of power spectrum implies, that the system presents an

oscillating dynamics seeded by the intrinsic noise. We carried out analytically a formula that describes the maximum frequency in function of the parameters of the model.

## 1.1 Biological context and existing literature

Calcium  $Ca^{2+}$  oscillations prove fundamental in many different life processes, including, among the others, muscle contraction, neural activity and fertilization [19]. At rest conditions, the calcium in the cell cytoplasm is kept at low concentration, while it is present at much higher concentration outside the cell, or inside small intracellular compartments as the endoplasmic reticulum, the sarcoplasmic reticulum and the mitochondria. Large gradients can indeed induce a sudden increase in the concentration of calcium dispersed inside the cellular *milieu*, by either releasing it from the internal stores or importing it from the outside environment, through specific voltage-gated channels.

In non-excitable cells, binding of an agonist, hormone or neurotransmitter, to cell-surface receptors initiates a cascade of reactions which promotes the production of the second messenger inositol trisphosphate (IP3). This latter diffuses through the cytoplasm and eventually binds to the IP3 receptors, positioned on the membrane of the endoplasmic reticulum. The IP3 receptors act also as channels: upon binding of the IP3, the channels open and let the  $Ca^{2+}$  to flow from the endoplasmic reticulum into the cell cytoplasm. Importantly, the release of calcium as mediated by the IP3 receptors can occasionally stimulate an additional release of  $Ca^{2+}$  from the endoplasmic reticulum. This is an autocatalytic process, usually termed calcium-induced calcium release (CICR) [20].

Different models have been developed in the past to describe the self-consistent generation of calcium oscillations. According to the pioneering model [21] sustained oscillations of cytosolic  $Ca^{2+}$  develop as mediated by the rise in IP3, triggered by external stimulation. This rise elicits the release of  $Ca^{2+}$  from an IP3-sensitive intracellular store, a process which in turn activate a further release of calcium from a second, independent compartment insensitive to IP3. Building on this formulation Goldbeter and collaborators [17, 18] have then elaborated a simplified scheme, particularly interesting for pedagogical reasons, where two distinct species, the cytosolic calcium and the calcium stored inside a IP3 sensitive compartments, are solely assumed to mutually interact. Working in this simplified setting, it was observed [22] that repetitive calcium spikes, evoked by external stimuli, are not necessarily linked to concomitant IP3 oscillations. The models mentioned above are deterministic in nature and, as such, assume the system to be ideally described in terms of continuum concentration amounts.

As opposed to this vision, one can favour an individual based description, which effectively accounts for the intrinsic discreteness of the scrutinized system. Stochastic effects are therefore present and stem from the finite size of the population of elementary constituents. Such stochastic contributions, endogenous to the system, can amplify via a resonant mechanism and so yield macroscopic oscillations in the discrete concentration in a region of the parameters for which a stable fixed point is predicted, as follows the deterministic linear stability analysis [1, 23]. Similar conclusions apply to spatially extended systems [24, 3, 10]. As concerns calcium dynamics, stochasticity has been mainly associated to external disturbances [25, 26]. The stochastic opening and closing of the channels have been for instance identified as a plausible cause of perturbation. At variance, Li and Hou [16] have recently investigated a discrete version of the Goldbeter model, showing that the inherent demographic noise can possibly drive stochastic oscillations, even when

the underlying deterministic system is in a non-oscillatory state. The analysis carried out in [16] relies on numerical simulations. However, the effect of finite size fluctuations can be also analytically appreciated by expanding the governing master equation under the so called Linear Noise Approximation scheme. In doing so, one can obtain a close prediction for the power spectrum of stochastic fluctuations and characterize the resonant frequency as a function of the parameters of the model.

We shall work along these lines, by revisiting the microscopic model [16], which we will slightly modify. We will then perform a complete analytical treatment of the model, recover the Goldbeter's scheme in the mean field limit and characterize the distribution of stochastic fluctuations in terms of a Fokker Planck equation derived from first principles. The stochastic oscillations observed in [16] are here interpreted as *quasi-cycles* of the discrete microscopic model, so building an ideal bridge with e.g. [1].

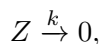
The chapter is organized as follows. In the next section we will introduce the stochastic model, inspired to [16] and constructed so to converge to the Goldbeter scheme [17, 18] in the deterministic limit. In section 1.2.1 we will then turn to study the governing master equation, under the linear noise approximation and elaborate on the role of stochastic fluctuations. We will in particular obtain a close prediction for the power spectrum of fluctuations that we will benchmark to direct simulations. An approximate expression for the resonant frequency is also derived and proved to be adequate.

## 1.2 Stochastic model and the master equation

We will hereafter introduce the stochastic a model for intracellular calcium oscillations. The model describes the process of calcium-induced calcium released (CICR), a biological process whereby calcium promotes calcium release from intracellular stores. As we shall discuss in the following the model is inspired to the formulation [16] and set up so to make contact, in the mean field, with the celebrated model proposed by Goldbeter and collaborators [18]. We will in particular consider two species, that we shall respectively denote  $Z$  e  $Y$ .  $Z$  stands for the calcium ions  $Ca^{2+}$  which are populating the cytosol, the liquid found inside cells.  $Y$  is meant to label the  $Ca^{2+}$  which are stored inside a specific compartment, insensitive to the IP3 and termed  $\mathcal{Y}$ . We will indicate with  $s$  the number of ions of type  $Z$ , i.e. dispersed in the cytoplasmic matrix. The integer  $q$  quantifies instead the abundance of species  $Y$ , the ions sequestered in the compartment.

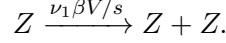
To progress in the model definition, we assume that the stochastic dynamics, which ultimately governs the evolution of the intracellular calcium, is an homogeneous Markov process. We will moreover label with  $V$  the volume of the cell.  $V$  defines in turn the characteristic size of the system. As we shall make clear in the following, the continuum deterministic limit is recovered by taking  $V \rightarrow \infty$ .

A  $Ca^{2+}$  ion can for instance migrate outside the cell, passing through specific channels which are hosted on the membrane walls. In term of chemical equation, one can ideally represent this event as:

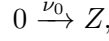


where the parameter  $k$  stands for the reaction rate associated to the hypothesized transformation. Conversely, calcium ions can reach the cytosol, coming from a second IP3 sensitive compartment, called  $\mathcal{X}$ . Following the CICR paradigm, this latter process

is autocatalytic and can be represented as:



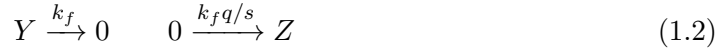
Elements of type  $Z$  can also come from the exterior of the cell, a process exemplified by:



To complete the formulation of the model, we also assume that  $Ca^{2+}$  can exit the IP3-insensitive compartment  $\mathcal{Y}$  to increment the population of cytosolic calcium according to the reactions <sup>1</sup>



The leaky transport from the IP3 insensitive pool  $\mathcal{Y}$  to the cytosol is here modeled as:



Finally, the ions can take the inverse path from the cytosol to the container  $\mathcal{Y}$ :



We wish to emphasize again that to each chemical equations introduced above, we have attached a quantity, constant or function of the concentration  $q/V$  and  $s/V$ , which quantifies the probability per unit of time for the reaction to eventually occur. The parameters  $\nu_0$ ,  $\nu_1 \beta$ ,  $\nu_3$  and  $\nu_2$ ,  $k$ ,  $k_f$  are bound to a microscopic, although artificial, description of the scrutinized process but will be later on shown to correspond to the control parameters that appear in the deterministic model pioneered by Goldbeter. More precisely,  $\beta$ ,  $\nu_0$ ,  $\nu_1$ ,  $k_f$  e  $k$  are positive constants,  $\beta$  controlling the degree of stimulation. The functions  $\nu_2$  and  $\nu_3$  are respectively associated to the pumping process and to the release of calcium from the intracellular store. Following [22], to take into account the cooperative nature of the two processes, as well as the positive feedback exerted on the transport by cytosolic  $Ca^{2+}$ , we posit:

$$\nu_2 \left( \frac{s}{V} \right) = V_{M2} \frac{(s/V)^n}{K_2^n + (s/V)^n} \quad \nu_3 \left( \frac{s}{V}, \frac{q}{V} \right) = V_{M3} \frac{(q/V)^m}{K_R^m + (q/V)^m} \frac{(s/V)^p}{K_A^p + (s/V)^p} \quad (1.4)$$

where  $V_{M2}$ ,  $V_{M3}$  denote the maximum rates of  $Ca^{2+}$  pumping into and release from the intracellular store. These processes are assumed to be mimicked by Hill like functions with cooperative indices respectively equal to  $n$  and  $m$ . The integer index  $p$  accounts instead for the degree of cooperation of the activation process.  $K_A$ ,  $K_2$  and  $K_R$  are threshold constants for pumping, release and activation.

---

<sup>1</sup>We will not indulge further on elaborating on a possible biological interpretation of the model. We rather insist on the fact that this is one of the possible microscopic, hence intrinsically stochastic formulation, which yields in the continuum limit to the aforementioned Golbeter model, as we will substantiate in the following. We have in particular decided to use two distinct chemical equations to model the  $Ca^{2+}$  release, as it was done in [16]. Alternatively, one could have mimicked the process by requiring.  $Y \xrightarrow{\nu_3 V/q} Z$ . The general conclusion that we will derive holds also if the latter choice is instead made. Similar considerations also apply to the last two pairs of reactions.

When it comes to the stochastic model, the state of the system at time  $t$  is known once the two integer quantities  $(s, q)$  are being assigned. The analysed process is intrinsically stochastic and, as such, can be rigorously described in terms of a master equation for the probability  $P(s, q, t)$  of seeing the system in the state  $(s, q)$  at the time of observation  $t$ . As a preliminary step, one needs to explicitly write down the transition rates  $T(\cdot|\cdot)$  from a given initial state (right entry) to the final state (left entry), compatible with the former, as dictated by above chemical equations. In formulae one gets:

$$\begin{aligned}
T(s-1, q|s, q) &= k \frac{s}{V} \\
T(s+1, q|s, q) &= \nu_0 + \nu_1 \beta + \nu_3 \left( \frac{s}{V}, \frac{q}{V} \right) + k_f \frac{q}{V} \\
T(s-1, q|s, q) &= \nu_2 \left( \frac{s}{V} \right) + k \frac{s}{V} \\
T(s, q+1|s, q) &= \nu_2 \left( \frac{s}{V} \right) \\
T(s, q-1|s, q) &= \nu_3 \left( \frac{s}{V}, \frac{q}{V} \right) + k_f \frac{q}{V}.
\end{aligned} \tag{1.5}$$

The master equation that rules the dynamics of the stochastic process under the Markov assumption can be cast in the form:

$$\begin{aligned}
\frac{\partial}{\partial t} P(s, q, t) &= -T(s+1, q|s, q)P(s, q, t) + T(s, q|s-1, q)P(s-1, q, t) \\
&\quad -T(s-1, q|s, q)P(s, q, t) + T(s, q|s+1, q)P(s+1, q, t) \\
&\quad -T(s, q+1|s, q)P(s, q, t) + T(s, q|s, q-1)P(s, q-1, t) \\
&\quad -T(s, q-1|s, q)P(s, q, t) + T(s, q|s, q+1)P(s, q+1, t).
\end{aligned} \tag{1.6}$$

Equation (1.6) can be written in a slightly more compact form:

$$\begin{aligned}
\frac{\partial}{\partial t} P(s, q, t) &= \left[ (\varepsilon_s^+ - 1)T(s-1, q|s, q) + (\varepsilon_s^- - 1)T(s+1, q|s, q) \right. \\
&\quad \left. + (\varepsilon_q^+ - 1)T(s, q-1|s, q) + (\varepsilon_q^- - 1)T(s, q+1|s, q) \right] P(s, q, t),
\end{aligned} \tag{1.7}$$

where use has been made of the so called step operators  $\varepsilon_q^\pm, \varepsilon_s^\pm$  defined as:

$$\begin{aligned}
\varepsilon_s^\pm f(s, q) &\equiv f(s \pm 1, q) \\
\varepsilon_q^\pm f(s, q) &\equiv f(s, q \pm 1).
\end{aligned}$$

The master equation provides an exact description of the stochastic dynamics. It is however difficult to handle it analytically. Progress in the analysis can be made via perturbative calculations to which will refer in the forthcoming section. Alternatively, the investigated system can be numerically simulated. By combining numerical and analytical tools, it is indeed possible to elaborate on the crucial role played by the stochastic fluctuations, stemming from the finite size and therefore intrinsic to the system. Before turning to discuss this important aspect, we devote the remaining part of this section to

deriving the mean field limit of the model, namely the underlying deterministic picture that can be formally recovered when operating in the thermodynamic limit  $V \rightarrow \infty$ .

To this end, we look after the average concentrations  $\langle s \rangle$  and  $\langle q \rangle$  respectively defined as:

$$\langle s \rangle = \sum_{s,q} sP(s, q, t) \quad \langle q \rangle = \sum_{s,q} qP(s, q, t).$$

Here the sums run over all positive integer pairs  $(s, q)$ . A closed system of equations for the above quantities can be derived starting from the master equation (1.6), and as follows a standard procedure that we will here detail with reference to  $\langle s \rangle$ . Let us start by multiplying both members of (1.6) times  $s$  and sum over all possible states  $(s, q)$ .

The left hand side of the master equation takes the form:

$$\sum_{s,q} s \frac{dP(s, q, t)}{dt} = \frac{d}{d\tau} \sum_{s,q} \frac{s}{V} P(s, q, t) = \frac{d \langle s \rangle}{d\tau},$$

where we have introduced the rescaled time  $\tau = t/V$ .

Consider now the first two terms on the right hand side. By implementing in the second term the change of variable  $s - 1 \rightarrow s$  one gets:

$$\begin{aligned} \sum_{s,q} s \left( -T(s+1, q|s, q)P(s, q, t) + T(s, q|s-1, q)P(s-1, q, t) \right) &= \\ &= \sum_{s,q} \left( -sT(s+1, q|s, q) + (s+1)T(s+1, q|s, q) \right) P(s, q, t) = \\ &= \langle T(s+1, q|s, q) \rangle. \end{aligned}$$

Similar considerations apply to the other two terms that appear in the right hand side of equation (1.6):

$$\begin{aligned} \sum_{s,q} s \left( -T(s-1, q|s, q)P(s, q, t) + T(s, q|s+1, q)P(s+1, q, t) \right) &= \\ &= \sum_{s,q} \left( -sT(s-1, q|s, q) + (s-1)T(s-1, q|s, q) \right) P(s, q, t) = \\ &= -\langle T(s-1, q|s, q) \rangle, \end{aligned}$$

where the second element of the sum has been transformed by operating the shift  $s+1 \rightarrow s$ . The remaining terms in the master equation are associated to changes in the species  $q$  and yield no contribution to the equation for  $\langle s \rangle$ . To clarify this point, let us consider the third pair of terms in the right hand side of equation (1.6). By replacing in the last of these terms  $q-1 \rightarrow q$  one gets:

$$\begin{aligned} \sum_{s,q} s \left( -T(s, q+1|s, q)P(s, q, t) + T(s, q|s, q-1)P(s, q-1, t) \right) &= \\ &= \sum_{s,q} \left( -sT(s, q+1|s, q) + sT(s, q+1|s, q) \right) P(s, q, t) = 0. \end{aligned}$$

Summing up, by collecting all terms together, the following equation for the average concentration  $\langle s \rangle$  is eventually found:

$$\frac{d \langle s \rangle}{d\tau} = \langle T(s+1, q|s, q) \rangle - \langle T(s-1, q|s, q) \rangle.$$

By recalling the expression for the transition rates, as given in equations (1.5), we obtain:

$$\frac{d \langle s \rangle}{d\tau} = \nu_0 + \nu_1\beta + \left\langle \nu_3 \left( \frac{s}{V}, \frac{q}{V} \right) \right\rangle + k_f \frac{\langle q \rangle}{V} - \left\langle \nu_2 \left( \frac{s}{V} \right) \right\rangle - k \frac{\langle s \rangle}{V}.$$

Consider for instance  $\left\langle \nu_3 \left( \frac{s}{V}, \frac{q}{V} \right) \right\rangle$ . In the limit  $V \rightarrow \infty$ , it is legitimate to neglect the correlations which formally implies setting:

$$\left\langle \nu_3 \left( \frac{s}{V}, \frac{q}{V} \right) \right\rangle \rightarrow \nu_3 \left( \frac{\langle s \rangle}{V}, \frac{\langle q \rangle}{V} \right).$$

In conclusion, by introducing:

$$\phi = \lim_{V \rightarrow \infty} \langle s \rangle / V \quad (1.8)$$

$$\psi = \lim_{V \rightarrow \infty} \langle q \rangle / V \quad (1.9)$$

and recalling eqs. (1.4) one gets:

$$\frac{d\phi}{d\tau} = \nu_0 + \nu_1\beta - \nu_2(\phi) - k\phi + k_f\psi + \nu_3(\phi, \psi). \quad (1.10)$$

A formal identical calculation can be carried out for the other species to eventually obtain:

$$\frac{d\psi}{d\tau} = -k_f\psi - \nu_3(\phi, \psi) + \nu_2(\phi). \quad (1.11)$$

Equations (1.10) and (1.11) constitute the deterministic approximation of the stochastic model. As anticipated, they match the classical model studied by Dupont and Goldbeter in [18]. This latter model displays a Hopf bifurcation: by tuning the control parameter  $\beta$ , a transition occurs which changes the stable stationary points into an oscillating solution. Three regimes can be in particular identified, depending on the value of the degree of cell stimulation  $\beta$ , and are schematically depicted in figure 1.1, adapted from [27]. Region II, delimited by the critical values  $\beta = b_1$  and  $\beta = b_2$ , identifies the domain where self-sustained oscillations of intracellular  $Ca^{2+}$  are predicted to occur as follows a straightforward linear stability analysis applied to system (1.10)-(1.11). In regions I and III, the concentration of  $Ca^{2+}$  converges to a stationary stable state. The asymptotic concentration increases linearly with the parameter  $\beta$ . For this reason, zones I and III are often referred to as to the regions of respectively low and high  $Ca^{2+}$  concentration.

Beyond the mean field prediction is instructive to simulate the master equation (1.6), which provides an exact description of the underlying stochastic dynamics. This task can be accomplished by resorting to the celebrated Gillespie scheme [28], a Monte Carlo based algorithm which produces realizations of the stochastic model which agree with the corresponding master equation (1.6). In figure 1.2 deterministic and stochastic simulations are confronted for a choice of the parameters that would position the system in region III. The deterministic solution (black online) approaches the asymptotic state, after an oscillatory transient that gets rapidly damped. At variance, persistent oscillations are observed in the stochastic model. Such sustained oscillations, also termed in the literature quasi-cycles, result from a resonant effect and originates from the amplification of the inherent finite sizes fluctuations. Interestingly,  $Ca^{2+}$  oscillations can hence develop

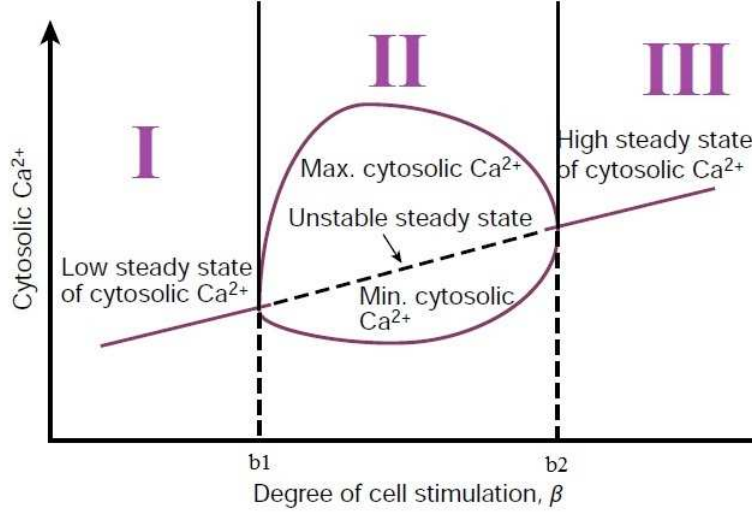


Figure 1.1: Schematic bifurcation diagram showing the domain and amplitude of intracellular  $Ca^{2+}$  oscillations as a function of the degree of cellular stimulation  $\beta$ , which act as control parameter. Sustained oscillations develop in region II, for a range of stimulation laying between two critical values of  $\beta$ , respectively denoted  $b_1$  and  $b_2$ . In region I and III, the system converges to stable stationary fixed point. The solid lines in region II stand for lowest and highest levels of cytosolic  $Ca^{2+}$  oscillations.

outside the region of the parameters for which a deterministic limit cycle is predicted to occur. This observation was already made in [16], based on simulative evidences. We shall take one step forward by characterizing the phenomenon analytically and so making contact with the concept of quasi-cycles as introduced above. To this end, we will compute the power spectrum of fluctuations and identify the, spontaneously selected, resonant frequency. The next section is entirely devoted to reporting about the calculations.

### 1.2.1 The role of finite size fluctuations: characterising the stochastic oscillations.

Consider the discrete concentration  $\frac{s}{V}$ . Following the linear noise approximation, also called the van Kampen ansatz [29], one can express  $s/V$  (resp.  $q/V$ ) as the sum of two distinct contributions. On the one side the deterministic solution, namely  $\phi(t)$  (resp.  $\psi$ ), which denotes the concentration in the mean field limit. The other contribution refers instead to the stochastic perturbation termed  $\xi$  (resp.  $\eta$ ) and assumed to scale as  $1/\sqrt{V}$ . In formulae:

$$\frac{s(t)}{V} = \phi(t) + \frac{\xi}{\sqrt{V}}, \quad (1.12)$$

$$\frac{q(t)}{V} = \psi(t) + \frac{\eta}{\sqrt{V}}. \quad (1.13)$$

In the limit for  $V \rightarrow \infty$  the stochastic contributions drop away and one is left with the deterministic concentrations  $\phi$  and  $\psi$ . Working at finite, although large  $V$ , one can



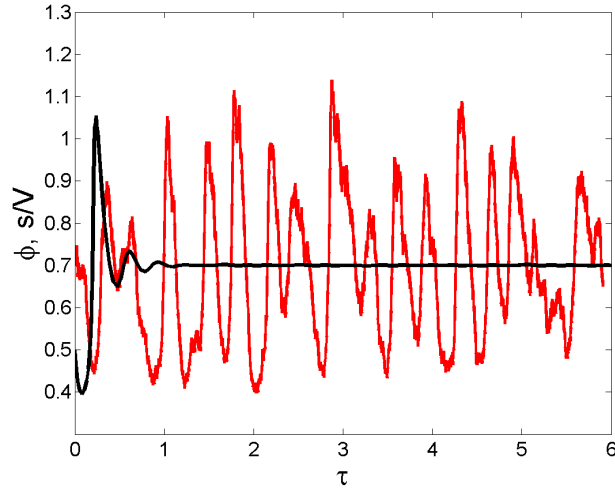


Figure 1.2: Time evolution of the intracellular calcium concentration  $\phi$ . Parameters are set so to have the system in region III, as identified in the main body of the chapter and in the caption of figure 1.1. The black solid line which converges to an asymptotic stable fixed point refers to the integration of the deterministic system (1.10) and (1.11). The wiggling curve (red online) follows stochastic simulations. Persistent oscillations are found, which display a characteristic frequency. This latter can be analytically predicted as discussed in section 1.2.1. Parameters are  $\beta = 0.823$ ,  $K_R = 2\mu\text{mol}/L$ ,  $k = 10\text{s}^{-1}$ ,  $K_A = 0.9\mu\text{mol}/L$ ,  $n = 2$ ,  $m = 2$ ,  $p = 4$ ,  $V_{M3} = 500\mu\text{mol}/(Ls)$ ,  $V_{M2} = 65\mu\text{mol}/(Ls)$ ,  $k_f = 1\text{s}^{-1}$ ,  $\nu_0 = 1(\mu\text{mol})/(Ls)$ ,  $\nu_1 = 7.3\mu\text{mol}/(Ls)$ ,  $K_2 = 1\mu\text{mol}/L$ . For this choice of the parameters, the critical values of  $\beta$  are respectively  $b_1 = 0.291$  and  $b_2 = 0.775$ .

carry out a perturbative expansion of the governing Master equation, the quantity  $1/\sqrt{V}$  acting as a small parameter. This is the van Kampen system size expansion [29], that allows one to recover the mean field equations at the leading order, and then characterize the distribution of fluctuations, at the next to leading order.

Let us start by noting that the step operators that appear in the left hand side of eq. (1.7), can be expanded as:

$$\varepsilon_s^\pm \simeq 1 \pm \frac{1}{\sqrt{V}} \frac{\partial}{\partial \xi} + \frac{1}{2V} \frac{\partial^2}{\partial \xi^2} \quad \varepsilon_q^\pm \simeq 1 \pm \frac{1}{\sqrt{V}} \frac{\partial}{\partial \eta} + \frac{1}{2V} \frac{\partial^2}{\partial \eta^2}.$$

It is then necessary to expand in series of  $1/\sqrt{V}$  the transition rates, which are non-linear function of the discrete concentrations. We shall hereafter outline the main step of the calculation with reference to the term  $T(s, q+1|s, q)$ , and then generalize the results to the other contributions. As a first step, let us introduce the van Kampen ansatz into the formula for  $T(s, q+1|s, q)$  as defined in (1.5):

$$T(s, q+1|s, q) = V_{M2} \frac{z^n}{K_2^n + z^n} = V_{M2} \frac{\left(\phi + \frac{\xi}{\sqrt{V}}\right)^n}{K_2^n + \left(\phi + \frac{\xi}{\sqrt{V}}\right)^n} = V_{M2} \frac{\phi^n \left(1 + \frac{\xi}{\phi\sqrt{V}}\right)^n}{K_2^n + \phi^n \left(1 + \frac{\xi}{\phi\sqrt{V}}\right)^n}.$$

A simple algebraic manipulation yields to:

$$\begin{aligned} T(s, q + 1 | s, q) &= \frac{V_{M2}\phi^n}{K_2^n + \phi^n} \left( 1 + n \frac{\xi}{\phi\sqrt{V}} \right) \left( 1 - n \frac{\xi}{\phi\sqrt{V}} \frac{\phi^n}{K_2^n + \phi^n} \right) \\ &\simeq V_{M2} \frac{\phi^n}{K_2^n + \phi^n} \left[ 1 + \frac{\xi}{\sqrt{V}} \frac{nK_2^n}{\phi(K_2^n + \phi^n)} \right], \end{aligned}$$

where use has been made of the approximate relations  $(1 + \epsilon)^n = 1 + n\epsilon + o(\epsilon)$  and  $\frac{1}{(1 + \epsilon)} = 1 - \epsilon + o(\epsilon)$ , for  $\epsilon \ll 1$ . In conclusion, by re-organizing the various terms, one gets the final expression:

$$T(s, q + 1 | s, q) \simeq V_{M2} \frac{\phi^n}{K_2^n + \phi^n} \left[ 1 + \frac{\xi}{\sqrt{V}} \frac{nK_2^n}{\phi(K_2^n + \phi^n)} \right] + o\left(\frac{1}{\sqrt{V}}\right).$$

Following a similar strategy for the other transition rates, one eventually obtains:

$$\begin{aligned} T(s + 1, q | s, q) &\simeq \nu_0 + \nu_1\beta + V_{M3} \frac{\psi^m}{K_R^m + \psi^m} \frac{\phi^p}{K_A^p + \phi^p} \left[ 1 + \frac{\eta}{\sqrt{V}} \frac{mK_R^m}{\psi(K_R^m + \psi^m)} + \frac{\xi}{\sqrt{V}} \times \right. \\ &\quad \left. \times \frac{pK_A^p}{\phi(K_A^p + \psi^p)} \right] + k_f \left( \psi + \frac{\eta}{\sqrt{V}} \right) \\ T(s - 1, q | s, q) &\simeq V_{M2} \frac{\phi^n}{K_2^n + \phi^n} \left[ 1 + \frac{\xi}{\sqrt{V}} \frac{nK_2^n}{\phi(K_2^n + \phi^n)} \right] + k \left( \phi + \frac{\xi}{\sqrt{V}} \right) \\ T(s, q + 1 | s, q) &\simeq V_{M2} \frac{\phi^n}{K_2^n + \phi^n} \left[ 1 + \frac{\xi}{\sqrt{V}} \frac{nK_2^n}{\phi(K_2^n + \phi^n)} \right] \\ T(s, q - 1 | s, q) &\simeq k_f \left( \psi + \frac{\eta}{\sqrt{V}} \right) + V_{M3} \frac{\psi^m}{K_R^m + \psi^m} \frac{\phi^p}{K_A^p + \phi^p} \left[ 1 + \frac{\eta}{\sqrt{V}} \frac{mK_R^m}{\psi(K_R^m + \psi^m)} + \right. \\ &\quad \left. + \frac{\xi}{\sqrt{V}} \frac{pK_A^p}{\phi(K_A^p + \psi^p)} \right]. \end{aligned}$$

Introduce now  $\Pi(\xi, \eta, t)$ , the distribution of fluctuations formally defined as:

$$\Pi(\xi, \eta, t) = P(s(\phi(t), \xi), q(\psi(t), \eta), t), \quad (1.14)$$

where  $s(\phi(t), \xi)$  and  $q(\psi(t), \eta)$  follow respectively eqs. (1.12) and (1.13). Taking the derivative of eq. (1.14) with respect to time yields:

$$\frac{\partial \Pi}{\partial t} = \frac{dP}{dt} = \frac{\partial P}{\partial t} + \frac{\partial P}{\partial s} V \dot{\phi}(t) + \frac{\partial P}{\partial q} V \dot{\psi}(t).$$

Hence:

$$\frac{\partial P}{\partial t} = \frac{\partial \Pi}{\partial t} - \frac{\partial P}{\partial s} V \dot{\phi}(t) - \frac{\partial P}{\partial q} V \dot{\psi}(t). \quad (1.15)$$

On the other hand:

$$\frac{\partial \Pi}{\partial \xi} = \frac{\partial P}{\partial s} \frac{\partial s}{\partial \xi} = \sqrt{V} \frac{\partial P}{\partial s} \quad \frac{\partial \Pi}{\partial \eta} = \frac{\partial P}{\partial q} \frac{\partial q}{\partial \eta} = \sqrt{V} \frac{\partial P}{\partial q},$$

which takes us to:

$$\frac{\partial P}{\partial s} = \frac{1}{\sqrt{V}} \frac{\partial \Pi}{\partial \xi} \quad \frac{\partial P}{\partial q} = \frac{1}{\sqrt{V}} \frac{\partial \Pi}{\partial \eta}.$$

Equation (1.15) can be therefore cast in the form:

$$\frac{\partial P}{\partial t} = \frac{\partial \Pi}{\partial t} - \frac{\partial \Pi}{\partial \xi} \sqrt{V} \dot{\phi}(t) - \frac{\partial \Pi}{\partial \eta} \sqrt{V} \dot{\psi}(t), \quad (1.16)$$

which transform into:

$$\frac{\partial P}{\partial t} \longrightarrow \frac{1}{V} \frac{\partial \Pi}{\partial \tau} - \frac{1}{\sqrt{V}} \frac{\partial \Pi}{\partial \xi} \dot{\phi}(\tau) - \frac{1}{\sqrt{V}} \frac{\partial \Pi}{\partial \eta} \dot{\psi}(\tau).$$

by operating the change of variable  $\tau \rightarrow t/V$ . To proceed in the analysis one needs to insert into the master equation (1.6) the approximate expressions for the transition rates, as well as the above relation for  $\partial P/\partial t$ . The terms can be therefore re-organized depending on their respective order in  $1/\sqrt{V}$ . At the leading order, namely the terms proportional to  $1/\sqrt{V}$ , one eventually recovers the mean field deterministic system for the continuum densities  $\phi$  and  $\psi$ . At the next to leading order, a Fokker-Planck for the distribution of the finite size fluctuations is instead obtained.

### 1.2.2 Leading order: the mean field limit

The contributions relative to  $1/\sqrt{V}$  result in:

$$\begin{aligned} -\frac{\partial \Pi}{\partial \xi} \frac{d\phi}{d\tau} - \frac{\partial \Pi}{\partial \eta} \frac{d\psi}{d\tau} = & \left( -\nu_0 - \nu_1 \beta - \nu_3(\phi, \psi) - k_f \psi + \nu_2(\phi) + k\phi \right) \frac{\partial \Pi}{\partial \xi} + \\ & + \left( k_f \psi + \nu_3(\phi, \psi) - \nu_2(\phi) \right) \frac{\partial \Pi}{\partial \eta}. \end{aligned}$$

By grouping together the terms proportional to  $\frac{\partial \Pi}{\partial \xi}$  (resp.  $\frac{\partial \Pi}{\partial \eta}$ ) and requiring their sum to return zero, one ends up with the following system of differential equations for the mean field concentrations  $\phi$  and  $\psi$ :

$$\begin{aligned} \frac{d\phi}{d\tau} &= \nu_0 + \nu_1 \beta + \nu_3(\phi, \psi) + k_f \psi - \nu_2(\phi) - k\phi \\ \frac{d\psi}{d\tau} &= -k_f \psi - \nu_3(\phi, \psi) + \nu_2(\phi). \end{aligned}$$

The above equations are identical to eqs. (1.10) and (1.11) as derived in the preceding section. However, the van Kampen expansion enables us to take one step forward in the study of the stochastic model. A rather complete characterization of the fluctuations can be in fact gained by operating at the next to leading approximation, as we shall outline in the remaining part of this section.

### 1.2.3 The next to leading approximation: the Fokker-Planck equation for the fluctuations.

Consider now the terms that scale as  $V^{-1}$  in the expansion of the master equation. In formulae one has:

$$\begin{aligned} \frac{\partial \Pi(\xi, \eta, \tau)}{\partial \tau} = & \left\{ \frac{1}{2} \left( k_f \psi + \nu_3(\phi, \psi) + \nu_2(\phi) \right) \partial_\eta^2 + \frac{1}{2} \left( \nu_0 + \nu_1 \beta + \nu_3(\phi, \psi) + k_f \psi + \nu_2(\phi) + \right. \right. \\ & \left. \left. + k\phi \right) \partial_\xi^2 + \partial_\eta \left[ \left( k_f + \nu_3(\phi, \psi) \frac{mK_R^m}{\psi(K_R^m + \psi^m)} \right) \eta + \left( \nu_3(\phi, \psi) \frac{pK_A^p}{\phi(K_A^p + \phi^p)} - \nu_2(\phi) \times \right. \right. \\ & \left. \left. \times \frac{nK_2^n}{\phi(K_2^n + \phi^n)} \right) \xi \right] + \partial_\xi \left[ - \left( k_f + \nu_3(\phi, \psi) \frac{mK_R^m}{\psi(K_R^m + \psi^m)} \right) \eta \left( k + \nu_2(\phi) \frac{nK_2^n}{\phi(K_2^n + \phi^n)} - \right. \right. \\ & \left. \left. - \nu_3(\phi, \psi) \frac{pK_A^p}{\phi(K_A^p + \phi^p)} \right) \xi \right] \right\} \Pi(\xi, \eta, \tau). \end{aligned}$$

This is a linear Fokker Planck equation, which can be put in the standard form:

$$\frac{\partial \Pi(\mathbf{x}, \tau)}{\partial \tau} = - \sum_{i=1}^2 \frac{\partial}{\partial x_i} A_i(\mathbf{x}) \Pi(\mathbf{x}, \tau) + \frac{1}{2} \sum_{i,j=1}^2 \frac{\partial^2}{\partial x_i \partial x_j} B_{i,j} \Pi(\mathbf{x}, \tau), \quad (1.17)$$

where we have introduced the vector  $\mathbf{x} = (x_1, x_2) = (\xi, \eta)$ . In the above eq.(1.17),  $A_i(\mathbf{x})$  represents the  $i$ -th component of the vector:

$$A(\mathbf{x}) = M\mathbf{x},$$

where  $M$  is a  $2 \times 2$  matrix:

$$M = \begin{pmatrix} -k - \nu_2(\phi) \frac{nK_2^n}{\phi(K_2^n + \phi^n)} + \nu_3(\phi, \psi) \frac{pK_A^p}{\phi(K_A^p + \phi^p)} & k_f + \nu_3(\phi, \psi) \frac{mK_R^m}{\psi(K_R^m + \psi^m)} \\ -\nu_3(\phi, \psi) \frac{pK_A^p}{\phi(K_A^p + \phi^p)} + \nu_2(\phi) \frac{nK_2^n}{\phi(K_2^n + \phi^n)} & -k_f - \nu_3(\phi, \psi) \frac{mK_R^m}{\psi(K_R^m + \psi^m)} \end{pmatrix}. \quad (1.18)$$

The terms  $B_{i,j}$  in equation (1.17) are the entries of the diagonal diffusion matrix  $B$ :

$$B = \begin{pmatrix} \nu_0 + \nu_1 \beta + \nu_3(\phi, \psi) + \nu_2(\phi) + k_f \psi + k\phi & 0 \\ 0 & k_f \psi + \nu_3(\phi, \psi) + \nu_2(\phi) \end{pmatrix}. \quad (1.19)$$

Notice that the coefficients of the above matrices  $M$  and  $B$  depend on time  $\tau$ , as the continuum concentration  $\phi$  and  $\psi$  do. The Fokker-Planck that we have derived makes it possible to characterize the distribution of fluctuations and explain, on solid interpretative ground, the emergence of the quasi-cycles as reported in figure 1.2. To this end, by building on the general approach first derived in [1] and later on exploited in e.g. [23], we will hereafter obtain a closed expression for the power spectrum of the stochastic fluctuations. It will be hence possible to determine a priori, and as a function of the parameters of the model, the frequency of the  $Ca^{2+}$  oscillations, which gets selected as follows the amplification of the intrinsic noise.

### 1.3 The power spectrum of fluctuations

A stochastic differential equation of the Langevin type can be associated to the Fokker Planck equation [29]. The Langevin equation describes the time evolution of the fluctuations, returning a global distribution which obeys to the corresponding Fokker Planck equation. For our case, the relevant Langevin equation, equivalent to eq. (1.17), reads:

$$\frac{d}{d\tau}\mathbf{x}_l(\tau) = \sum_{j=1}^2 M_{l,j}\mathbf{x}_j(\tau) + \lambda_l(\tau) \quad l = 1, 2; \quad (1.20)$$

where  $\mathbf{x}_l$  is the  $l$ -th component of the vector  $\mathbf{x} = (\xi, \eta)$  and  $\lambda_l(\tau)$  stands for a stochastic variable which satisfies the following conditions:

$$\langle \lambda_l(\tau) \rangle = 0 \quad \langle \lambda_l(\tau)\lambda_j(\tau') \rangle = B_{l,j}\delta(\tau - \tau').$$

It should be noticed that the amplitude of the noise term is controlled by the diffusion matrix  $B$  and ultimately relates to the chemical parameters of the model. In other words, the noise follows the microscopic formulation of the problem and it is not imposed as an external source of disturbance.

To study the emergence of regular patterns in time, the quasi-cycles, it is convenient to Fourier transform the Langevin equation (1.20):

$$-i\omega\hat{x}_l(\omega) = \sum_{j=1}^2 M_{l,j}\hat{x}_j(\omega) + \hat{\lambda}_l(\omega) \quad l = 1, 2; \quad (1.21)$$

where  $\hat{\cdot}$  stands for the Fourier transform and  $\omega$  represents the Fourier frequency. The contribution  $\hat{\lambda}(\omega)$  verifies:

$$\langle \hat{\lambda}_l(\omega) \rangle = 0 \quad \langle \hat{\lambda}_l(\omega)\hat{\lambda}_j^*(\omega) \rangle = B_{l,j}, \quad (1.22)$$

where  $\hat{\lambda}_j^*(\omega)$  denotes the complex conjugate of  $\hat{\lambda}_j(\omega)$ . Eq. (1.21) yields:

$$\hat{x}_l(\omega) = \sum_{j=1}^2 (-i\omega I_{l,j} - M_{l,j})^{-1} \hat{\lambda}_j(\omega) = \sum_{j=1}^2 \Phi_{l,j}^{-1}(\omega) \hat{\lambda}_j(\omega) \quad l = 1, 2;$$

where  $\Phi(\omega) = -i\omega I - M$ . The power spectrum can be calculated as:

$$\begin{aligned} P_l(\omega) &= \langle |\hat{x}_l(\omega)|^2 \rangle = \langle \hat{x}_l(\omega)\hat{x}_l^*(\omega) \rangle = \left\langle \sum_{j,r=1}^2 \Phi_{l,j}^{-1}(\omega) \hat{\lambda}_j(\omega) (\Phi_{l,r}^*)^{-1}(\omega) \hat{\lambda}_r^*(\omega) \right\rangle = \\ &= \sum_{j,r=1}^2 \Phi_{l,j}^{-1}(\omega) \langle \hat{\lambda}_j(\omega)\hat{\lambda}_r^*(\omega) \rangle (\Phi^\dagger)_{l,r}^{-1}(\omega) = \sum_{j,r=1}^2 \Phi_{l,j}^{-1}(\omega) B_{j,r} (\Phi^\dagger)_{l,r}^{-1}(\omega) \end{aligned}$$

where use has been made of eq. (1.22) and where we have introduced  $\Phi^\dagger = (\Phi^*)^T$ . In conclusion, one gets:

$$P_l(\omega) = \sum_{j,r=1}^2 \Phi_{l,j}^{-1}(\omega) B_{j,r} (\Phi^\dagger)_{l,r}^{-1}(\omega) \quad l = 1, 2. \quad (1.23)$$

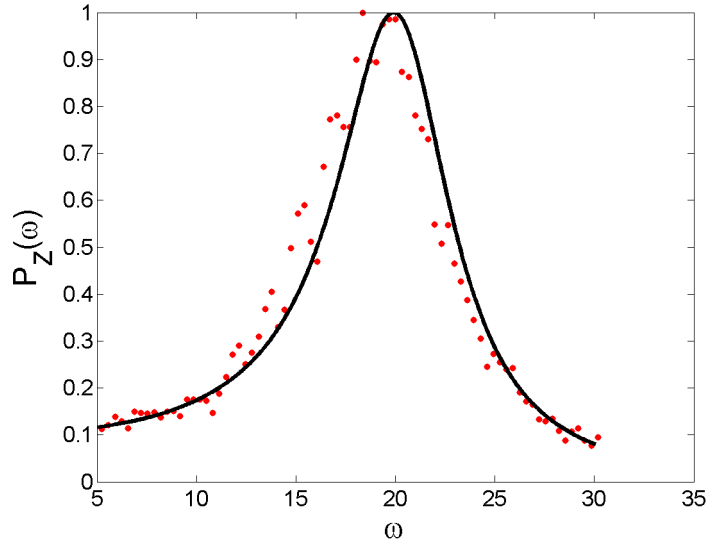


Figure 1.3: The power spectrum of fluctuations as a function of  $\omega$  is plotted for species  $Z$ . The solid line stands for the theoretical prediction (1.24), while the symbols refer to the stochastic simulations averaged over 200 independent realizations. The power spectrum is normalized by the maximum. The parameters are set as in figure 1.2. The system is hence initialized to fall in region III, as depicted in the schematic diagram of figure 1.1.

After some algebraic manipulation, Eq. (1.23) yields to the following explicit forms:

$$P_Z(\omega) = \frac{a_Z + b_Z \omega^2}{(\omega^2 - \Omega^2)^2 + \Gamma^2 \omega^2} \quad (1.24)$$

$$P_Y(\omega) = \frac{a_Y + b_Y \omega^2}{(\omega^2 - \Omega^2)^2 + \Gamma^2 \omega^2}, \quad (1.25)$$

where  $\Gamma = -\text{tr}(M)$ ,  $\Omega = \sqrt{\det(M)}$   $a_Z = B_{1,1}M_{2,2}^2 - 2B_{1,2}M_{1,2}M_{2,2} + B_{2,2}M_{1,2}^2$ ,  $b_Z = B_{1,1}$ ,  $b_Y = B_{2,2}$  e  $a_Y = B_{2,2}M_{1,1}^2 - 2B_{1,2}M_{2,1}M_{1,1} + B_{1,1}M_{2,1}^2$ .

To test the adequacy of the theory we can plot the power spectrum of fluctuation of species  $Z$  around the mean field stationary point, for a choice of the parameters that falls outside the region of deterministic oscillations and compare the prediction to the numerical profile obtained by averaging over many realizations of the stochastic dynamics. The comparison is displayed in figure 1.3. A clear peak is found in the power spectrum, thus confirming that the stochastic oscillations as seen in figure 1.2 stem from finite size fluctuations. The agreement between theory and numerical simulations is excellent. Quasi cycles can therefore develop outside the region of mean field order, and the associated frequency can be adequately estimated via perturbative analytical means.

An approximate estimate for the resonant frequency, where the peak of the power spectrum is positioned, can be analytically worked out. Let us assume legitimate to neglect, as a first approximation, the term proportional to  $\omega^2$  in the numerator of  $P_Z(\omega)$ , see eq. (1.24). Then  $P_Z(\omega)$  is maximum when the denominator is minimum, namely

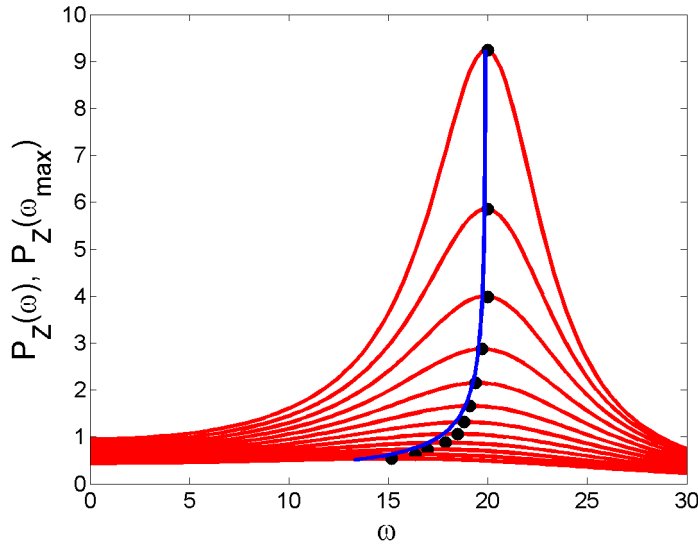


Figure 1.4: The power spectrum of fluctuations  $P_Z$  as a function of  $\omega$ , for different choices of  $\beta$ . is plotted for species  $Z$ . The symbols identify the location of the maxima, while the solid line is obtained by plotting  $P_Z(\omega_{max})$ , as a function of  $\beta$ . The quantity  $\omega_{max}$  follows the approximate eq. (1.27).

when  $|\det\Phi(\omega)|$  takes the smallest possible value. Denote by  $\lambda_i$   $i = 1, 2$  the eigenvalues of matrix  $M$ . Hence:

$$|\det\Phi(\omega)| = \prod_{j=1}^2 (-i\omega - \lambda_j)(i\omega - \lambda_j^*).$$

Since  $M$  is by definition a real matrix, the eigenvalues  $\lambda_i$  can be either real or complex conjugate. If they are real, then  $|\det\Phi(\omega)| = (\omega^2 + \lambda_1^2)(\omega^2 + \lambda_2^2)$ . If they are complex  $\lambda_1 = \lambda_2^* = \lambda$ . If one posits  $\lambda = \lambda_R + i\lambda_I$ , then:

$$|\det\Phi(\omega)| = |\omega^2 + (\lambda_R^2 - \lambda_I^2) + 2i\lambda_R\lambda_I|^2. \quad (1.26)$$

This latter case is of interest to us, as quasi-cycles can develop only if the corresponding mean field dynamics approaches the asymptotic stationary state, via damped oscillations. The condition for the minimum of (1.26) readily translates into the final expression for the resonant frequency  $\omega_{max}$ :

$$\omega_{max} = \sqrt{\lambda_I^2 - \lambda_R^2}. \quad (1.27)$$

In figure 1.4 the theoretical power spectrum of fluctuations is plotted for different values of  $\beta$ . The symbols identify the position of the peaks while the solid line refers to the approximate formula  $P_Z(\omega_{max})$ , where  $\omega_{max}$  is given by (1.27). This comparison points to the correctness of formula (1.27), which therefore encodes all the necessary information to estimate the resonant frequency as a function of the parameters of the model.

## 1.4 Conclusion

Calcium oscillations are crucial for the functioning of the cellular machinery and for this reasons have been widely investigated, both experimentally and theoretically. Dynamical models have been proposed, to different levels of sophistication, which make it possible to reproduce *in silico* the processes that underly the emergence of sustained  $Ca^{2+}$  oscillations. Most of the models so far discussed in the literature are of deterministic inspiration and, as such, omit the inherent stochastic perturbations, which stem from individual based effects. This latter are particularly important at low concentrations, a regime which is certainly of interest when it comes to modeling intracellular calcium oscillations.

Recently, Li and Hou [16] have put forward a microscopic version of the celebrated Goldbeter model [17, 18], a paradigmatic scheme for calcium dynamics, which assumes two species in mutual interaction. Working in such a generalized stochastic setting, it was shown numerically [16] that the intrinsic noise can drive stochastic oscillations, termed in [1] quasi cycles, also outside the region where a deterministic limit cycle is predicted to occur.

Starting from this observation, and to make contact with the theoretical literature devoted to the phenomenon of quasi-cycles, we have here carried out an analytical study of a stochastic  $Ca^{2+}$  model [16]. The analysis is carried out under the linear noise approximation and allows us to obtain a close prediction for the power spectrum of stochastic fluctuations. This latter displays an isolated peak, whose reference frequency appears to be controlled by the chemical parameters of the model, as e.g. the degree of external stimulation  $\beta$ . The validity of the theory is confirmed by direct numerical simulations of the examined stochastic model.

In conclusion, by building on recent advances on the study of noise induced oscillations in stochastic population dynamics models, we have here cast on solid mathematical ground the numerical observations of [16], so confirming that intrinsic noise can play an important, although often neglected, role in the onset of intracellular calcium oscillations.

We have shown that the van Kampen expansion works well on the classical approximation and that it allows us to understand some phenomena that are not explicitly taken into account in the deterministic limit. However, for very low concentration, or in a model with an absorbing boundary, it may happen that the linear approximation does not yield a satisfying description of the behaviour of the fluctuations. For this reason, in the next chapter, we will consider three different models to elaborate on the validity of non linear noise approximation. Moreover, we will explicitly perform the van Kampen expansion beyond the Gaussian approximation to quantify analytically the skewed behaviour of the distribution of the fluctuations. Performing such extended expansion we will obtain a generalized Fokker-Planck equation, that describes the behaviour of the fluctuations. From the Fokker-Planck equation, with a standard procedure, it is possible to obtain a system of ordinary differential equations for the moments of the unknown distribution. The knowledge of the moments enable one to rebuild the profile of the distribution of fluctuations.



## Chapter 2

# Validity of van Kampen expansion beyond Gaussian-approximations

This chapter is devoted to describe the validity of the van Kampen expansion beyond the classical Gaussian approximation. To achieve this result, we have used two different models. In the first one a complex network of autocatalytic chemical reactions is studied both numerically and analytically. The van Kampen perturbative scheme is implemented, beyond the second order approximation, so to capture the non Gaussianity traits as displayed by the simulations. The method is targeted for the first model to the characterization of the third moments of the distribution of fluctuations, originating from a system of four populations in mutual interaction under an auto-catalytic chemical reaction scheme. The theory predictions agree well with the simulations, pointing to the validity of the van Kampen expansion beyond the conventional Gaussian solution. The second model is a one-dimensional stochastic version of a voter model with an absorbing boundary. The distribution of fluctuations is analytically characterized within the generalized van Kampen expansion, accounting for higher-order corrections. The theoretical is shown to successfully capture the non-Gaussian traits of the sought distribution returning an excellent agreement with the simulations, for all times and arbitrarily close to the absorbing barrier. At large times, a compact analytical solution for the distribution of fluctuations is also obtained, bridging the gap with previous investigations [23]. In the final part of the chapter we consider a third model, a stochastic version of the logistic equation, and we compare the van Kampen expansion to the Wentzel–Kramers–Brillouin approximation.

### 2.1 Analytical study of non Gaussian fluctuations in a stochastic scheme of autocatalytic reactions

The cell is a complex structural unit, that defines the building block of living systems [30]. It is made of by a tiny membrane, constituted by a lipid bilayer, which encloses a finite volume and protects the genetic material stored inside. The membrane is semi-permeable: nutrients can leak in and serve as energy storage to support the machinery functioning. Metabolism converts energy into molecules, i.e. building cell components, and releases by-product. Evolution certainly guided the ancient supposedly minimalistic cell entities, the so-called protocells [31],[32],[33], through subsequent steps towards the

delicate and complex biological devices that we see nowadays. Focusing on primordial cell units, back at the origin of life, the most accredited scenario dictates that chemical reactions occurred inside vesicles, small cell-like structures in which the outer membrane takes the form of a lipid bilayer [33]. Vesicles possibly defined the scaffold of prototypical cell models, while it is customarily believed that autocatalytic reactions might have been at play inside primordial protocell. The shared view is that protocell's volume might have been occupied by interacting families of replicators, organized in autocatalytic cycles. A chemical reaction is called autocatalytic if one of the reaction products is itself a catalyst for the chemical reaction. Even if only a small amount of the catalyst is present, the reaction may start off slowly, but will quickly develop once more catalyst is produced. If the reactant is not replaced, the process will again slow down producing the typical sigmoid shape for the concentration of the product. All this is for a single chemical reaction, but of greater interest is the case of many chemical reactions, where one or more reactions produce a catalyst for some of the other reactions. Then the whole collection of constituents is called an autocatalytic set. Autocatalytic reactions have been invoked in the context of studies on the origin of life as a possible solution of the famous Eigen's paradox [34]. This is a puzzling logic concept which limits the size of self replicating molecules to perhaps a few hundred base pairs. However, almost all life on Earth requires much longer molecules to encode their genetic information. This problem is handled in living cells by the presence of enzymes which repair mutations, allowing the encoding molecules to reach large enough sizes. In primordial organisms, autocatalytic cycles might have contributed to the inherent robustness of the system, translating in a degree of microscopic cooperation that successfully prevented the Eigen's evolutionary derive towards self-destruction to occur. It is therefore of interest to analyze the coupled dynamics of chemicals organized in extended cycles of autocatalytic reactions.

It is in this context that our work is positioned. We will in particular consider a model of autocatalytic reactions confined within a bounded region of space. The model was pioneered by Togashi and Kaneko [35] and more recently revisited by [2],[3]. It was in particular shown that fluctuations stemming from the intimated discreteness of the scrutinized medium can seed a resonant effect yielding to organized macroscopic patterns, both in time [2] and space [3].

As we shall clarify in the forthcoming discussion, the model here examined is intrinsically stochastic and falls in the realm of the so called individual-based description. The microscopic dynamics follows explicit rules governing the interactions among individuals and with the surrounding environment. Starting from the stochastic scenario and performing the perturbative development (the van Kampen expansion [29]) with respect to a small parameter which encodes the amplitude of finite size fluctuations, one obtains, at the leading order, the mean-field equations, i.e. the idealized continuum description for the concentration amount. These latter govern in fact the coupled evolution of the average population amount, as in the spirit of the deterministic representation. Including the next-to-leading order corrections, one obtains a description of the fluctuations, as a set of linear stochastic differential equations. Such a system can be hence analyzed exactly, so allowing us to quantify the differences between the stochastic formulation and its deterministic analogue. This analysis was performed in [2] with reference to the a-spatial version of model, and in [3] where the notion of space is instead explicitly included.

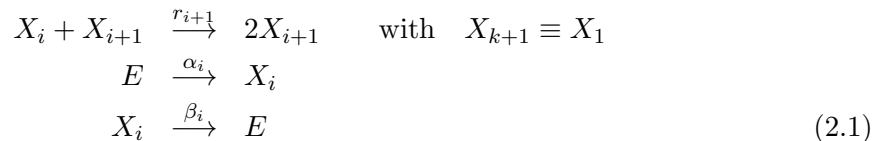
In this section, we take one step forward by analytically characterizing the fluctuations beyond the second order in the van Kampen perturbative scheme [29, 36], i.e. the Gaus-

sian approximation, and so quantifying higher contributions in the hierarchy of moments of the associated distribution. As we shall demonstrate, and with reference to the analyzed case study, we can successfully quantify non Gaussian fluctuations, within the van Kampen descriptive scenario, in agreement with the recent investigations of Grima and collaborators [37] and previous indications of Risken and Vollmer [38]. Indeed, the aim of our work is to recover an analytical description of the asymmetry in the distribution of the fluctuations already observed in [35]. As we will show in the following sections, accounting for higher orders in the van Kampen system size expansion, allows one to obtain a more accurate prediction of the moments, which explains the skewed numerical profile of the fluctuations pointed out in [35]. This work has been in part develop during my master stage, but took to completion in the early stage of my PhD training, with the implementation and extension of dedicated numerical simulation.

The section is organized as follows. In the following subsection we will introduce the model under scrutiny. Then we will turn to discussing the associated master equation, derive the mean field equation, and characterize the fluctuations within the Gaussian approximation. Non Gaussian traits are revealed via numerical (stochastic) simulations for small system sizes. These features are analytically inspected and explained by working in the framework of a generalized Fokker-Planck formulation where the role of the finite population is explicitly accommodated for.

### 2.1.1 The stochastic Kaneko model

The autocatalytic reaction scheme as introduced in [2] describes the dynamics of  $k$  species which interact according to the following rules



where  $X_i$  denotes an element of the  $i$ -th species, while  $E$  is the null constituent or vacancies. The parameter  $r_i$  (with  $r_{k+1} \equiv r_1$ ) is the autocatalytic process rate, while  $\alpha_i$  and  $\beta_i$  are the rates at which the molecules appear and disappear from the system. The size of the system is denoted by  $N$ , then  $\sum_{i=1}^k n_i + n_E = N$ , where  $n_E$  is the number of  $E$ .

It is worth emphasizing that the concept of vacancies  $E$  enables us to accommodate for a finite carrying capacity of the hosting volume. The approach can be readily extended to the case where the space is accounted for by formally dividing the volume in small patches, each being characterized by a limited capacity. Species can then migrate between neighbors cells, therefore visiting different regions of the spatial domain in which they are confined. This generalization is discussed in [3]. We will here solely consider the a-spatial version of the model, aiming at characterizing the fluctuations beyond the canonical Gaussian approximation. In the following, we will introduce the master equation that rules the stochastic dynamics of the system defined by the closed set of chemical equations (2.1).

### 2.1.2 The master equation and its expansion

Let us start by introducing the master equation that governs the evolution of the stochastic system described above. First, it is necessary to write down the transition rates  $T(\mathbf{n}'|\mathbf{n})$  from the state  $\mathbf{n}$  to the state  $\mathbf{n}'$ , where  $\mathbf{n} \equiv (n_1, \dots, n_k)$  is the vector whose components define the number of elements of each species at time  $t$ . These transition rates are

$$\begin{aligned} T(n_1, \dots, n_i - 1, n_{i+1} + 1, \dots, n_k | \mathbf{n}) &= r_{i+1} \frac{n_i}{N} \frac{n_{i+1}}{N}, \\ T(n_1, \dots, n_i + 1, \dots, n_k | \mathbf{n}) &= \alpha_i \left( 1 - \frac{\sum_{j=1}^k n_j}{N} \right), \\ T(n_1, \dots, n_i - 1, \dots, n_k | \mathbf{n}) &= \beta_i \frac{n_i}{N}. \end{aligned}$$

In this way, the differential equation for the probability  $P(\mathbf{n}, t)$  reads

$$\begin{aligned} \frac{d}{dt} P(\mathbf{n}, t) &= \sum_{i=1}^k (\varepsilon_i^+ \varepsilon_{i+1}^-) T(n_1, \dots, n_i - 1, n_{i+1} + 1, \dots, n_k) P(\mathbf{n}, t) + \\ &\quad \sum_{i=1}^k (\varepsilon_i^- - 1) T(n_1, \dots, n_i + 1, n_{i+1}, \dots, n_k) P(\mathbf{n}, t) + \\ &\quad \sum_{i=1}^k (\varepsilon_i^+ - 1) T(n_1, \dots, n_i - 1, n_{i+1}, \dots, n_k) P(\mathbf{n}, t) \end{aligned} \quad (2.2)$$

where  $\varepsilon_i^\pm$  are the step operators which act on an arbitrary function  $f(\mathbf{x})$  as  $\varepsilon_i^\pm f(\mathbf{x}) = f(\dots, x_i \pm 1, \dots)$ .

As we have already underline in the previous chapter the above description is exact: no approximations have yet been made. At this stage we could resort to numerical simulations of the underlying chemical reactions by means of the Gillespie algorithm [28, 39]. This method produces realizations of the stochastic dynamics which are formally equivalent to those found from the master equation (2.2). Averaging over many realizations enables us to calculate quantities of interest. We will comment on the results of such simulations, in the following. A different route is however possible which consists in drastically simplifying the master equation, via a perturbative calculation, the van Kampen system size expansion [29, 36]. We will again notice that it is effectively an expansion in powers of  $N^{-1/2}$ , which to the leading order ( $N \rightarrow \infty$ ) gives the deterministic equations describing the system, while at next-to-leading order returns the finite  $N$  corrections to these. The van Kampen ansatz is:

$$\frac{n_i}{N} = \phi_i + \frac{\xi_i}{\sqrt{N}}. \quad (2.3)$$

where  $\xi_i$  is the  $i$ -th component of the  $k$ -dimensional stochastic variable  $\boldsymbol{\xi} = (\xi_1, \xi_2, \dots)$ . To proceed in the analysis we make use of the working ansatz (2.3) into the master equation (2.2). Then, it is straightforward to show that the operator  $\varepsilon_i^\pm$  can be approximated as:

$$\varepsilon_i^\pm = 1 \pm \frac{1}{N^{1/2}} \frac{\partial}{\partial \xi_i} + \frac{1}{2N} \frac{\partial^2}{\partial \xi_i^2} \pm \frac{1}{3! N^{3/2}} \frac{\partial^3}{\partial \xi_i^3} + \dots$$

The first step in the perturbative calculation consists in expliciting in the master equation the dependence on the concentration vector  $\mathbf{y} = \mathbf{n}/N$ . It is legitimate to assume that this latter quantity changes continuously with time, as far as each instantaneous variation is small when compared to the system size. We therefore proceed by defining the following distribution:

$$\Pi(\boldsymbol{\xi}, t) = P(\mathbf{y}, t) = P\left(\boldsymbol{\phi}(t) + \frac{\boldsymbol{\xi}}{\sqrt{N}}, t\right).$$

A simple manipulation yields to:

$$\frac{\partial P}{\partial t} = -\sqrt{N} \sum_{i=1}^k \frac{\partial \Pi}{\partial \xi_i} \frac{d\phi_i}{dt} + \frac{\partial \Pi}{\partial t}.$$

Similarly one can act on the right hand side of Eq. (2.2) and hierarchically organize the resulting terms with respect to their  $N$ -dependence. The outcome of such algebraic calculation are reported in the following. We will in particular limit our discussion to the Gaussian approximation, by neglecting, at this stage, the  $N^{-3/2}$  terms. We will then return on this important issue and discuss the specific role that is played by  $N^{-3/2}$  corrections.

### 2.1.3 The $N^{-1/2}$ terms

As concerns the terms of order  $N^{-\frac{1}{2}}$  one obtains:

$$\begin{aligned} -\frac{1}{\sqrt{N}} \sum_{i=1}^k \frac{\partial \Pi}{\partial \xi_i} \frac{d\phi_i}{d\tau} &= \frac{1}{\sqrt{N}} \sum_{i=1}^k (r_{i+1}\phi_i\phi_{i+1} - r_i\phi_{i-1}\phi_i) \frac{\partial \Pi}{\partial \xi_i} \\ &+ \frac{1}{\sqrt{N}} \sum_{i=1}^k \left[ \beta_i\phi_i - \alpha_i \left( 1 - \sum_{m=1}^k \phi_m \right) \right] \frac{\partial \Pi}{\partial \xi_i} \end{aligned}$$

where the rescaled time  $\tau$  is defined as  $\tau = t/N$ . Thus the following system of differential equations holds for the concentration amount  $\phi_i$

$$\frac{d\phi_i}{d\tau} = r_i\phi_{i-1}\phi_i - r_{i+1}\phi_i\phi_{i+1} + \alpha_i \left( 1 - \sum_{m=1}^k \phi_m \right) - \beta_i\phi_i, \quad (2.4)$$

which in turn corresponds to working within the so-called mean field approximation and eventually disregard finite size corrections. We should emphasize that Eqs. (2.4) are obtained by elaborating on the exact stochastic chemical model and exploring the limit for infinite system size  $N \rightarrow \infty$ .

To make contact with previous investigations [2] we shall assume the simplifying setting with  $\beta_i = \beta$ ,  $\alpha_i = \alpha$  and  $r_i = r \forall i$ . Under this condition, all species asymptotically converge to the fixed point  $\phi^*$  which is readily calculated as:

$$\alpha \left( 1 - \sum_{m=1}^k \phi^* \right) - \beta\phi^* = 0 \quad \longrightarrow \quad \phi^* = \frac{\alpha}{k\alpha + \beta}. \quad (2.5)$$

We now turn to numerical simulation based on the Gillespie algorithm and discuss the case with  $k = 4$  species. As reported in Fig. 2.1, once the initial transient has

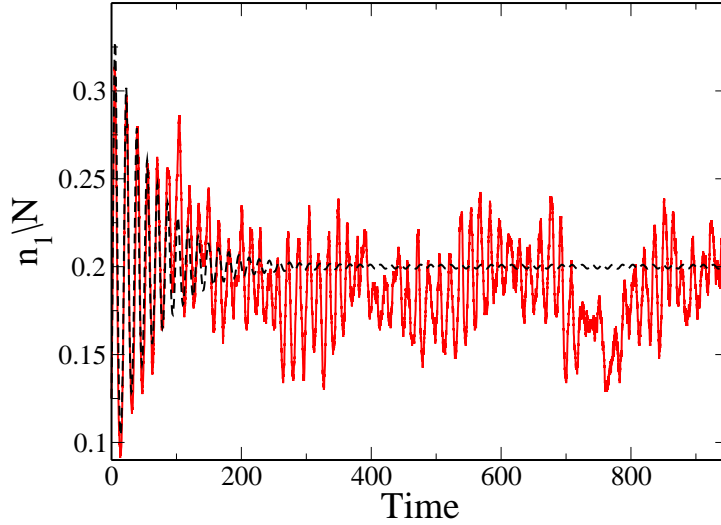


Figure 2.1: Temporal evolution of one of the species concentrations for a system composed by 4 species and parameters set as  $N = 8190$ ,  $r_i = 10$  and  $\alpha_i = \beta_i = 1/64 \forall i$ . The noisy (red online) line represents one stochastic realization thought the Gillespie algorithm [28, 39], while the dashed black line shows the numerical solution of the deterministic system given by Eq. (2.4).

died out, the numerically recorded time series keep on oscillating around the reference value as specified by relation (2.5). The mean field dynamics has conversely relaxed to the deputed equilibrium value. These oscillations stem from the finite size corrections to the idealized mean field dynamics and will be inspected in the following. We will be in particular concerned with characterizing the statistical properties of the observed signal, and quantify via rigorous analytical means the moments of the distribution of the fluctuations.

#### 2.1.4 The $N^{-1}$ corrections

Finite size effects related to the  $N^{-1}$  corrections result in the Fokker-Planck equation:

$$\frac{\partial \Pi}{\partial \tau} = - \sum_{i=1}^k \frac{\partial}{\partial \xi_i} \left[ A_i(\boldsymbol{\xi}) \Pi \right] + \frac{1}{2} \sum_{j=1}^k \sum_{i=1}^k \frac{\partial^2}{\partial \xi_i \partial \xi_j} \left[ b_{ij} \Pi \right] \quad (2.6)$$

which governs the evolution of the distribution  $\Pi(\cdot)$ . Here  $A_i(\boldsymbol{\xi})$  reads:

$$A_i(\boldsymbol{\xi}) = (r_i \phi_{i-1} - r_{i+1} \phi_{i+1}) \xi_i - r_{i+1} \phi_i \xi_{i+1} + r_i \phi_i \xi_{i-1} - \alpha_i \sum_{m=1}^k \xi_m - \beta_i \xi_i,$$

while  $b_{ij}$  stands for the element  $ij$  of matrix  $B$  defined as:

$$b_{ij} = \begin{cases} r_{i+1} \phi_i \phi_{i+1} + r_i \phi_i \phi_{i-1} + \alpha_i (1 - \sum_{m=1}^k \phi_m) + \beta_i \phi_i & \text{if } i = j \\ -r_{i+1} \phi_i \phi_{i+1} & \text{if } j = i + 1 \\ -r_i \phi_{i-1} \phi_i & \text{if } j = i - 1 \\ 0 & \text{if } |i - j| > 1. \end{cases}$$

For the sake of clarity we shall introduce the matrix  $M$  of elements  $m_{ij}$  defined as:

$$m_{ij} = \begin{cases} r_i\phi_{i-1} - r_{i+1}\phi_{i+1} - \alpha_i - \beta_i & \text{if } i = j \\ -r_{i+1}\phi_i - \alpha_i & \text{if } j = i + 1 \\ r_i\phi_i - \beta_i & \text{if } j = i - 1 \\ -\alpha_i & \text{if } |i - j| > 1 \end{cases}$$

and so rewrite  $A_i$  as:

$$A_i = \sum_{j=1}^k m_{ij}\xi_j.$$

The Fokker-Planck equation (2.6) has been previously obtained in [2] and shown to explain the regular oscillations displayed in direct stochastic simulations. The oscillations, in fact, materialize in a peak in the power spectrum of fluctuations which can be analytically calculated working in the equivalent context of the Langevin equation. Here, we take a different route and reconstruct the distribution of fluctuations through the calculation of the associated moments. To allow for analytical progress, we will assume again identical chemical reactions rates for all species, namely  $r_i = r$ ,  $\beta_i = \beta$  and  $\alpha_i = \alpha \forall i$ . Moreover, we will focus on the fluctuations around the equilibrium and so require  $\phi_i = \phi^* \forall i$ . Under these conditions the matrix  $M$  is circulating and can be cast in the form:

$$M = \begin{bmatrix} m_0 & m_1 & m_2 & m_2 & \dots & m_3 \\ m_3 & m_0 & m_1 & m_2 & \dots & m_2 \\ m_2 & m_3 & m_0 & m_1 & \dots & m_2 \\ \dots & \dots & \dots & \dots & \dots & \dots \\ m_1 & m_2 & m_2 & m_2 & \dots & m_0 \end{bmatrix}.$$

with  $m_0 = -\alpha - \beta$ ,  $m_1 = -r\phi^* - \alpha$ ,  $m_2 = -\alpha$ , and  $m_3 = r\phi^* - \alpha$ . The  $k \times k$  matrix reads instead:

$$B = \begin{bmatrix} b_0 & b_1 & 0 & \dots & 0 & b_1 \\ b_1 & b_0 & b_1 & \dots & 0 & 0 \\ 0 & b_1 & b_0 & \dots & 0 & 0 \\ \dots & \dots & \dots & \dots & \dots & \dots \\ b_1 & 0 & 0 & \dots & b_1 & b_0 \end{bmatrix};$$

where  $b_0 = 2r\phi^*\phi^* + \alpha(1 - k\phi^*) + \beta\phi^*$ , and  $b_1 = -r\phi^*\phi^*$ . We recall that the solution of the Fokker-Planck equation (2.6) is a multivariate Gaussian which is univocally characterized by the associated families of first and second moments. Working within this setting, it is hence sufficient to derive the analytical equations that control the time evolution of the first two moments of the distribution. We will in particular provide closed analytical expressions for the asymptotic moments and draw a direct comparison with the numerical experiments.

### 2.1.5 Analytical estimates of the fluctuations distribution moments

Define the moment of order  $p$  for  $\xi_i$  the quantity

$$\langle \xi_i^p \rangle = \int \Pi(\boldsymbol{\xi}) \xi_i^p d\boldsymbol{\xi}$$

Let us illustrate the analytical procedure that is here adopted, with reference to  $\langle \xi_i^2 \rangle$ . To this end we start from Eq. (2.6) and multiply it on both sides by the factor  $\xi_i^2$ . Integrating over  $\mathbb{R}^k$  in  $d\boldsymbol{\xi} = (d\xi_1, d\xi_2, \dots, d\xi_k)$ , yields:

$$\int \xi_i^2 \frac{\partial}{\partial \tau} \Pi(\boldsymbol{\xi}, \tau) d\boldsymbol{\xi} = \int \xi_i^2 \sum_i \frac{\partial}{\partial \xi_i} A_i(\boldsymbol{\xi}) \Pi(\boldsymbol{\xi}, \tau) d\boldsymbol{\xi} + \int \xi_i^2 \frac{1}{2!} \sum_{i,j} \frac{\partial^2}{\partial \xi_i \partial \xi_j} b_{i,j}(\boldsymbol{\xi}) \Pi(\boldsymbol{\xi}, \tau) d\boldsymbol{\xi}. \quad (2.7)$$

Consider the right hand side of Eq. (2.7) and operate two successive integrations by parts. Just two terms survive, as it can be trivially argued for. Hence, bringing out the time derivative from the integral at the left hand side of Eq. (2.7), the sought equation for the second moments reads:

$$\langle \dot{\xi}_i^2 \rangle = 2m_{i,i} \langle \xi_i^2 \rangle + 2m_{i,i-1} \langle \xi_i \xi_{i-1} \rangle + 2m_{i,i+1} \langle \xi_i \xi_{i+1} \rangle + 2m_{i,i+2} \langle \xi_i \xi_{i+2} \rangle + b_{i,i} \quad (2.8)$$

where  $i = 1, \dots, 4$ . Use has been made of the definitions of the coefficients  $m_{ij}$ . With analogous steps one immediately obtains the differential equation that governs the time evolution of quantity  $\langle \xi_i \xi_j \rangle$ :

$$\begin{aligned} \langle \dot{\xi}_i \xi_j \rangle = & m_{i,i} \langle \xi_i \xi_{i+1} \rangle + m_{i+1,i} \langle \xi_i^2 \rangle + m_{i,i+1} \langle \xi_{i+1}^2 \rangle + m_{i,i+2} \langle \xi_{i+1} \xi_{i+2} \rangle \\ & + m_{i+1,i+1} \langle \xi_i \xi_{i+1} \rangle + m_{i+1,i+2} \langle \xi_i \xi_{i+2} \rangle + m_{i+1,i} \langle \xi_i^2 \rangle \\ & + m_{i,i+3} \langle \xi_{i+3} \xi_{i+1} \rangle + b_{i,i+1}. \end{aligned} \quad (2.9)$$

which, in practice, encodes the degree of temporal correlation between species  $i$  and  $j$ . The picture is completed by providing the equations for the first moments which read:

$$\langle \dot{\xi}_i \rangle = m_{i,i} \langle \xi_i \rangle + m_{i,i-1} \langle \xi_{i-1} \rangle + \langle \xi_i \rangle m_{i,i+1} - m_{i,i+2} \langle \xi_{i+2} \rangle.$$

Taking into account all possible permutations of the involved indexes  $i, j$ , both ranging in the interval from 1 to 4, and recalling the Eq.s (2.8)–(2.9), one eventually obtains a closed system of ten coupled ordinary differential equations. For the simplified case  $r_i = r$ ,  $\alpha_i = \alpha$ ,  $\beta_i = \beta \forall i$ , this latter can be cast in a compact form by introducing the matrix:

$$K = \begin{pmatrix} 2m_0 & 2m_1 & 2m_2 & 2m_3 & 0 & 0 & 0 & 0 & 0 & 0 \\ m_3 & 2m_0 & m_1 & m_2 & m_1 & m_1 & m_2 & m_3 & 0 & 0 \\ m_2 & m_3 & 2m_0 & m_1 & 0 & m_1 & 0 & m_2 & m_3 & 0 \\ m_1 & m_2 & m_3 & 2m_0 & 0 & 0 & m_1 & 0 & m_2 & m_3 \\ 0 & 2m_3 & 0 & 0 & 2m_0 & 2m_1 & 2m_2 & 0 & 0 & 0 \\ 0 & m_2 & m_3 & 0 & m_3 & 2m_0 & m_1 & m_1 & m_2 & 0 \\ 0 & m_1 & 0 & m_3 & m_2 & m_3 & 2m_0 & 0 & m_1 & m_2 \\ 0 & 0 & 2m_2 & 0 & 0 & 2m_3 & 0 & 2m_0 & 2m_1 & 0 \\ 0 & 0 & m_1 & m_2 & 0 & m_2 & m_3 & m_3 & 2m_0 & m_1 \\ 0 & 0 & 0 & 2m_1 & 0 & 0 & 2m_2 & 0 & 2m_3 & 2m_0 \end{pmatrix}$$

By further defining:

$$\mathbf{X} = [\langle \xi_1^2 \rangle \quad \langle \xi_1 \xi_2 \rangle \quad \langle \xi_1 \xi_3 \rangle \quad \langle \xi_1 \xi_4 \rangle \quad \langle \xi_2^2 \rangle \quad \langle \xi_2 \xi_3 \rangle \quad \langle \xi_2 \xi_4 \rangle \quad \langle \xi_3^2 \rangle \quad \langle \xi_3 \xi_4 \rangle \quad \langle \xi_4^2 \rangle]$$

and the vector

$$D = [b_0 \quad b_1 \quad 0 \quad b_1 \quad b_0 \quad b_1 \quad 0 \quad b_0 \quad b_1 \quad b_0]$$



one gets

$$\dot{\mathbf{X}} = K\mathbf{X} + D.$$

As anticipated, we focus in particular on the late time evolution of the system, i.e. when the fluctuations' distribution has converged to its asymptotic form. This request translates into the mathematical condition  $\dot{\mathbf{X}} = 0$ , which implies dealing with an algebraic system of equations. Given the peculiar structure of the problem, and by invoking a straightforward argument of symmetry <sup>1</sup>, one can identify three families of independent unknowns, namely:

$$\begin{aligned} \langle \xi_1^2 \rangle &= \langle \xi_2^2 \rangle = \langle \xi_3^2 \rangle = \langle \xi_4^2 \rangle =: \Gamma_1 \\ \langle \xi_1 \xi_2 \rangle &= \langle \xi_1 \xi_4 \rangle = \langle \xi_2 \xi_3 \rangle = \langle \xi_3 \xi_4 \rangle =: \Gamma_2 \\ \langle \xi_1 \xi_3 \rangle &= \langle \xi_2 \xi_4 \rangle =: \Gamma_3. \end{aligned} \tag{2.10}$$

Closed analytical expressions for the unknowns  $\Gamma_1, \Gamma_2$  and  $\Gamma_3$  as a function of the chemical parameters can be derived and take the form:

$$\begin{aligned} \Gamma_1 &= \frac{2b_0}{5\alpha} - \frac{b_1}{5\alpha} \\ \Gamma_2 &= -\frac{b_0}{10\alpha} + \frac{3b_1}{10\alpha} \\ \Gamma_3 &= -\frac{b_0}{10\alpha} - \frac{b_1}{5\alpha}. \end{aligned} \tag{2.11}$$

In deriving the above, we have assumed a further simplifying condition, namely  $\alpha = \beta$ . The adequacy of the predictions is tested in Fig. 2.2, where  $\Gamma_1$  and  $\Gamma_2$  are plotted versus the independent parameter  $\alpha$ . Recalling the explicit forms of  $b_0$  and  $b_1$  one can immediately appreciate that  $\Gamma_3$  is indeed independent of  $\alpha$ . For this reason we here avoid to include  $\Gamma_3$  in Fig. 2.2. One can moreover make use of the knowledge of the moments to reconstruct the profile of the distribution  $\Pi(\boldsymbol{\xi})$ . In particular, and due to the symmetry of the model, we solely focus on the marginal distribution  $\Pi(\xi) = \Pi(\xi_i)$  for  $i = 1, \dots, 4$ . In practice, we project the distribution in a one-dimensional subspace by integrating over three out of four scalar independent variables  $\xi_i$ . In Fig. 2.3, a comparison between theory and stochastic simulations (relative to small  $N$  values) is drawn. While the agreement is certainly satisfying, deviations from the predicted Gaussian profile manifest as the population size shrinks. As we shall demonstrate, these distortions, which materialize in a skewed distribution, can be successfully explained within an extended interpretative framework that moves from the van Kampen system size expansion. In the following section we will hence extend the calculation beyond the Gaussian approximation. In doing so we will operate in the general setting for  $\alpha \neq \beta$ , but then specialize on the choice  $\alpha = \beta$  to drastically reduce the complexity of the inspected problem.

### 2.1.6 Beyond the Gaussian approximation

We shall here go back to discussing the higher orders,  $N^{-3/2}$  corrections to the Fokker-Planck equation. We will in particular consider the various terms that contribute to the generalized Fokker-Planck equation grouping them as a function of the order of the

---

<sup>1</sup>It can be shown (see Fig. 1 of [2]) that the four families of chemicals evolve in pairs. Odd species  $k = 1, 3$  are mutually synchronized. The same applies to the even pairs  $k = 2, 4$ .

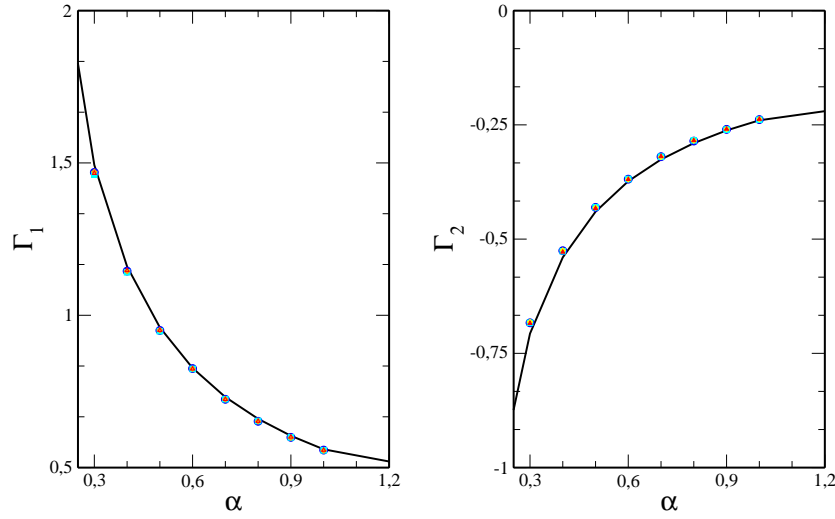


Figure 2.2: Plots of the moments  $\Gamma_1$  and  $\Gamma_2$  as functions of  $\alpha$ . The black lines show the theoretical predictions given by Eq. (2.11), while the (colored online) symbols represent the numerical simulations of the stochastic problem. Each symbol corresponds to a different component of the family according to (2.10). Parameters are set as  $N = 2000$ ,  $\alpha = \beta$ .

derivative involved. The order  $N^{-3/2}$  terms that involve the first derivatives can be expressed as:

$$\begin{aligned} \sum_{i=1}^k \left[ \frac{\partial}{\partial \xi_i} - \frac{\partial}{\partial \xi_{i+1}} \right] r_{i+1} \xi_i \xi_{i+1} \Pi(\boldsymbol{\xi}, \tau) &= \sum_{i=1}^k \frac{\partial}{\partial \xi_i} [r_{i+1} \xi_i \xi_{i+1} - r_i \xi_{i-1} \xi_i] \Pi(\boldsymbol{\xi}, \tau) \\ &= - \sum_{i=1}^k \sum_{j=1}^k \frac{\partial}{\partial \xi_i} l_{ij} \xi_i \xi_j \Pi(\boldsymbol{\xi}, \tau), \end{aligned}$$

where  $l_{ij}$  are the elements of the  $k \times k$  circulant matrix  $L$  which, for  $r_i = r \quad \forall i$  reads:

$$L = \begin{pmatrix} 0 & -r & 0 & \dots & 0 & r \\ r & 0 & -r & \dots & \dots & 0 \\ 0 & r & 0 & \dots & \dots & \dots \\ \dots & \dots & \dots & \dots & \dots & \dots \\ \dots & \dots & \dots & \dots & -r & 0 \\ 0 & \dots & \dots & r & 0 & -r \\ -r & 0 & \dots & 0 & r & 0 \end{pmatrix}.$$

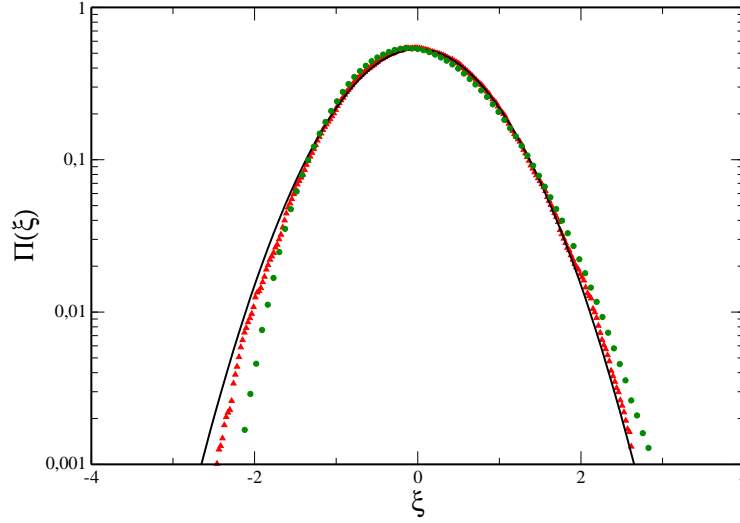


Figure 2.3: Comparison between the stationary marginal Gaussian distribution and the stochastic simulations (the y-axis has a logarithmic scale). The solid (red on line) line shows the theoretical prediction according to the van Kampen theory. The (green online) circles represent the numerical distribution for a system with  $N = 200$ , while the (red online) triangles refer to a system with  $N = 2000$ . For all the curves  $r = 10$ ,  $\alpha = \beta = 0.1$ .

The order  $N^{-3/2}$  contribution which depends on the second derivatives can be also expressed in a matricial form. In fact, we have:

$$\frac{1}{2} \left[ \frac{\partial^2}{\partial \xi_i^2} \beta_i \xi_i - \frac{\partial^2}{\partial \xi_i^2} \alpha_i \sum_w \xi_w + r_{i+1} \frac{\partial^2}{\partial \xi_i^2} (\xi_i \phi_{i+1} + \phi_i \xi_{i+1}) + r_i \frac{\partial^2}{\partial \xi_i^2} (\xi_i \phi_{i-1} + \phi_i \xi_{i-1}) \right. \\ \left. + 2r_{i+1} \frac{\partial}{\partial \xi_i} \frac{\partial}{\partial \xi_{i+1}} (\xi_i \phi_{i+1} + \phi_i \xi_{i+1}) \right] \Pi(\boldsymbol{\xi}, \tau) = \sum_{i=1}^k \sum_{j=1}^k \frac{\partial}{\partial \xi_i \partial \xi_j} d_{ij},$$

where the  $k \times k$  matrix  $D$  of elements  $d_{ij}$ , for  $r_i = r \forall i$ , reads:

$$d_{ij} = \begin{cases} \beta_i \xi_i - \alpha \sum_w \xi_w + r(\xi_i \phi^* + \xi_{i+1} \phi^*) + r(\xi_i \phi^* + \xi_{i-1} \phi^*) & \text{if } i = j \\ -r(\xi_i \phi^* + \xi_{i+1} \phi^*) & \text{if } j = i + 1 \\ -r(\xi_i \phi^* + \xi_{i-1} \phi^*) & \text{if } j = i - 1 \\ 0 & \text{otherwise.} \end{cases}$$

Finally, the third order derivatives contribute as:

$$\left[ -\frac{1}{3!} \frac{\partial^3}{\partial \xi_i^3} \alpha_i (1 - \sum_m \phi_m) + \frac{1}{3!} \left[ \frac{\partial}{\partial \xi_i} - \frac{\partial}{\partial \xi_{i+1}} \right]^3 r_{i+1} \phi_i \phi_{i+1} + \frac{1}{3!} \frac{\partial^3}{\partial \xi_i^3} \beta_i \phi_i \right] \Pi(\boldsymbol{\xi}, \tau) = \\ - \sum_{i,j,w} \frac{\partial^3}{\partial \xi_i \partial \xi_j \partial \xi_w} e_{ijw} \Pi(\boldsymbol{\xi}, \tau),$$

where we introduced the matrix  $E$  defined as:

$$e_{ijw} = \begin{cases} r(\phi^*)^2 & j = i & w = i + 1 \\ r(\phi^*)^2 & j = i - 1 & w = i - 1 \\ r(\phi^*)^2 & j = i + 1 & w = i \\ -r(\phi^*)^2 & j = i + 1 & w = i + 1 \\ -r(\phi^*)^2 & j = i & w = i - 1 \\ -r(\phi^*)^2 & j = i - 1 & w = i \\ -[\beta\phi^* - \alpha(1 - k\phi^*)] & i = j = w. \end{cases}$$

In conclusion, one gets the following equation for the distribution  $\Pi(\boldsymbol{\xi}, \tau)$  [40]:

$$\begin{aligned} \frac{\partial \Pi(\boldsymbol{\xi}, \tau)}{\partial \tau} = & - \sum_{i=1}^k \frac{\partial}{\partial \xi_i} [A_i(\boldsymbol{\xi}) \Pi(\boldsymbol{\xi}, \tau)] + \frac{1}{2} \sum_{i,j=1}^k \frac{\partial^2}{\partial \xi_i \partial \xi_j} [b_{ij} \Pi(\boldsymbol{\xi}, \tau)] \\ & - \frac{1}{N^{1/2}} \sum_{i=1}^k \frac{\partial}{\partial \xi_i} [C_i(\boldsymbol{\xi}) \Pi(\boldsymbol{\xi}, \tau)] + \frac{1}{2N^{1/2}} \sum_{i,j=1}^k \frac{\partial^2}{\partial \xi_i \partial \xi_j} [d_{ij}(\boldsymbol{\xi}) \Pi(\boldsymbol{\xi}, \tau)] \\ & - \frac{1}{3!N^{1/2}} \sum_{i,j,w=1}^k \frac{\partial^3}{\partial \xi_i \partial \xi_j \partial \xi_w} [e_{ijw} \Pi(\boldsymbol{\xi}, \tau)], \end{aligned} \quad (2.12)$$

where:

$$C_i(\boldsymbol{\xi}) = \sum_{j=1}^k l_{ij} \xi_i \xi_j.$$

We will refer to the latter as to the *generalized Fokker-Planck equation*. In the following section we will discuss the corrections to the Gaussian approximation as deduced by the above mathematical framework.

### 2.1.7 Non Gaussian corrections to the moments of the distribution

Starting from Eq. (2.12) we shall now assume  $k = 4$  and calculate the first three moments of the asymptotic distribution of the fluctuations around the mean field equilibrium. Clearly, the derivation can be in principle extended to evaluate the contribution of higher moments. The algebraic complexity of such an extension is however considerable and for this reason the third is the largest moment here characterized. The conclusions are nevertheless rather interesting as evaluating the third moment allows us to quantify the observed degree of skewness in the distribution of fluctuations.

When it comes to the first moment one gets:

$$\begin{aligned} \frac{d}{dt} \langle \xi_i \rangle = & m_{i,i} \langle \xi_i \rangle + m_{i,i-1} \langle \xi_{i-1} \rangle + m_{i,i+1} \langle \xi_i \rangle + m_{i,i+2} \langle \xi_{i+2} \rangle \\ & + \frac{1}{N^{1/2}} [l_{i,i-1} \langle \xi_i \xi_{i-1} \rangle + l_{i,i+1} \langle \xi_i \xi_{i+1} \rangle]. \end{aligned} \quad (2.13)$$

This equation differs from the one obtained in section 2.1.5 for the additional contribution

$$\frac{1}{N^{1/2}} [l_{i,i-1} \langle \xi_i \xi_{i-1} \rangle + l_{i,i+1} \langle \xi_i \xi_{i+1} \rangle] \quad .$$

Thanks to the symmetry of the system, which ultimately stems from having assumed  $r_i = r \forall i$ , we can operate in a highly simplified framework. We notice in fact that

the above term is function of the second moments, which have been estimated above and quantified as  $\langle \xi_i \xi_{i+1} \rangle = \langle \xi_i \xi_{i-1} \rangle = \Gamma_2 + o(1/\sqrt{N})$ . Further we observe that  $l_{i,i-1} = -l_{i,i+1}$ . Hence the corrections to the Gaussian solution as exemplified in Eq. (2.13) contribute with an overall term of order  $N^{-3/2}$ , which can be legitimately neglected at this level of approximation. In conclusion the equation for the first moments is identical to that obtained in section 2.1.5.

Working in complete analogy, for the second moments we find:

$$\begin{aligned} \langle \xi_i^2 \rangle &= 2m_{i,i} \langle \xi_i^2 \rangle + 2m_{i,i+2} \langle \xi_i \xi_{i+2} \rangle + 2m_{i,i+1} \langle \xi_i \xi_{i+1} \rangle + 2m_{i,i-1} \langle \xi_i \xi_{i-1} \rangle + b_{i,i} \\ &\quad + \frac{2}{N^{1/2}} [l_{i,i+1} \langle \xi_i^2 \xi_{i+1} \rangle + l_{i,i-1} \langle \xi_i^2 \xi_{i-1} \rangle], \end{aligned}$$

for the variance of each involved species (recalling that the first moments are indeed null) and

$$\begin{aligned} \langle \xi_i \xi_{i+1} \rangle &= m_{i,i} \langle \xi_i \xi_{i+1} \rangle + m_{i,i+2} \langle \xi_{i+1} \xi_{i+2} \rangle + m_{i,i+1} \langle \xi_{i+1}^2 \rangle + m_{i+1,i} \langle \xi_i^2 \rangle \\ &\quad + m_{i+1,i+1} \langle \xi_i \xi_{i+1} \rangle + m_{i+1,i+2} \langle \xi_i \xi_{i+2} \rangle + m_{i,i+1} \langle \xi_i^2 \rangle + m_{i,i+3} \langle \xi_{i+1} \xi_{i+3} \rangle \\ &\quad + \frac{1}{2} b_{i,i+1} + \frac{1}{2} b_{i+1,i} + \frac{1}{N^{1/2}} [l_{i,i+1} \langle \xi_i \xi_{i+1}^2 \rangle + l_{i,i-1} \langle \xi_i \xi_{i-1} \xi_{i+1} \rangle \\ &\quad + l_{i+1,i} \langle \xi_i^2 \xi_{i+1} \rangle + l_{i+1,i+2} \langle \xi_i \xi_{i+2} \xi_{i+1} \rangle], \end{aligned}$$

for the mutual correlation between distinct populations. The index  $i$  ranges from 1 to 4. Again the extra contributions are limited to the terms stored in square brackets and prove to be negligible at this level of approximation. In fact the third order correlations therein involved should scale as  $N^{-1/2}$  as requested by a simple consistency argument and as we shall prove a posteriori. Then, also in this case, thanks to the specific form of the matrix  $L$ , the additional contribution, stemming from third order moments, vanishes. We come hence to the conclusion that the second moments are identical to those calculated in the preceding section 2.1.5 working within the Gaussian ansatz.

Let us now turn to calculating the third moments. After a lengthy derivation we end up with:

$$\begin{aligned} \langle \xi_i^3 \rangle &= 3m_0 \langle \xi_i^3 \rangle + 3m_3 \langle \xi_i^2 \xi_{i-1} \rangle + 3m_2 \langle \xi_i^2 \xi_{i+2} \rangle + 3m_1 \langle \xi_i^2 \xi_{i+1} \rangle + 3b_0 \langle \xi_i \rangle \\ &\quad + \frac{3}{N^{1/2}} [m_4 \langle \xi_i^2 \rangle + m_3 \langle \xi_i \xi_{i+1} \rangle + m_3 \langle \xi_i \xi_{i-1} \rangle + 3m_2 \langle \xi_i \xi_{i+2} \rangle] + \frac{m_5}{N^{1/2}} \\ &\quad + \frac{1}{N^{1/2}} [3r \langle \xi_i^3 \xi_{i-1} \rangle - 3r \langle \xi_i^3 \xi_{i+1} \rangle], \end{aligned}$$

where  $m_0 = -2\alpha$ ,  $m_1 = -\alpha - r/5$ ,  $m_2 = -\alpha$ ,  $m_3 = -\alpha + r/5$ ,  $m_4 = 2r/5$ ,  $m_5 = m_6 = 0$ ,  $m_7 = -2r/5$ ,  $m_8 = r/25$  and  $m_9 = -r/5$ . Here again, and as anticipated in the preceding discussion, we have chosen the simplifying setting with  $\alpha = \beta$ , which consequently implies  $\phi^* = 1/5$ . Elaborating on the symmetry one can identify five families of independent moments, which obey to the above and the following differential equations:

$$\begin{aligned} \frac{d}{dt} \langle \xi_i^2 \xi_{i-1} \rangle &= 3m_0 \langle \xi_i^2 \xi_{i-1} \rangle + 2m_3 \langle \xi_i \xi_{i-1}^2 \rangle + 2m_1 \langle \xi_i \xi_{i+1} \xi_{i-1} \rangle + 2m_2 \langle \xi_i \xi_{i-1} \xi_{i+2} \rangle \\ &\quad + m_3 \langle \xi_i^2 \xi_{i+2} \rangle + m_1 \langle \xi_i^3 \rangle + m_2 \langle \xi_i^2 \xi_{i+1} \rangle + b_0 \langle \xi_{i-1} \rangle + 2b_1 \langle \xi_i \rangle \\ &\quad + \frac{1}{N^{1/2}} [m_3 \langle \xi_{i-1}^2 \rangle + m_6 \langle \xi_i \xi_{i+1} \rangle + m_3 \langle \xi_{i+1} \xi_{i-1} \rangle + m_2 \langle \xi_{i-1} \xi_{i+2} \rangle + m_7 \langle \xi_i^2 \rangle] \\ &\quad - \frac{m_8}{N^{1/2}} + \frac{1}{N^{1/2}} [-2r \langle \xi_{i-1} \xi_i^2 \xi_{i+1} \rangle + 2r \langle \xi_{i-1}^2 \xi_i^2 \rangle + r \langle \xi_i^2 \xi_{i-1} \xi_{i+2} \rangle - r \langle \xi_i^3 \xi_{i-1} \rangle], \end{aligned}$$

and

$$\begin{aligned} \frac{d}{dt} \langle \xi_i^2 \xi_{i+1} \rangle &= 3m_0 \langle \xi_i^2 \xi_{i+1} \rangle + 2m_3 \langle \xi_i \xi_{i-1} \xi_{i+1} \rangle + 2m_1 \langle \xi_i \xi_{i+1}^2 \rangle + 2m_2 \langle \xi_i \xi_{i+1} \xi_{i+2} \rangle \\ &+ m_3 \langle \xi_i^3 \rangle + m_1 \langle \xi_i^2 \xi_{i+2} \rangle + m_2 \langle \xi_i^2 \xi_{i-1} \rangle + b_0 \langle \xi_{i+1} \rangle + 2b_1 \langle \xi_i \rangle \\ &+ \frac{1}{N^{1/2}} [m_3 \langle \xi_{i+1}^2 \rangle + m_6 \langle \xi_i \xi_{i+1} \rangle + m_3 \langle \xi_{i+1} \xi_{i+3} \rangle + m_2 \langle \xi_{i+1} \xi_{i+2} \rangle + m_7 \langle \xi_i^2 \rangle] \\ &+ \frac{m_8}{N^{1/2}} + \frac{1}{N^{1/2}} [-2r \langle \xi_{i+1}^2 \xi_i^2 \rangle + 2r \langle \xi_{i-1} \xi_{i+1} \xi_i^2 \rangle + r \langle \xi_i^3 \xi_{i+1} \rangle - r \langle \xi_i^2 \xi_{i+1} \xi_{i+2} \rangle], \end{aligned}$$

for adjacent populations with respect to the assumed ordering. For next-to-neighbors correlation one gets:

$$\begin{aligned} \frac{d}{dt} \langle \xi_i^2 \xi_{i+2} \rangle &= 3m_0 \langle \xi_i^2 \xi_{i+2} \rangle + 2m_3 \langle \xi_i \xi_{i-1} \xi_{i+2} \rangle + 2m_1 \langle \xi_i \xi_{i+1} \xi_{i+2} \rangle + 2m_2 \langle \xi_i \xi_{i+2}^2 \rangle \\ &+ m_3 \langle \xi_i^2 \xi_{i+1} \rangle + m_1 \langle \xi_i^2 \xi_{i-1} \rangle + m_2 \langle \xi_i^3 \rangle + b_0 \langle \xi_{i+2} \rangle + \frac{1}{N^{1/2}} [-r \langle \xi_i^2 \xi_{i+1} \xi_{i+2} \rangle \\ &+ r \langle \xi_{i-1} \xi_{i+2} \xi_i^2 \rangle] + \frac{1}{N^{1/2}} [m_2 \langle \xi_{i+2}^2 \rangle + m_4 \langle \xi_i \xi_{i+2} \rangle + m_3 \langle \xi_{i-1} \xi_{i+2} \rangle \\ &+ m_3 \langle \xi_{i+1} \xi_{i+2} \rangle]. \end{aligned}$$

Finally, for correlations that involve three distinct species, we find:

$$\begin{aligned} \frac{d}{dt} \langle \xi_i \xi_{i+1} \xi_{i-1} \rangle &= 3m_0 \langle \xi_i \xi_{i+1} \xi_{i-1} \rangle + m_3 \langle \xi_{i+1} \xi_{i-1}^2 \rangle + m_1 \langle \xi_{i+1}^2 \xi_{i-1} \rangle + m_2 \langle \xi_{i+2} \xi_{i+1} \xi_{i-1} \rangle \\ &+ m_3 \langle \xi_i^2 \xi_{i-1} \rangle + m_1 \langle \xi_i \xi_{i+2} \xi_{i-1} \rangle + m_3 \langle \xi_i \xi_{i+1} \xi_{i+2} \rangle + m_2 \langle \xi_i \xi_{i-1}^2 \rangle \\ &+ m_1 \langle \xi_i^2 \xi_{i+1} \rangle + m_2 \langle \xi_i \xi_{i+1}^2 \rangle + b_1 \langle \xi_{i-1} \rangle + b_1 \langle \xi_{i+1} \rangle + \frac{1}{N^{1/2}} [m_9 \langle \xi_{i-1} \xi_i \rangle \\ &+ m_9 \langle \xi_{i+1} \xi_i \rangle + m_7 \langle \xi_{i-1} \xi_{i+1} \rangle] + \frac{1}{N^{1/2}} [-r \langle \xi_{i+1}^2 \xi_i \xi_{i-1} \rangle + r \langle \xi_{i+1} \xi_i \xi_{i-1}^2 \rangle]. \end{aligned}$$

Clearly, the fourth moments enter the equation for the third ones. To close the system and so enable for quantitative predictions, we can estimate the zero-th order contribution to the fourth moments by recalling the Gaussian solution as obtained in Section 2.1.5 and neglecting the  $1/\sqrt{N}$  terms. In formula:

$$\begin{aligned} \langle \xi_i^4 \rangle &= 3(\langle \xi_i^2 \rangle)^2 \\ \langle \xi_i^3 \xi_j \rangle &= 3\langle \xi_i^2 \rangle \langle \xi_i \xi_j \rangle \\ \langle \xi_i^2 \xi_j^2 \rangle &= \langle \xi_i^2 \rangle \langle \xi_j^2 \rangle + 2(\langle \xi_i \xi_j \rangle)^2 \\ \langle \xi_i^2 \xi_j \xi_k \rangle &= \langle \xi_i^2 \rangle \langle \xi_j \xi_k \rangle + 2\langle \xi_i \xi_j \rangle \langle \xi_i \xi_k \rangle. \end{aligned}$$

The above quantities can be analytically estimated at equilibrium and expressed as a function of respectively  $\Gamma_1$ ,  $\Gamma_2$ ,  $\Gamma_3$ , as derived in section 2.1.5.

### 2.1.8 The asymptotic evolution of the third moments

Let us now write down the system of differential equations that controls the dynamics of the five independent families of moments of order three<sup>2</sup>. Such a system takes the form

$$\dot{\mathbf{X}} = V\mathbf{X} + S, \quad (2.14)$$

<sup>2</sup>The system reduces to five families of independent moments as follows a the inherent symmetry of the problem to which we alluded in the preceding discussion.

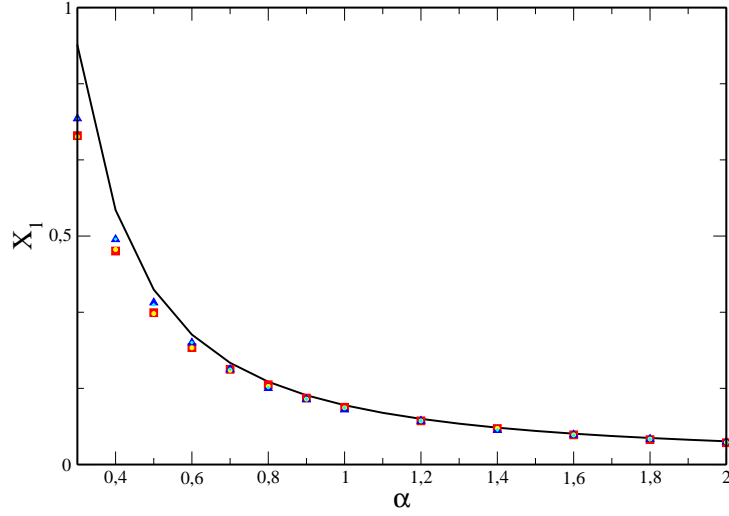


Figure 2.4: Plots of  $X_1$  (see Eq. (2.15)) as functions of the parameter  $\alpha$ , for a system with  $\beta = \alpha$ ,  $N = 200$  and  $r = 10$ . The solid black lines represent the numerical solution of the system (2.14), while the symbols refer to the stochastic simulations (each of the four symbols is associated to a different species).

where  $\mathbf{X}$  is

$$\mathbf{X} = [\langle \xi_i^3 \rangle \quad \langle \xi_i^2 \xi_{i+1} \rangle \quad \langle \xi_i^2 \xi_{i-1} \rangle \quad \langle \xi_i^2 \xi_{i+2} \rangle \quad \langle \xi_i \xi_{i+1} \xi_{i-1} \rangle], \quad (2.15)$$

and the matrix of coefficients  $V$  reads:

$$V = \begin{pmatrix} 3m_0 & 3m_1 & 3m_3 & 3m_2 & 0 \\ m_3 & 3m_0 & 2m_1 + m_2 & m_1 & 2m_3 + 2m_2 \\ m_1 & 2m_3 + m_2 & 3m_0 & m_3 & 2m_1 + 2m_2 \\ m_2 & m_3 & m_1 & 3m_0 + 2m_2 & 2m_3 + 2m_1 \\ 0 & m_2 + m_1 & m_3 + m_2 & m_3 + m_1 & 3m_0 + m_1 + m_3 + m_2 \end{pmatrix}.$$

Finally the vector  $S$  is:

$$S = 1/\sqrt{N} [s_1 \quad s_2 \quad s_3 \quad s_4 \quad s_5],$$

where:

$$\begin{aligned} s_1 &= 3m_4\Gamma_1 + 6m_3\Gamma_2 + 3m_2\Gamma_3 \\ s_2 &= m_3\Gamma_1 + m_7\Gamma_1 + m_3\Gamma_3 + m_2\Gamma_2 + m_6\Gamma_2 + m_8 \\ &\quad + [-2r(\Gamma_1)^2 + 2r\Gamma_3\Gamma_1 - 2r\Gamma_3\Gamma_2 + 2r\Gamma_1\Gamma_2] \\ s_3 &= m_3\Gamma_1 + m_7\Gamma_1 + m_3\Gamma_3 + m_2\Gamma_2 + m_6\Gamma_2 - m_8 \\ &\quad + [2r(\Gamma_1)^2 - 2r\Gamma_1\Gamma_3 + 2r\Gamma_3\Gamma_2 - 2r\Gamma_1\Gamma_2] \\ s_4 &= m_4\Gamma_3 + 2m_3\Gamma_2 + m_2\Gamma_1 \\ s_5 &= m_7\Gamma_3 + 2m_9\Gamma_2. \end{aligned}$$

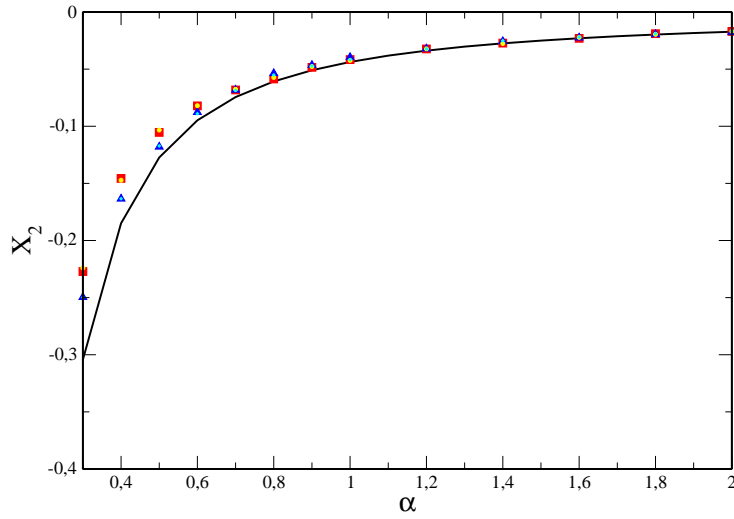


Figure 2.5: Plots of  $X_2$  as functions of the parameter  $\alpha$ . For the parameters' setting and the explanation of the symbols see caption of Fig. 2.4.

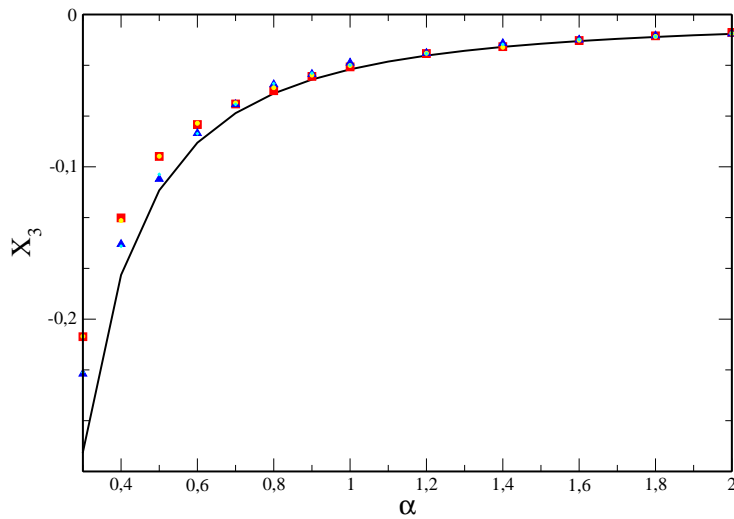


Figure 2.6: Plots of  $X_3$  as functions of the parameter  $\alpha$ . For the parameters' setting and the explanation of the symbols see caption of Fig. 2.4.



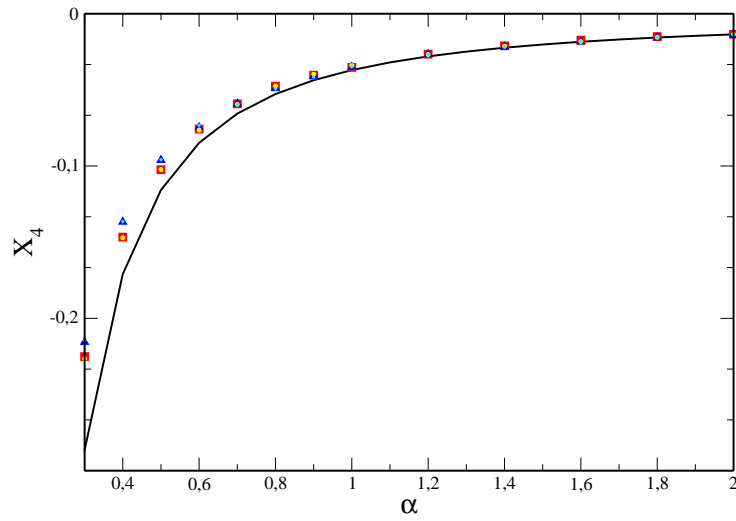


Figure 2.7: Plots of  $X_4$  as functions of the parameter  $\alpha$ . For the parameters' setting and the explanation of the symbols see caption of Fig. 2.4.

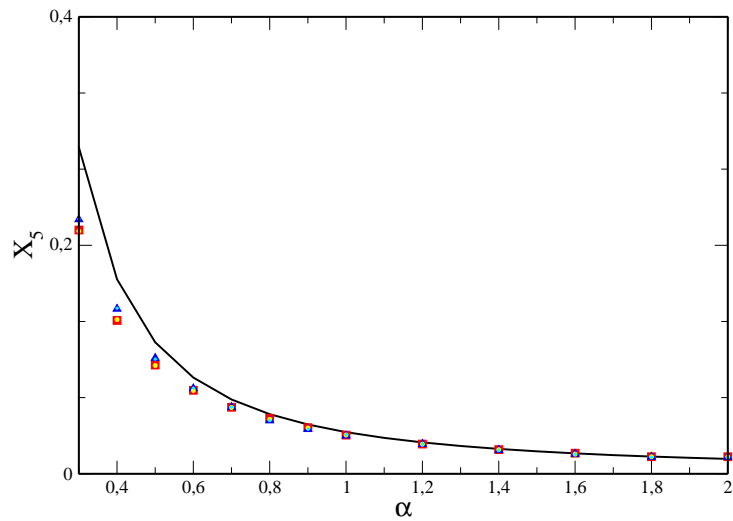


Figure 2.8: Plots of  $X_5$  as functions of the parameter  $\alpha$ . For the parameters' setting and the explanation of the symbols see caption of Fig. 2.4.

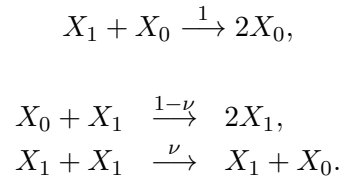
We now turn to numerical simulations to validate the correctness of the theory. Stochastic simulations are performed for small systems ( $N = 200$ ) and the time evolution of the third moments is monitored for each of the considered species and by varying the parameter  $\alpha$ , while keeping  $r$  unchanged. Results are displayed in Figs. 2.4–2.8, where the simulations outcome (symbols) are compared to the theory predictions. The agreement has to be considered satisfactory, a conclusion which a posteriori validates the theory assumptions and in particular confirms the predictive ability of the van Kampen expansion beyond the Gaussian approximation [37, 29]. We notice that the overlap between simulations and theory is less accurate for small values of  $\alpha$ . This discrepancy may be due to the related to the fact that small values of  $\alpha$  means reactions less probable and thus the dynamics is slow. Increasing the simulation time or averaging over more realizations would help increasing the match.

For this specific case we have reached a good agreement between theory and numerical simulations. Moreover, the complexity of the model makes it hard to extend the analysis beyond the order of approximation here concluded. To eventually checks the adequacy of the generalized van Kampen expansion, testing its convergence at a different order, we shall consider in the next section a single one dimensional version of the Voter model in the presence of an absorbing boundary.

## 2.2 Voter model

In this section we start by the stochastic version of the Voter model introduced in [2] and we will analytically demonstrate that by extending the van Kampen expansion to include higher orders corrections, beyond the classical approximation, allows us to accurately reproduce the observed distribution of fluctuations *at any time*. Non Gaussian traits reflecting the presence of the absorbing barrier are nicely captured by the method, which proves therefore accurate *also close to the boundary*. Even more interesting, the van Kampen solution is shown to converge at late times to the distribution calculated in [2], this latter being hence explained within a sound and universal descriptive picture.

Let us start by introducing the stochastic discrete voter model. As in the spirit of [2], we consider a system made of  $N$  elements in mutual interactions, possibly organized in different species. Label with  $X_1$  the elements of a specific species and with  $X_0$  all the other entities. The following chemical equations are proposed to rule the microscopic dynamics:



The master equation which stems from the above system reads:

$$\begin{aligned} \frac{d}{dt}P_n(t) &= (\epsilon_n^- - 1)[T(n+1|n)P_n(t)] \\ &\quad + (\epsilon_n^+ - 1)[T(n-1|n)P_n(t)], \end{aligned} \quad (2.16)$$

where  $P_n(t)$  is the probability of photographing the system at time  $t$  in a configuration with  $n$  individuals belonging to the population of  $X_1$  and  $\epsilon_n^\pm$  are the step operators [29].

The transition rates are given by:

$$\begin{aligned} T(n+1|n) &= (1-\nu) \frac{(N-n)}{N} \frac{n}{N} \\ T(n-1|n) &= \frac{n}{N} \frac{N-n}{N} + \nu \frac{n}{N} \frac{n}{N}, \end{aligned}$$

where the initial states are the right entries and the final states the left ones. As follows the above,  $n=0$  is an absorbing state while  $n=N$  corresponds to a reflecting barrier. As usual, the van Kampen approach requires imposing:

$$\frac{n}{N} = \phi(t) + \frac{\xi}{\sqrt{N}}, \quad (2.17)$$

where  $1/\sqrt{N}$  plays the role of a small parameter and paves the way to the perturbative expansion hereafter discussed. By inserting the working ansatz (2.17) into the master equation (2.16), and hierarchically organizing the resulting terms with respect to their  $N$ -dependence, one obtains at the first order the mean-field deterministic equation for the continuum concentration  $\phi(\tau)$  ( $\tau$  being the rescaled time  $t/N$ ), namely  $d\phi/d\tau = -\nu\phi$ , whose solution reads  $\phi(\tau) = \phi_0 \exp(-\nu\tau)$ . Higher order contributions results in a generalized Fokker-Planck equation for the new probability  $\Pi(\xi, \tau) = P(\phi(\tau) + \xi/\sqrt{N}, \tau)$ . By truncating the expansion at the second order yields the standard Fokker-Planck equation, which predicts Gaussian fluctuations. Allowing instead for higher order corrections, generates a cascade of terms whose relative weights are controlled by the finite size  $N$ . After a lengthy algebraic derivation one ends up with:

$$\begin{aligned} \frac{\partial \Pi}{\partial \tau} &= \sum_{k=1}^{\infty} \frac{1}{(k+1)!} \frac{1}{N^{(k-1)/2}} \frac{\partial^{k+1}}{\partial \xi^{k+1}} \left[ f(\phi, k+1) \Pi \right] \\ &+ \sum_{k=1}^{\infty} \frac{1}{k!} \frac{1}{N^{(k-1)/2}} \frac{\partial^k}{\partial \xi^k} \left[ g(\phi, \xi, k) \Pi \right] \\ &+ \sum_{k=3}^{\infty} \frac{1}{(k-1)!} \frac{1}{N^{(k-1)/2}} \frac{\partial^{k-1}}{\partial \xi^{k-1}} \left[ q(\xi^2, k-1) \Pi \right], \end{aligned} \quad (2.18)$$

where:

$$\begin{aligned} f(\phi, k) &= \begin{cases} 2\phi - 2\phi^2 - \nu\phi + 2\nu\phi^2 & \text{for } k \text{ even} \\ \nu\phi & \text{for } k \text{ odd} \end{cases} \\ g(\xi, \phi, k) &= \begin{cases} 2\xi - 4\phi\xi + 4\nu\phi\xi - \nu\xi & \text{for } k \text{ even} \\ \nu\xi & \text{for } k \text{ odd} \end{cases} \\ q(\xi, k^2) &= \begin{cases} 2\xi^2(\nu-1) & \text{for } k \text{ even} \\ 0 & \text{for } k \text{ odd.} \end{cases} \end{aligned}$$

Formally, the positiveness of the probability  $\Pi(\cdot)$  is not guaranteed a priori under the generalized Fokker-Planck evolution, an observation that was made rigorous in [41, 42]. However, with reference to specific case studies [38], it was shown that unphysical negative values are just occasionally attained by  $\Pi(\xi, \tau)$ , and punctually localized in the tails of the distribution. The phenomenon fades off when including a sufficiently large number of terms in the development. The adequacy of the prediction can be a posteriori evaluated via a direct comparison with the numerical experiments.

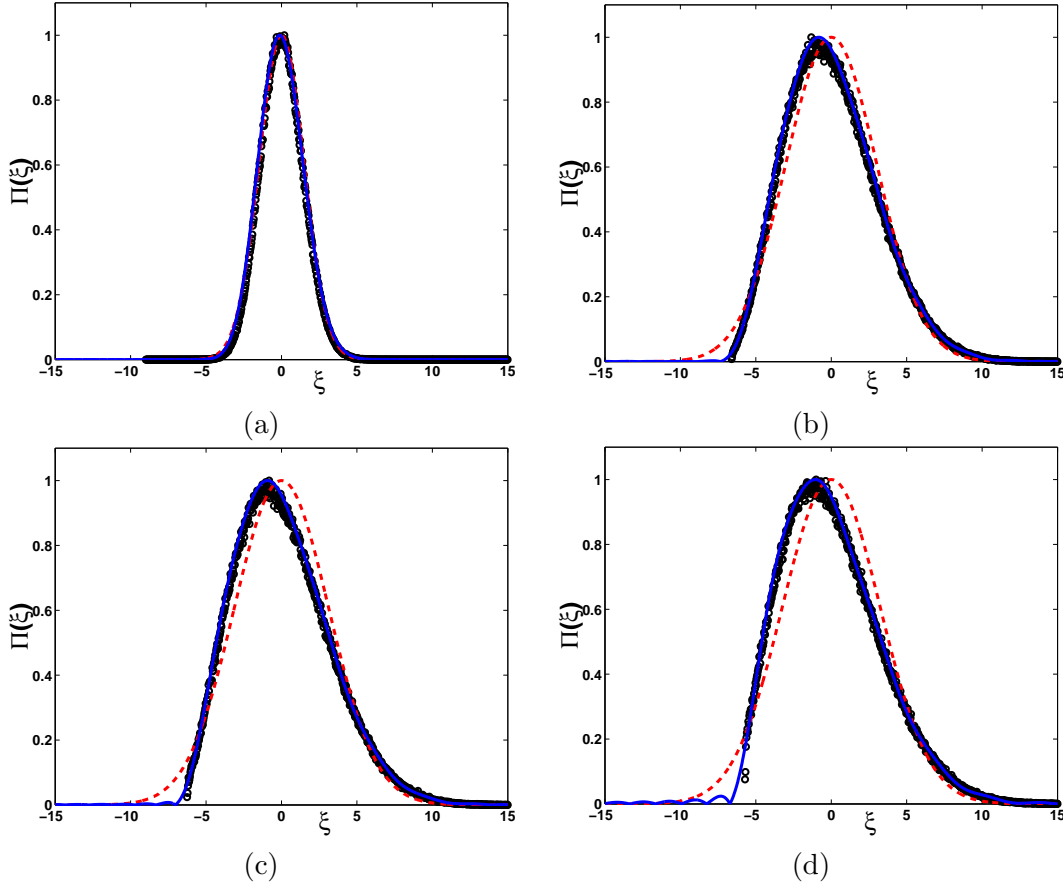


Figure 2.9: The distribution of fluctuations at distinct rescaled times  $\tau$ . The snapshots refer to: (a)  $\tau = 5$ , (b)  $\tau = 36$ , (c)  $\tau = 41$  and (d)  $\tau = 50$ . The symbols stand for direct stochastic simulations. The solid lines represent the theoretical predictions as obtained within the generalized Fokker Planck scenario. We have in particular truncated the sums in the Fokker-Planck (2.18) to  $k = 3$  ( $1/N^{3/2}$  corrections) and included 200 moments in the final estimates of the generating function. The dashed lines refer to the Gaussian solutions obtained working within the van Kampen expansion at the, conventional, next to leading approximation ( $1/N^{1/2}$  terms). Here  $\nu = 0.01$  and the distributions are normalized so to have the maximum equal to one.

To progress with the calculation, we set off to estimate the moments of the sought distribution  $\Pi(\xi, \tau)$ . Let us recall that the moment of order  $h$  is defined as

$$\langle \xi^h \rangle = \int_{-\infty}^{\infty} \Pi(\xi) \xi^h d\xi.$$

Multiply both sides of the generalized Fokker-Planck equation by the factor  $\xi^h$  and inte-

grate over  $\mathbb{R}$  in  $d\xi$ . A straightforward manipulation yields to:

$$\begin{aligned}
\frac{d}{d\tau}\langle\xi^h\rangle = & \\
& + \sum_{k=1}^{h-2} \frac{1}{(k+1)!} \frac{f(\phi, k+1)}{N^{(k-1)/2}} \frac{h!(-1)^{k+1}}{(h-(k+1))!} \langle\xi^{h-(k+1)}\rangle \\
& + \sum_{k=1}^{h-1} \frac{1}{k!} \frac{g(\phi, \xi, k)}{N^{(k-1)/2}} \frac{h!(-1)^k}{(h-k)!} \langle\xi^{h-k+1}\rangle \\
& + \sum_{k=3}^{h+2} \frac{1}{(k-1)!} \frac{q(\xi^2, k-1)}{N^{(k-1)/2}} \frac{h!(-1)^{k-1}}{(h-(k-1))!} \langle\xi^{h-(k-1)+2}\rangle
\end{aligned} \tag{2.19}$$

where use has been made of the supposed regularity of the distribution  $\Pi(\xi, \tau)$  to drop out the boundary terms resulting from integrating by parts <sup>3</sup>.

We therefore dispose of a closed system of first order differential equations for the moments of the distribution  $\Pi(\xi, \tau)$ . We can integrate it numerically and so estimate the quantities  $\langle\xi^h\rangle$ , for all  $h$ , at any time  $\tau$ . The knowledge of the moments enables us to immediately reconstruct the characteristic function, and so recover, upon Fourier transform inversion, the distribution  $\Pi(\xi, \tau)$ . The predicted profiles are displayed in Fig. 2.9 (solid line) for different times. A comparison is drawn with the outcome of direct stochastic simulations based on the exact Gillespie algorithm [28] (symbols), returning excellent agreement. The distribution of fluctuations displays clear non-Gaussian traits. It gets in fact more and more skewed as time progresses, reflecting the non trivial interplay with the absorbing boundary. Surprisingly, and at odds with what customarily believed, the van Kampen ansatz proves accurate well beyond the Gaussian approximation that is often invoked to justify its intrinsic validity. As a corollary, it seems tempting to argue that the transformation (2.17) from discrete to continuum variables is an *exact one*, and not just an approximation that presumably descends from the central limit theorem, as occasionally speculated.

It is also very instructive to analyze the asymptotic fate of the distribution of fluctuations, as predicted within the realm of the van Kampen theory. Based on intuition, we expect that when time goes to infinity, the distribution  $\Pi(\xi, \tau)$  converges to a Dirac delta centered in zero. Indeed, plugging into the moments' equations (2.18), the asymptotic mean-field solution  $\phi = 0$ , and looking for stationary solutions of the obtained system (i.e. setting the derivatives to zero), one readily gets  $\langle\xi^h\rangle = 0 \forall h$ , the moments of a delta function. However, for times large enough that  $\phi \simeq 0$ , but before the system has relaxed to its stationary state, the generalized Fokker-Planck equation (2.18) reads:

$$\frac{\partial\Pi}{\partial\tau} = \nu \frac{\partial}{\partial\xi} (\xi\Pi) + \frac{2-\nu}{2\sqrt{N}} \frac{\partial^2}{\partial\xi^2} (\xi\Pi), \tag{2.20}$$

where we have only retained the term in  $1/\sqrt{N}$  dropping higher orders corrections. Per-

<sup>3</sup>In the definition of the moments we integrate from  $-\infty$  to  $\infty$ . In principle, the maximum extent of the allowed (negative) fluctuations is limited by the presence of the absorbing boundary. Strictly, the lower extreme of the above integral should read  $-\sqrt{(N)}\phi(\tau)$ . Assuming however that the distribution of fluctuations  $\Pi(\xi, \tau)$  is exactly zero at  $\xi = -\sqrt{(N)}\phi(\tau)$ , one recovers the same equations for the moments as those obtained by formally extending the domain of integration to  $-\infty$ .

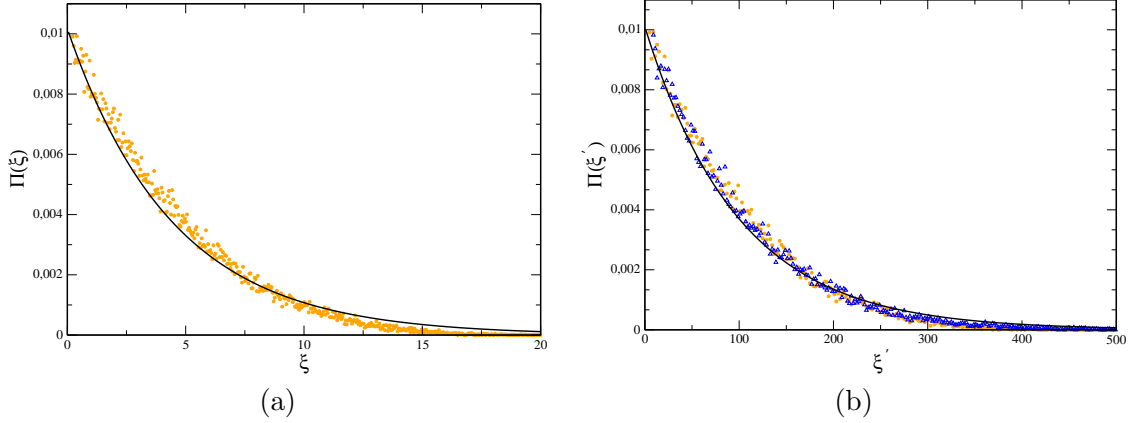


Figure 2.10: The distribution of fluctuations at large times. Right panel: the distribution  $\Pi(\xi', \tau)$  is plotted as function of the rescaled  $\xi'$ . Symbols refer to numerical simulations relative to distinct  $N$ . In particular,  $N = 500$  (circles) and  $N = 1000$  (triangles). The solid line stands for the (normalized) solution (2.23). Here  $\nu = 0.01$  and the distributions are normalized to unit. Left panel: the distribution  $\Pi(\xi, \tau)$  is plotted versus  $\xi$  at  $\tau = 388$ . Symbols refer to the simulations, while the solid line stands for the (normalized) solution (2.23) after the change of variable  $\xi' \rightarrow \xi\sqrt{N}$  is performed.

form now the scaling  $\xi \rightarrow \xi'/\sqrt{N}$ . The equation (2.20) can be cast in the form:

$$\frac{\partial \Pi}{\partial \tau} = \nu \frac{\partial}{\partial \xi'} (\xi' \Pi) + \frac{2 - \nu}{2} \frac{\partial^2}{\partial \xi'^2} (\xi' \Pi). \quad (2.21)$$

The large time distribution  $\Pi(\xi', \tau)$  is therefore insensitive to the system size  $N$  and bears consequently universal traits. Equation (2.21) can be solved analytically (see also [2]) to give:

$$\begin{aligned} \Pi(\xi', \tau) &= \frac{2\nu}{2 - \nu} \frac{1}{1 - e^{-\nu\tau}} \exp \left[ \frac{2\nu(\xi' + \xi'_0 e^{-\nu\tau})}{(2 - \nu)(1 - e^{-\nu\tau})} \right] \\ &\times \left( \frac{\xi'}{\xi'_0} e^{\nu\tau} \right)^{-\frac{1}{2}} I_1 \left( \frac{4\nu\sqrt{\xi'_0 \xi'} e^{\nu\tau}}{(2 - \nu)(e^{\nu\tau} - 1)} \right), \end{aligned} \quad (2.22)$$

where  $I_1(\cdot)$  is the modified Bessel function of the first kind. For large  $\tau$ , recalling that  $I_1(x) \simeq x/2$  when  $x$  is small, one can approximate Eq. (2.22) as:

$$\Pi(\xi', \tau) \propto \xi'_0 \left( \frac{2\nu}{2 - \nu} \right)^2 \exp \left( -\frac{2\nu}{2 - \nu} \xi' \right) \exp(-\nu\tau), \quad (2.23)$$

Operating with the rescaled variable  $\xi'$ , which, it is worth emphasizing, emerges naturally within the van Kampen expansion, when the large time limit is being considered, it is equivalent to inserting into the governing master equation the modified ansatz  $n = N\phi + \xi'$ . This latter corresponds to the strategy adopted in [2] for the specific choice  $\alpha = 0$ . In other words, and interestingly enough, the expected fluctuations  $\xi'$  are comparable to the discrete population size  $n$ , when the absorbing boundary is being approached. We have therefore recovered exactly the same solution as obtained in [2], while working within the

generalized, but conventional, van Kampen approach. The adequacy of (2.23) is challenged in 2.10 versus numerical simulation returning a perfect quantitative agreement. Notice that different distribution profiles recorded at distinct values  $N$ , nicely superpose when the rescaled fluctuations  $\xi'$  is employed.

As a side remark, we stress that the same conclusion can be drawn working in the Fourier space and operating under analogous approximations. Retaining only  $1/\sqrt{N}$  corrections in (2.19), assuming  $\phi \rightarrow 0$  and performing the scaling  $\langle \eta^h \rangle = \langle \xi^h \rangle N^{\frac{h}{2}}$ <sup>4</sup>, one immediately obtains the following  $N$  independent differential equations for the moments evolution:

$$\frac{\partial}{\partial \tau} \langle \eta^h \rangle = -\nu h \langle \eta^h \rangle + \frac{h(h-1)}{2} (2-\nu) \langle \eta^{h-1} \rangle. \quad (2.24)$$

Equations (2.24), here obtained within the extended van Kampen scenario, could be also derived via the alternative, supposedly distinct, approach discussed in [2]. Equations (2.24) can be in fact straightforwardly deduced from Eq. (2.21) (see also Eq. (8) in [2]) following the same strategy for the evaluation of the moments as outlined above.

In conclusion, the van Kampen approximation works effectively for *all times*, well beyond the Gaussian approximation and in a regime where the presence of the absorbing boundary is definitely important. The method returns in fact the correct asymptotic solution (a delta function centered in the origin), but also converges to the large time solution calculated in [2], which is therefore contextualized within a general descriptive picture. At moderate times, after the Gaussian approximation has broken down, direct comparisons with the numerical experiments, as reported in this section, testify on the excellent predictive ability of the van Kampen theory. This is an important observation, that will certainly motivate using the van Kampen machinery beyond the limited domains of applications for which it was originally conceived, and/or later referred to [2]. Future investigations will be targeted to extending the current analysis to cases where the absorbing boundary competes with a non trivial stable fixed point, as well as models for which the notion of space is explicitly accounted for [3, 24].

Up to now, we have shown two different models, for which we have demonstrated a posteriori the validity of the van Kampen expansion beyond the Gaussian approximation. In the next section we compare the generalized van Kampen expansion and the WKB approximation. We focus in particular on extinction dynamics, i.e. the transition from the vicinity of a non-trivial fixed point of the deterministic dynamics to a trivial fixed point. In the linear-noise approximation the phenomenon of extinction it is so rare to be negligible. When the extinction phenomenon is not longer negligible, higher corrections prove essential. To draw the comparison between WKB and the van Kampen approach and quantify their predictive ability, we will perform simulations and calculations for a stochastic version of the logistic equation.

## 2.3 WKB versus generalized van Kampen system size expansion: the stochastic logistic equation

### 2.3.1 Introduction

Here we will focus on extinction dynamics, that is, transitions from the vicinity of a non-trivial fixed point of the deterministic dynamics, to a trivial fixed point where all

---

<sup>4</sup>This is equivalent, in Fourier space, to the transformation  $\xi \rightarrow \xi'/\sqrt{N}$  of the original fluctuation  $\xi$ .

the individuals have become extinct. If the parameters of the models are chosen so that the two fixed points are not too close, then extinctions will be rare and the state of the system will continue to fluctuate about the non-trivial fixed point for a long period of time. In this situation the van Kampen system-size expansion [29] has proved to be a powerful tool. Essentially the method gives the deterministic equations to leading order in an expansion in (inverse) system-size, and linear stochastic corrections to this result at next-to-leading order. This linear approximation, sometimes called the linear-noise approximation, corresponds to Gaussian fluctuations, and is an excellent approximation if extinctions are so rare as to be negligible.

In principle, extinction events can be incorporated into the system-size expansion by going beyond the Gaussian approximation, and including non-linear terms in the stochastic differential equation giving the approximate stochastic dynamics. This should give rise to a tail on one side of the probability distribution function which will characterise the extinction process. These higher-order calculations have only been carried out recently, and then only by a few authors [37, 7, 43]. In addition if there are only a few individuals in the system, extinction effects will be very important, and one may have to go to quite high-order in the expansion to get an accurate form for what will be a very non-Gaussian distribution.

By contrast, the standard technique to look at rare events from one metastable state to another is to use a WKB-like approximation [44]. This goes under many names: large deviation theory [45], the instanton method, Freidlin-Wentzell theory [46], amongst others. It consists of postulating that the dominant contribution to the probability distribution is exponentially small in  $N$ , the system-size, that is, is of the order of  $e^{-NS}$ . Here  $S$  is a function of variables describing the system in the deterministic limit which turns out to satisfy a Hamilton-Jacobi equation. The corresponding Hamiltonian, known as the FreidlinWentzell Hamiltonian, can be used to describe the extinction trajectories, even though they are stochastic in nature.

The aim of this section is to explore the connection between the van Kampen system-size expansion at higher-order and the WKB method. They have a very different basis, and to the best of our knowledge, their predictive power in regimes where extinctions are important have not been compared. We will carry out the explicit assessment of their range of validity and comparison with numerical simulations on a specific stochastic system with one degree of freedom to minimise numerical errors. In the case of the WKB method, most of the steps can be performed analytically, which also makes the interpretation of the results more straightforward. A simple dynamical system with a stable non-trivial fixed point and an unstable trivial fixed point is the logistic equation  $\dot{\phi} = r\phi[1 - (\phi/k)]$ , and the stochastic model we will choose to study will have this equation as its deterministic limit.

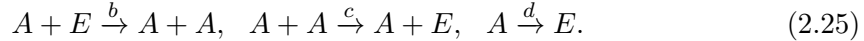
### 2.3.2 Model

In this section we will introduce the model as an individual based model, and write down the master equation, which governs its stochastic dynamics. The two techniques we are comparing can be viewed as different approximations for these dynamics. We will describe them in this section and apply them to the model in the following section.

As discussed in the Introduction probably the simplest model which contains the features which we wish to explore is a system containing identical individuals denoted by  $A$ . We assume that there are  $n$  such individuals, and since the size of the system is taken



to be characterised by an integer  $N$ , we suppose that there are  $(N - n)$  nulls denoted by  $E$ . These are vacancies, which in a spatial version of the model would denote spaces which could potentially be colonised by a individual. If the only processes are (asexual) birth, competition and death, then we may define the well-mixed model through the reactions



The last equation, for instance, indicates that an individual of type  $A$  dies at a rate  $d$  to give a vacancy,  $E$ . Simple combinatorics then gives the rate at which the number of individuals increases from  $n$  to  $(n + 1)$  to be given by  $b(n/N)(N - n)/N$ . A more accurate statement of these rates would replace one of the  $N$  factors in the denominator by  $(N - 1)$ , but since we wish to keep the analysis as simple as possible we will not do this. If we scale the time by a factor of  $N$ , then the transition rate from state  $n$  to state  $(n + 1)$  may be written as:

$$T(n + 1|n) = bn \left(1 - \frac{n}{N}\right). \quad (2.26)$$

Similarly, the transition rate from state  $n$  to state  $(n - 1)$  is

$$T(n - 1|n) = n \left(d + c\frac{n}{N}\right), \quad (2.27)$$

where once again factors of  $N(N - 1)$  and  $n(n - 1)$  have been replaced by  $N^2$  and  $n^2$  respectively. Since the transition rates  $T(n + 1|n)$  and  $T(n - 1|n)$  define the model, this choice simply corresponds to a slight variant of the standard model, which can be justified on grounds of simplicity.

The master equation is an equation for the rate of change with time of the probability of finding  $n$  individuals in the system at time  $t$ , denoted by  $P(n, t)$ . Since this is simply the rate of transitions into the state  $n$  minus the rate of transitions out of state  $n$ , it reads:

$$\begin{aligned} \frac{dP(n, t)}{dt} &= T(n|n + 1)P(n + 1, t) \\ &+ T(n|n - 1)P(n - 1, t) \\ &- T(n - 1|n)P(n, t) - T(n + 1|n)P(n, t). \end{aligned} \quad (2.28)$$

This equation cannot be solved exactly, so we need to resort to either numerical methods or approximation techniques. It is frequently simpler to simulate [28] the processes given in Eq. (2.25), rather than numerically solve the master equation, and the results we give in Section III to assess the accuracy of the approximation techniques are found in this way. We now briefly outline the two approximation methods that we use in this section.

### 2.3.3 The van Kampen system size expansion

The first, the van Kampen system-size expansion has as the leading-order approximation the deterministic differential equation found by taking the limit  $N \rightarrow \infty$ . In the case of the model just described, this is the logistic equation given in the Introduction. However this equation emerges as the leading order approximation to the model defined by Eqs. (2.26) and (2.27), and does not have to be postulated independently. The next-to-leading order gives a linear stochastic differential equation, which describes Gaussian fluctuations about

the deterministic equation. If the intention is to simply study the stochastic dynamics of the model well away from the boundaries, it is usually sufficient to work to this order. However it is possible to go higher orders to obtain non-Gaussian corrections to the probability distribution function (pdf). One of the main aims of this section is to argue that these higher-order corrections enable reliable estimates for the pdf to be obtained very close to the boundaries.

To apply the van Kampen expansion we first write down the master equation (2.28) in terms of step-operators  $\mathcal{E}^\pm$  defined by  $\mathcal{E}^\pm f(n) = f(n \pm 1)$ , where  $f$  is an arbitrary function:

$$\begin{aligned} \frac{dP(n, t)}{dt} &= (\mathcal{E}^+ - 1) [T(n-1|n)P(n, t)] \\ &+ (\mathcal{E}^- - 1) [T(n+1|n)P(n, t)]. \end{aligned} \quad (2.29)$$

The ansatz which forms the basis of the method is to write:

$$\frac{n}{N} = \phi(t) + \frac{\xi}{\sqrt{N}}. \quad (2.30)$$

Here  $\phi(t)$  is the solution of the deterministic equation valid in the limit  $N \rightarrow \infty$  and  $\xi$  is the (continuous) stochastic variable which gives the deviation of the stochastic trajectory from this deterministic value. The pdf when written in terms of  $\xi$  is denoted as  $\Pi(\xi, t)$ , thus  $P(n, t) = \Pi(\xi, t)$ . Let us quickly reviewed the main step of the calculation already discussed in the previous section. After the change of variables (2.30), the left-hand side of the master equation (2.28) becomes:

$$\frac{dP}{dt} = \frac{\partial \Pi}{\partial t} - \sqrt{N} \frac{\partial \Pi}{\partial \xi} \frac{d\phi}{dt}. \quad (2.31)$$

The right-hand side of the master equation in the form (2.29) can also be written in terms of  $\phi$  and  $\xi$  by (i) eliminating  $n$  in the transition rates (2.26) and (2.27) using Eq. (2.30), and (ii) noting that the step-operators may be written as

$$\mathcal{E}^\pm = 1 + \sum_{\ell=1}^{\infty} \frac{(\pm 1)^\ell}{\ell!} \frac{1}{N^{\ell/2}} \frac{\partial^\ell}{\partial \xi^\ell}. \quad (2.32)$$

Equating the left-hand and right-hand sides of the master equation, after rescaling time by introducing  $\tau = t/N$ , we can match inverse powers of  $N^{1/2}$  to obtain a set of equations for the dynamics of the process. This is carried out explicitly in 2.3.6. At leading order — obtained by matching the coefficients of  $N^{-1/2}$  — one finds the equation:

$$\frac{d\phi}{d\tau} = r\phi \left( 1 - \frac{\phi}{k} \right), \quad (2.33)$$

where  $r = b - d$  and  $k = (b - d)/(b + c)$ . This is the logistic equation, which could be guessed as the deterministic of the model, even if the identification of the constant  $k$  is not so obvious. This has the solution:

$$\phi(\tau) = \frac{k\phi_0}{[k - \phi_0]e^{-r\tau} + \phi_0}, \quad (2.34)$$

where  $\phi_0 \equiv \phi(0)$ . This has the required feature that, as long as  $\phi_0 \neq 0$ , then  $\phi(\tau) \rightarrow \phi^*$  as  $t \rightarrow \infty$ , where  $\phi^* = k$  is the non-trivial fixed point.

Once the leading-order contributions have been extracted the left-hand side is simply  $\partial\Pi/\partial\tau$ , but the right-hand side contains derivatives of  $\Pi$  with respect to  $\xi$  of all orders. The resulting equation has the general structure:

$$\begin{aligned} \frac{\partial\Pi}{\partial\tau} &= \sum_{k=1}^{\infty} \frac{1}{N^{k/2}} \frac{\partial^k}{\partial\xi^k} [f_k(\xi)\Pi] \\ &+ \sum_{k=0}^{\infty} \frac{1}{N^{k/2}} \frac{\partial^{k+1}}{\partial\xi^{k+1}} \left[ g_k(\phi, \xi)\Pi + h_k(\phi) \frac{\partial\Pi}{\partial\xi} \right], \end{aligned} \quad (2.35)$$

where the explicit form of the functions  $f_k$ ,  $g_k$  and  $h_k$  are given in 2.3.6.

To proceed in the analysis we introduce the moment of order  $q$  of the distribution  $\Pi$ :

$$\langle \xi^q \rangle = \int \xi^q \Pi(\xi) d\xi. \quad (2.36)$$

From the generalized Fokker-Planck equation (2.35) one can obtain a set of ordinary differential equations for the coupled evolution of the first  $q$  moments of the distribution  $\Pi$ . The method is straightforward [29] and consists in multiplying both sides of equation (2.35) by  $\xi^q$  and carrying out an integration over the variable  $\xi$ . One eventually ends up with the following equation for any integer for the moment  $\langle \xi^q \rangle$  ( $q$  being an arbitrary positive integer):

$$\begin{aligned} \frac{d \langle \xi^q \rangle}{d\tau} &= \sum_{k=2}^{q+1} \frac{h_{k-1}(-1)^{k-1} q! \langle \xi^{q-(k-1)+2} \rangle}{(k-1)!(q-(k-1))! N^{(k-1)/2}} \\ &+ \sum_{k=1}^q \frac{g_k(-1)^k q! \langle \xi^{q-k+1} \rangle}{k! N^{(k-1)/2} (q-k)!} \\ &+ \sum_{k=1}^{q-1} \frac{(-1)^{k+1} q! f_{k+1} \langle \xi^{q-(k+1)} \rangle}{(k+1) N^{(k-1)/2} (q-(k+1))!}. \end{aligned} \quad (2.37)$$

The explicit form of  $g_k$ ,  $f_{k+1}$ ,  $h_{k-1}$  can be found in 2.3.6. From (2.37), one can write down a system of ordinary differential equations for the first  $q$  moments of the distribution of fluctuations. Notice, however, that the equation for the  $q$ -th moment depends on higher moments. The obtained system is hence ill posed, and dedicated truncation strategies need to be imposed to eventually recover a closed, self-consistent formulation for the problem at hand. For the case of the model here examined, higher moments contribute with terms that can be safely neglected when operating at a given order of the expansion in powers  $1/\sqrt{N}$ . This entails the possibility of implementing a rather natural truncation scheme, on which we will return in the forthcoming section. Once complemented by a dedicated closure, system (2.37) can be solved numerically and the estimated moments used to reconstruct the sought distribution via Fourier inversion, as we will point out in the following section.

### 2.3.4 The WKB expansion

The second method hereafter outlined, the WKB approximation, involves a different form of scaling. The starting point is the master equation (2.28), but written in terms of

$x = n/N$  and  $N$ , rather than  $n$ . To this end we write  $P(n, t) = P(Nx, t) = \Pi(x, t)$  and  $T_{\pm}(n \pm 1|n) = N\Omega_{\pm}(x)$ , so that:

$$\Omega_+(x) = bx(1-x), \quad \Omega_-(x) = c(d+cx). \quad (2.38)$$

We assume that  $N$  is so large that  $x$  is effectively continuous. Looking for the quasi-stationary solution of the master equation (2.28) in one of the basin of the attraction of the stable fixed point imply dealing with the following problem:

$$\begin{aligned} \Omega_-\left(x + \frac{1}{N}\right)\Pi\left(x + \frac{1}{N}\right) + \Omega_+\left(x - \frac{1}{N}\right)\Pi\left(x - \frac{1}{N}\right) \\ - [\Omega_-(x) + \Omega_+(x)]\Pi(x) = 0. \end{aligned} \quad (2.39)$$

To solve the above time-independent equation for the stationary distribution, we apply the WKB approximation [44, 47] to  $\Pi(x)$  as

$$\Pi(x) = K(x) \exp(-NS(x)) \left[1 + O\left(\frac{1}{N}\right)\right], \quad (2.40)$$

where both of  $S(x)$  and  $K(x)$  are of the order of unity. Substituting (2.40) into (2.39), Taylor expanding with respect to  $N^{-1}$  and collecting together the leading order terms yield:

$$\sum_{r=\pm 1} \Omega_r(x) [\exp(rS'(x)) - 1] = 0, \quad (2.41)$$

where  $S'(x) = dS(x)/dx$ . The above equation can be seen as a stationary Hamilton-Jacobi equation  $H(x, S'(x)) = 0$  for  $S$  with Hamiltonian

$$H(x, p) = \sum_{r=\pm 1} \Omega_r(x) [\exp(rp) - 1], \quad (2.42)$$

where  $p = S'(x)$ . From equation (2.42) one gets the following Hamilton's equations:

$$\begin{cases} \dot{x} = \frac{\partial H}{\partial p} = \sum_{r=\pm 1} \Omega_r(x) \exp(rp) \\ \dot{p} = -\frac{\partial H}{\partial x} = -\sum_{r=\pm 1} [\exp(rp) - 1] \frac{\partial \Omega_r(x)}{\partial x}, \end{cases} \quad (2.43)$$

where the dot denotes differentiation with respect to time.

From the solution of these equations one finds the so called fluctuation trajectories  $x_f$  and the corresponding momenta  $p_f$ . For the zero energy solution  $H = 0$  that we are interested in, the action calculated along a given fluctuation trajectory reads:

$$S_f = \int_{t_0}^t p_f \dot{x}_f dt'. \quad (2.44)$$

From Hamilton's equations (2.43) one readily find the trivial solution  $p_f = 0$ , provided:

$$\dot{x} = \Omega_+(x) - \Omega_-(x). \quad (2.45)$$

This is customarily called the relaxation trajectory and corresponds to the deterministic approximation to the examined model. In fact, multiplying both sides of the original master equation by  $n$  and summing over all possible states one gets:

$$\frac{d \langle n \rangle}{dt} = N\Omega_+(x) - N\Omega_-(x), \quad (2.46)$$

where  $\langle n \rangle = \sum_n nP(n, t)$ . Dividing then by  $N$  and performing the continuum limit, one ends up with equation (2.45), namely the deterministic limit. The relaxation trajectory eventually converges to the stable fixed point. Here, we are rather interested into solutions of the Hamilton's equations (2.43) with  $p_f \neq 0$ , which enables us to explore trajectories not allowed in the mean field limit.

The non trivial solution of equations (2.43) reads:

$$p = \ln \frac{\Omega_-(x)}{\Omega_+(x)}; \quad \dot{x} = \Omega_-(x) - \Omega_+(x). \quad (2.47)$$

The action associated to this path might be calculated (see 2.3.7) to finally give:

$$\begin{aligned} S(x) &= \frac{(d+cx)\ln(d+cx)}{c} + \frac{(b-bx)\ln(b-bx)}{b} \\ &- \frac{(d+cx)}{c} - \frac{(b-bx)}{b} + \frac{(d+c)}{c} \\ &- \frac{(c+d)}{b} \ln \left[ \frac{b(d+c)}{c+b} \right]. \end{aligned} \quad (2.48)$$

We recall that the solution that we are looking for is in the form:

$P(x) = K(x) \exp(-NS(x))$ . One therefore needs to estimate the amplitude factor  $K(x)$ . At the next to leading order expansion of the stationary master equation (2.39) one gets the following partial differential equation for the unknown function  $K(x)$ :

$$\frac{\partial H}{\partial p} \frac{K'}{K} = -\frac{1}{2} p' \frac{\partial^2 H}{\partial p^2} - \frac{\partial^2 H}{\partial p \partial x}. \quad (2.49)$$

For the interesting case  $p \neq 0$ , with  $p(x)$  specified by equation (2.47), one can solve equation (2.49) to obtain:

$$K(x) = \frac{A}{\sqrt{\Omega_+(x)\Omega_-(x)}}, \quad (2.50)$$

where  $A$  is a constant to be determined. For the sake of completeness we hereafter provide the expression for  $K(x)$  which applies to the case  $p = 0$ :

$$K(x) = \frac{B}{\Omega_+(x) - \Omega_-(x)}, \quad (2.51)$$

To find the constant  $A$  in equation (2.50) we expand the quasi-stationary distribution  $\Pi(x)$  in the vicinity of the fixed point  $x = x^*$ , that is the non trivial fixed point:

$$\begin{aligned} \Pi(x) &\approx \frac{A}{\sqrt{\Omega_+(x^*)\Omega_-(x^*)}} \exp \left( -NS(x^*) \right. \\ &\left. - \frac{N}{2} S''(x^*)(x-x^*)^2 \right), \end{aligned} \quad (2.52)$$

where use had been made of the fact that  $S'(x^*) = \ln(\Omega_-(x^*)/\Omega_+(x^*)) = 0$ . A straightforward calculation allows us to write:

$$S''(x^*) = (b+c)^2/b(c+d)^2,$$

and therefore:

$$\Pi(x) \approx \frac{A}{\Omega_+(x^*)} \exp[-NS(x^*)] \exp\left(-\frac{\lambda}{2}(x-x^*)^2\right), \quad (2.53)$$

where  $\lambda = N(b+c)^2/b(c+d)$ . By imposing the normalization condition for  $\Pi(x)$  we obtain the following expression for  $A$ :

$$A = \sqrt{\frac{\lambda}{2\pi}} \exp[NS(x^*)] \Omega_+(x^*). \quad (2.54)$$

which eventually yields:

$$\begin{aligned} \Pi(x) &= \sqrt{\frac{NS''(x^*)}{2\pi}} \left[ \frac{\Omega_+(x^*)\Omega_-(x^*)}{\Omega_+(x)\Omega_-(x)} \right]^{1/2} \times \\ &\times \exp -N[S(x) - S(x^*)]. \end{aligned} \quad (2.55)$$

In conclusion, we have derived a closed analytical expression for the quasi-stationary distribution  $\Pi$ , under the WKB working hypothesis. In the following section we will test the adequacy of formula (2.55), and of the homologous prediction obtained in the framework of the van Kampen expansion, by performing a direct comparison with the outcome of stochastic simulations.

### 2.3.5 Numerical simulations

As discussed in the preceding section, by operating under the WKB procedure, one can derive a closed analytical expression for the quasi-distribution  $\Pi$  around the deterministic fixed point  $x^*$ . On the other hand, by extending the van Kampen analysis beyond the Gaussian order of approximation, we have obtained a set of coupled differential equations for the moments of the distribution of fluctuations. The knowledge of the moments enables us in principle to reconstruct the corresponding distribution via a standard Fourier inversion. In this Section we aim at comparing the two theoretical predictions, and assess their respective validity versus direct simulations of the stochastic dynamics.

While it is straightforward to display the result of the WKB analysis, some comments are mandatory as concerns the interpretation of the calculation based on the van Kampen system expansion. To recover the stationary distribution of fluctuations we consider the ensemble of first  $q$  moments and impose a truncation in the van Kampen expansion at e.g. order  $1/N^2$ , namely two orders beyond the conventional Gaussian approximation. To obtain a closed system for the unknown moments, we omit in the equation for  $d < \xi^q > / d\tau$  the term proportional to  $< \xi^{q+1} > / \sqrt{N}$ , more specifically the contribution  $k = 2$  in the first sum of the left hand side of equation (2.37). In principle, one cannot formally drop such term, our expansion being targeted to the order  $1/N^2$ , which requires including terms up to  $1/N^{3/2}$  in the equation for the moments. On the other hand, the error committed when neglecting a contribution proportional to  $1/\sqrt{N}$  in the equation for the  $q$ -th moment, becomes rapidly negligible when approaching the first moments of the hierarchy. More precisely, the imposed closure will impact the  $j$ -th moment equation with an associated error that we can estimate of order  $1/N^{(q-j-1)/2}$ , from the structure of the ruling equations (2.37). In other words, only the equations for moments  $j = q - 1$  and

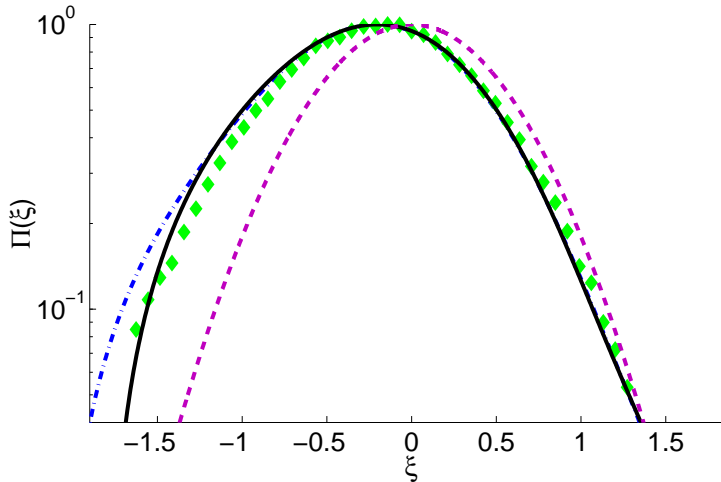


Figure 2.11: The (green) diamonds stand for the distribution in lin-log scale rebuilt from the Gillespie's algorithm simulation. The (black) solid line is the theoretical profile obtained following the van Kampen strategy, with the first thirty moments, arrested to order of  $1/N^2$ . The blue dot-dashed line is instead obtained by arresting the distribution to order of  $N^{-1}$ . The (purple) dashed-line refers to the so-called Gaussian approximation (order  $1/N^{1/2}$  in the van Kampen expansion). The parameters used are:  $N = 1000$   $c = 0.5$   $b = 0.3$   $d = 0.2$ . For this choice of the parameters the fixed point of the deterministic dynamics is  $\phi^* = 0.125$ .

$j = q - 2$  are affected by the imposed truncation, all other errors being negligible at the considered order of expansion. If  $q$  is large, one can therefore hope that the errors in the last three equations of the hierarchy are sufficiently localized to not compromise the estimate of a large subset of moments. The comparison with the simulations will provide an a posteriori validation of the proposed approximation.

As an additional remark, we recall that we are here interested at the asymptotic distribution of fluctuations, around the non trivial fixed point of the deterministic dynamics. This implies setting to zero the derivatives  $d \langle \xi^q \rangle / d\tau$  in equation (2.37), after having imposed  $\phi = \phi^*$  in the functions  $f_k, g_k$  and  $h_k$ , as defined in 2.3.6. The system of differential equations for the evolution of the moments is hence transformed into an algebraic system that can be readily solved by matrix inversion. The distribution of fluctuation is finally determined by Fourier inverting its corresponding moments expansion. In the following, we will report results obtained when considering the first thirty moments in the expansion, i.e. considering the first  $q = 30$  algebraic equations for the stationary moments.

In figure 2.11 we compare the distributions of fluctuations obtained via the van Kampen procedure, at different order of approximations. The Gaussian solution, obtained by truncating the expansion at the order  $1/\sqrt{N}$ , is displayed with a dashed line (purple online). The point-dashed line and the solid line refer respectively to the van Kampen approximation at order  $1/N^{3/2}$  and one at  $1/N^2$ . The symbols stand for the distribution rebuilt from direct stochastic simulations, based on the Gillespie's algorithm, for the system (2.25). When the order of the approximation is increased, the theoretical distribution tends to adjust nicely on the numerical profile.

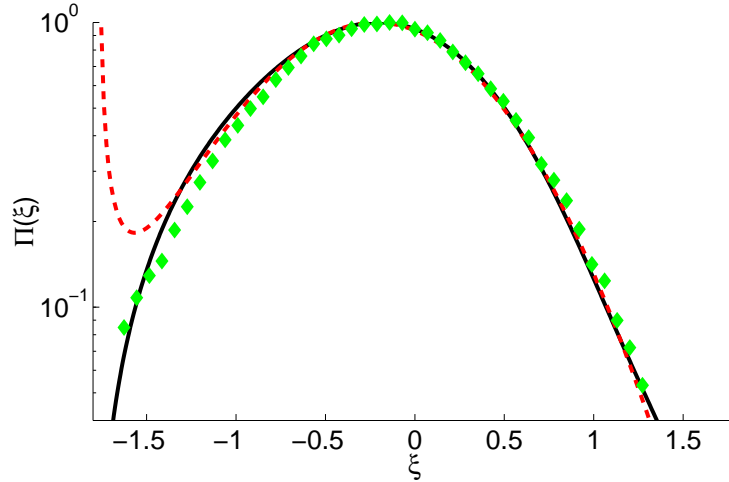


Figure 2.12: The (green) diamonds stand for the distribution in lin-log scale rebuilt from the Gillespie's algorithm simulation. The (black) solid line represents the van Kampen approximation with the first thirty moments, and the expansion arrested to order of  $1/N^2$ . The (red) dashed line is the WKB approximation. The parameters used are:  $N = 1000$   $c = 0.5$   $b = 0.3$   $d = 0.2$ . For this choice of the parameters the fixed point of the deterministic dynamics is  $\phi^* = 0.125$ .

In figure 2.12 the performance of the van Kampen systems size expansion and the WKB scheme are respectively compared. The solid line stands for the distribution of fluctuations obtained via the extended van Kampen system size calculation at order  $1/N^2$ , while the dashed line refers to the WKB analysis. As in figure 2.11, the symbols represents the numerically determined profile. In both cases the agreement with the numerics is satisfying and the overall skewness of the distribution appears to be properly captured by the theories. The WKB solution tends to deviate from the expected profile for negative fluctuations amount (at system sizes of few tens of individuals), when the van Kampen approximation, at the considered order of expansion, prove still adequate. The fact that the van Kampen solution interpolate correctly the simulated data, constitutes an a posteriori validation of the implemented closure strategy.

### 2.3.6 Details of van Kampen expansion

By inserting in the master equation (2.28) the development of the step operator (2.32) and the van Kampen ansatz, the resulting equation is the (2.35). We consider as an example the following term of the master equation:

$$(\epsilon_n^+ - 1)[T(n-1|n)P_n(t)] = \left( \sum_{k=0}^{\infty} \frac{1}{k!} \frac{1}{N^{k/2}} \frac{\partial^k}{\partial \xi^k} - 1 \right) \left[ (d\phi + d\xi/\sqrt{N} + c\phi^2 + 2c\phi\xi/\sqrt{N} + c\xi^2/N)\Pi(\xi) \right].$$

It is possible to observe that for  $k = 0$  the operator in the brackets is null, because



the value of the first term of the Taylor expansion is equal to one, so we obtain:

$$(\epsilon_n^+ - 1)[T(n-1|n)P_n(t)] = \left( \sum_{k=1}^{\infty} \frac{1}{k!} \frac{1}{N^{k/2}} \frac{\partial^k}{\partial \xi^k} \right) \left[ (d\phi + d\xi/\sqrt{N} + c\phi^2 + 2c\phi\xi/\sqrt{N} + c\xi^2/N)\Pi(\xi) \right].$$

We divided the contributions depending on the different power in  $\xi$  for the derivative and we obtain:

$$\begin{aligned} & \left( \sum_{k=1}^{\infty} \frac{1}{k!} \frac{1}{N^{k/2}} \frac{\partial^k}{\partial \xi^k} (d\phi + c\phi^2)\Pi \right) + \left( \sum_{k=1}^{\infty} \frac{1}{k!} \frac{1}{N^{k/2+1/2}} \frac{\partial^k}{\partial \xi^k} (2c\phi\xi + d\xi)\Pi \right) \\ & + \left( \sum_{k=1}^{\infty} \frac{1}{k!} \frac{1}{N^{k/2+1}} \frac{\partial^k}{\partial \xi^k} [c\xi^2]\Pi \right). \end{aligned} \quad (2.56)$$

Collecting together the terms proportional to different powers of  $N$  in the first order, we recover the mean field equation (2.33), that corresponds to the term of the development for  $k=1$ . The leading order results in the following generalized Fokker-Planck equation:

$$\begin{aligned} \frac{\partial \Pi}{\partial \tau} &= \sum_{k=2}^{\infty} \frac{1}{k!} \frac{1}{N^{k/2-1}} \frac{\partial^k}{\partial \xi^k} (d\phi + c\phi^2 + (-1)^k (b\phi - b\phi^2))\Pi \\ &+ \sum_{k=1}^{\infty} \frac{1}{k!} \frac{1}{N^{k/2-1/2}} \frac{\partial^k}{\partial \xi^k} (2c\phi\xi + d\xi + (-1)^k (+b\xi - 2b\phi\xi))\Pi \\ &+ \sum_{k=1}^{\infty} \frac{1}{k!} \frac{1}{N^{k/2}} \frac{\partial^k}{\partial \xi^k} [(c\xi^2 - b\xi^2(-1)^k)\Pi]. \end{aligned}$$

We denote by:

$$f_k(\phi) = (d\phi + c\phi^2 + (-1)^k (b\phi - b\phi^2)) \quad (2.57)$$

$$f_k = \begin{cases} (b+d)\phi + (c-b)\phi^2 & \text{if } k \text{ is odd} \\ (d-b)\phi + (b+c)\phi^2 & \text{if } k \text{ is even.} \end{cases} \quad (2.58)$$

For the other two terms we obtain:

$$g_k(\xi, \phi) = (2c\phi\xi + d\xi + (-1)^k (+b\xi - 2b\phi\xi))$$

$$g_k(\xi, \phi) = \begin{cases} [(2c-2b)\phi + (b+d)]\xi & \text{if } k \text{ is even} \\ [(2b+2c)\phi + (d-b)]\xi & \text{if } k \text{ is odd.} \end{cases} \quad (2.59)$$

$$h_k(\xi) = c\xi^2 - b\xi^2(-1)^k$$

$$h_k(\xi^2) = \begin{cases} (c-b)\xi^2 & \text{if } k \text{ is even} \\ (b+c)\xi^2 & \text{if } k \text{ is odd.} \end{cases} \quad (2.60)$$

Rearranging the terms in the sums, we obtain the generalized Fokker Planck, equation (2.35) in the main body of the section.

Now we want to calculate the equation of the moments at any order. By focusing on the right hand side we multiply both sides by  $\xi^q$  and integrating over  $\mathbb{R}$ . We obtain the following equation:

$$\int \sum_{k=1}^{\infty} \frac{1}{(k+1)!} \frac{1}{N^{(k-1)/2}} \xi^q \frac{\partial^{k+1}}{\partial \xi^{k+1}} [f_{k+1}(\phi)\Pi] d\xi + \int \sum_{k=1}^{\infty} \frac{1}{k!} \frac{1}{N^{(k-1)/2}} \xi^q \frac{\partial^k}{\partial \xi^k} [g_k(\phi\xi)\Pi] d\xi \\ + \int \sum_{k=2}^{\infty} \frac{1}{(k-1)!} \frac{1}{N^{(k-1)/2}} \xi^q \frac{\partial^{k-1}}{\partial \xi^{k-1}} [h_{k-1}(\xi^2)\Pi] d\xi.$$

Concentrate on the first term:

$$\int \sum_{k=1}^{\infty} \frac{1}{(k+1)!} \frac{1}{N^{(k-1)/2}} \xi^q \frac{\partial^{k+1}}{\partial \xi^{k+1}} [f_{k+1}(\phi)\Pi] d\xi = \sum_{k=1}^{\infty} \frac{1}{(k+1)!} \frac{1}{N^{(k-1)/2}} f_{k+1}(\phi) \int \xi^q \frac{\partial^{k+1}}{\partial \xi^{k+1}} \Pi d\xi.$$

The only non-null terms are those corresponding to  $k+1 \leq q$ :

$$\sum_{k=1}^{\infty} \frac{1}{(k+1)!} \frac{1}{N^{(k-1)/2}} f_{k+1}(\phi) \int \xi^q \frac{\partial^{k+1}}{\partial \xi^{k+1}} \Pi d\xi = \\ \sum_{k=1}^{q-1} \frac{1}{(k+1)!} \frac{1}{N^{(k-1)/2}} f_{k+1}(\phi) \frac{(-1)^{k+1} q!}{(q-(k+1))!} \int \xi^{q-(k+1)} \Pi d\xi = \\ \sum_{k=1}^{q-1} \frac{1}{(k+1)!} \frac{1}{N^{(k-1)/2}} f_{k+1}(\phi) \frac{(-1)^{k+1} q!}{(q-(k+1))!} < \xi^{q-(k+1)} > .$$

Similarly for all the other terms we obtain finally the following moments equation:

$$\frac{d \langle \xi^q \rangle}{d\tau} = \sum_{k=2}^{q+1} \frac{h_{k-1}(-1)^{k-1} q! \langle \xi^{q-(k-1)+2} \rangle}{(k-1)!(q-(k-1))! N^{(k-1)/2}} \\ + \sum_{k=1}^q \frac{g_k(-1)^k q! \langle \xi^{q-k+1} \rangle}{k! N^{(k-1)/2} (q-k)!} \\ + \sum_{k=1}^{q-1} \frac{f_{k+1}(-1)^{k+1} q! \langle \xi^{q-(k+1)} \rangle}{(k+1) N^{(k-1)/2} (q-(k+1))!}.$$

### 2.3.7 Details of WKB approximation

We here calculate the function  $S(x)$ , along the trajectory with  $p \neq 0$ . Recall that

$$S(x) = \int_{x^*}^x p \, dx, \quad (2.61)$$

where the integral extends from the fixed point  $x^*$  to  $x$ . By using condition  $p = \ln(\Omega_+/\Omega_-)$  we get:

$$S(x) = \int_{x^*}^x \ln \left[ \frac{d+cx}{b-bx} \right] dx. \quad (2.62)$$

By setting  $y = d+cx$ , we find

$$\int \ln[d+cx] dx = c^{-1} \int \ln y dy = c^{-1} [y \ln y - y].$$

In complete analogy, imposing  $y = b - bx$ , implies

$$\int \ln[b - bx]dx = -b^{-1} \int \ln y dy = -b^{-1}[y \ln y - y].$$

Combining together:

$$\begin{aligned} S(x) &= \frac{(d + cx) \ln(d + cx)}{c} + (1 - x) \ln(b - bx) \\ &- \frac{(d + cx)}{c} - (1 - x) + \text{constant}. \end{aligned} \quad (2.63)$$

At the fixed point:

$$S(x^*) = (c^{-1} + b^{-1})k \ln k - (c^{-1} + b^{-1})k + \text{constant}. \quad (2.64)$$

where  $k = \frac{b(c+d)}{(c+b)}$ .

After some manipulation one eventually finds the final expression (2.48).

## 2.4 Conclusion

In this chapter we have presented three different models, and in all of them we have used the van Kampen expansion beyond the classical approximation. Here we have been interested in extending the perturbative calculation beyond the second order approximation and challenge its adequacy in capturing the deviation from the idealized Gaussian behavior. Recent support on the validity of the van Kampen higher orders calculation have been provided by Grima and collaborators [37].

We here have brought one more evidence on the accuracy of the procedure within a rather complex model the first considered in this chapter, where different species are simultaneously made to interact. Numerical simulations performed in a stochastic setting with modest sizes of the population involved, so to magnify the role played by finite size corrections, confirm the correctness of the theory predictions. Due to the complexity of the proposed model, it is not possible to evaluate a large gallery of successive moments and so reconstruct the full distribution of fluctuations. The analysis is hence limited to the third moments, which however quantify the degree of skewness of the recorded fluctuations.

In the second model [7], we returned on the issue of the validity of the van Kampen ansatz, working within a considerably simpler setting, the voter model, that enables us to explicitly calculate all the moments of the distribution at any order of the expansion. We were hence able to recover a general and exact analytical solution for the distribution of fluctuations that agreed very well with the simulations.

In the last section we have considered a logistic model with a stable non-trivial fixed point and an unstable trivial fixed point. The stochastic model was chosen so as to obtain a logistic equation as its deterministic limit. We were interested in characterizing the distribution of fluctuations, a question of paramount importance if one aims to study the extinction dynamics. Stochastic fluctuations may, in fact, drive the system from the vicinity of a non-trivial fixed point of the deterministic dynamics, to a trivial fixed point where all the individuals have become extinct. For sufficiently large population sizes, extinction will be rare and the state of the system will fluctuate about the non-trivial fixed

point for a long time. In this situation the van Kampen system-size expansion constitutes a powerful analytical tool to estimate the distribution of fluctuations. As we have already discussed, the method gives the deterministic equations to leading order in an expansion in (inverse) system-size. The linear stochastic corrections are found at the next-to-leading order, giving an excellent approximation of the dynamics if extinctions are so rare as to be negligible. When the size of the population is reduced, non Gaussian traits prove crucial and one needs to go beyond the conventional order to eventually resolve the skewness of the distribution. Alternatively, a WKB-like perturbation scheme can be implemented to derive a closed analytical approximation for the distribution of fluctuations. The method consists on postulating that the dominant contribution to the probability distribution scales as  $e^{-NS(x)}$  where  $N$  is the system-size and  $S(x)$  is a solution of a fictitious Hamilton-Jacobi equation that is self-consistently derived by carrying out the perturbative analysis. The corresponding Hamiltonian can be used to describe the extinction trajectories, and consequently the distribution of the stochastic fluctuations. The theoretical predictions have been compared to the results of the numerical simulations, obtained by solving the examined stochastic model via the standard Gillespie's algorithm [28]. In both cases the agreement has to be considered satisfactory. The advantage of the WKB method over the generalized expansion resides in that the former enables one to recover a closed analytical expression for the distribution of fluctuations. At variance, the latter requires calculating the fixed point of a large set of algebraic equations for the moments of the distribution, a step that can be only performed numerically. We also recall that the extended van Kampen method must be accompanied by a dedicated truncation strategy, to get a fully consistent system for the unknown moments. The validity of the imposed closure can only be tested a posteriori by a direct comparison with numerical, or experimentally available, data.

## Chapter 3

# Spatial model: Stochastic Turing pattern formation

This chapter, together with the following, concerns the study of reaction-diffusion models as possible mechanisms for generating spatial patterns. Indeed, spatial patterns are ubiquitous in nature: the early patterning in the embryo of the fruit fly, spatial patterning in slime moulds, chemical oscillating reaction and bacterial patterns [48]. Much of the research in developmental biology, both experimental and theoretical, aims at elucidating the mechanisms which underlay pattern formation. The first explanation theory was put forward by Turing in the classical paper [9], devoted to morphogenesis. From then on reaction diffusion theory became an established field of research.

In this chapter we will study the problem of pattern formation in a generic two species reaction-diffusion model, under the hypothesis that only one species can diffuse. For such systems, the classical Turing instability cannot take place. At variance, by working in the generalized setting of a stochastic formulation, Turing like patterns can develop, through finite-size corrections. General conditions are given for the stochastic Turing patterns to occur. The predictions of the theory are tested for a specific case of study.

### 3.1 Stochastic Turing Patterns for systems with one diffusing species

Spatio temporal self-organized patterns [48] can spontaneously emerge in a reaction-diffusion system. A small perturbation of a homogeneous fixed point can for example amplify, as follows a symmetry breaking instability seeded by diffusion, and eventually yield to a steady state non homogeneous solution. These are the Turing patterns [9], recurrently investigated in chemistry [49, 50] and biology [48].

The majority of studies devoted to the Turing instability consider two, mutually interacting, species. More specifically, and following the customarily accepted paradigm, one species activates the production of the other, this latter acting through an inhibitor feedback. Systems of three [51] simultaneously diffusing species have been also considered and shown to display a rich zoology of possible patterns and instabilities. Patterns can also develop if only one species is allowed to diffuse in the embedding medium, provided the system is composed of at least three coupled species [52]. In contrast, it is well known [52] that two species systems where only one species can migrate, cannot undergo Turing

instability. Models however exist which fall within this category [18]. For this reason, it is of general interest to theoretically explore the possibility of bifurcation patterns of such systems, beyond the classical Turing framework. This chapter aims at elaborating along these lines, by considering the generalized concept of stochastically driven patterns.

Reaction-diffusion systems are in fact generally studied by resorting to deterministic mathematical models. The continuum concentrations of the interacting species is hence monitored over space and in time. As opposed to this, one can develop an individual based description of the scrutinized dynamics, which effectively accounts for the inherent discreteness of the system. Stochastic contributions, stemming from finite size corrections, can thus modify the idealized mean field picture and occasionally return alternative scenarios to interpret available data.

In a series of recent publications, the effect of the intrinsic noise was indeed shown to create stochastic patterns, in a region of the parameters for which macroscopically ordered structures do not occur. When the deterministic dynamics predicts a stable homogeneous state, the stochastic component can amplify via a resonant mechanism, giving birth to stochastic Turing patterns [53, 10, 12, 54]. The effect of finite size fluctuations can be characterized with numerical simulations, but also analytically via the van Kampen system size expansion. As previously discussed this allows to expand the governing master equation, which accounts for the role of demographic fluctuations. At the first order of the expansion, the deterministic mean-field model is obtained, while the second order contributions form an equation for the stochastic fluctuations.

Working in this context, we will consider a simple birth and death model, with two species, of which one can diffuse. The reaction rates are assumed to be generic non linear functions of the concentration amount. Conditions for the emergence of stochastic Turing patterns are derived. More concretely, stochastic Turing patterns can materialize if the power spectrum of fluctuations has at least a peak for a non zero spatial wave number  $k$  for  $\omega$ , the Fourier time frequency, equal to zero. We will here prove that a non trivial maximum of the power spectrum exists, if the system matches specific conditions that we shall mathematically characterize. The validity of our conclusions are tested for a simple non linear model, which falls in the general class of models inspected. With reference to this specific case study, we perform stochastic simulations through the Gillespie's algorithm and confirm a posteriori the adequacy of the predictions.

The chapter is organized as follows. In the next section we will prove that, over a continuum support, the Turing instability cannot take place for reaction-diffusion models with two interacting species of which only one is allowed to diffuse [52]. If space is instead discrete, Turing like pattern can in principle take place, but only if the non diffusing species acts as a self-activator. However, when the condition for the instability are met, the most unstable mode  $k$  is always located in  $\pi$ , a trivial consequence of the imposed discretization. As we shall here demonstrate, accounting for the intrinsic finite size fluctuations allows one to obtain a more complex landscape of possible instabilities. In Section 3.3 we introduce the stochastic birth and death model that we shall use as a reference case study. The model is completely general and the reaction rates are assumed to depend on the species concentration, via generic non linear functions. Then, in Section 3.4, we first derive the mean-field deterministic limit: the only request that we shall put forward has to do with the existence of a stable fixed point for the aspatial mean-field system. We then proceed to derive the Fokker-Planck equation that describes the fluctuations. From this, in Section 3.5, we calculate the power spectrum of fluctuations,

and find the mathematical conditions for having stochastic Turing patterns. We turn in Section 3.6 to considering a particular non-linear model, to verify the correctness of our predictions. Finally, in Section 3.7 we sum up and conclude.

### 3.2 Deterministic reaction-diffusion system with one diffusing species

Let us start by considering two species respectively characterized by the continuum concentrations  $\phi(\mathbf{r}, t)$  and  $\psi(\mathbf{r}, t)$ . Here  $\mathbf{r}$  stands for the spatial variable and  $t$  represents time. Imagine the following general system to rule the dynamics of the concentrations:

$$\begin{aligned} \frac{\partial \phi}{\partial t} &= f(\phi, \psi) + D \nabla^2 \phi \\ \frac{\partial \psi}{\partial t} &= g(\phi, \psi), \end{aligned} \tag{3.1}$$

where  $\nabla^2$  is the standard Laplacian operator and the functions  $f(\cdot, \cdot)$  and  $g(\cdot, \cdot)$  account for the interactions among the species. As anticipated we are focusing on the specific case study where just one species, specifically  $\phi$ , is allowed to diffuse,  $D$  denoting its diffusion coefficient. Notice that  $\psi$  is also function of the spatial variable  $\mathbf{r}$ , as it depends on the concentration  $\phi$ , the species which can in turn migrate. We shall here assume that a fixed point of the homogeneous system exists. This is a uniform solution  $\phi(\mathbf{r}) = \hat{\phi}$ ,  $\psi(\mathbf{r}) = \hat{\psi}$ , with  $\hat{\phi}$  and  $\hat{\psi}$  constants, such that  $f(\hat{\phi}, \hat{\psi}) = g(\hat{\phi}, \hat{\psi}) = 0$ . We shall furthermore assume that the fixed point  $(\hat{\phi}, \hat{\psi})$  is stable. In the following we will prove that no Turing instability can occur, if just one species can diffuse.

To this end we consider a small perturbation  $\mathbf{w}$  of the initial homogeneous stationary state, in formulae:

$$\mathbf{w} = \begin{pmatrix} \phi - \hat{\phi} \\ \psi - \hat{\psi} \end{pmatrix}. \tag{3.2}$$

Since  $|\mathbf{w}|$  is by hypothesis small we can linearize system (3.1) around the fixed point and so eventually obtain:

$$\dot{\mathbf{w}} = \mathcal{J} \mathbf{w} + \mathbf{D} \nabla^2 \mathbf{w}, \quad \mathbf{D} = \begin{pmatrix} D & 0 \\ 0 & 0 \end{pmatrix}. \tag{3.3}$$

where  $\dot{\mathbf{w}}$  represents the time derivative of  $\mathbf{w}$  and  $\mathcal{J}$  is the Jacobian matrix defined as:

$$\mathcal{J} = \begin{pmatrix} f_\phi & f_\psi \\ g_\phi & g_\psi \end{pmatrix}, \tag{3.4}$$

where e.g.  $f_\phi$  stands for  $\partial f / \partial \phi$  evaluated at the fixed point  $(\hat{\phi}, \hat{\psi})$ . Similar definitions apply to the other entries of the matrix  $\mathcal{J}$ .

To solve the above system (3.3), subject to specific boundary conditions, one can introduce the eigenfunctions  $\mathbf{W}_k(\mathbf{x})$  of the Laplacian, such that

$$-\nabla^2 \mathbf{W}_k(\mathbf{x}) = k^2 \mathbf{W}_k(\mathbf{x}),$$

for all  $k \in \sigma$ , where  $\sigma$  is a suitable (unbounded) spectral set. Then we expand

$$\mathbf{w}(\mathbf{x}, t) = \sum_{k \in \sigma} c_k e^{\lambda^{(k)} t} \mathbf{W}_k(\mathbf{x}), \tag{3.5}$$

where the constants  $c_k$  refer to the initial condition. This is equivalent to performing a Fourier-like transform of the original equation. The function  $\lambda(k)$ , also called dispersion relation, controls the growth (or damping) of the perturbation. More specifically the solution of the linearized system (3.3) exists if

$$\det(\lambda I - \tilde{\mathcal{J}}) = 0, \quad (3.6)$$

where  $\det(\cdot)$  is the determinant and

$$\tilde{\mathcal{J}} = \begin{pmatrix} f_\phi - Dk^2 & f_\psi \\ g_\phi & g_\psi \end{pmatrix}. \quad (3.7)$$

A simple calculation yields:

$$\lambda(k) = \frac{(\text{Tr } \mathcal{J} - Dk^2) + \sqrt{(\text{Tr } \mathcal{J} - Dk^2)^2 - 4(\det \mathcal{J} - Dk^2 g_\psi)}}{2}, \quad (3.8)$$

where  $\text{Tr}(\cdot)$  denotes the trace. Since we are interested in the growth of unstable perturbations, we have here selected the largest  $\lambda(k)$ . The Turing instability occurs if one can isolate a finite domain in  $k$  for which  $\lambda(k) > 0$ . In formulae:

$$\begin{aligned} & (\text{Tr } \mathcal{J} - Dk^2) + \sqrt{(\text{Tr } \mathcal{J} - Dk^2)^2 - 4(\det \mathcal{J} - Dk^2 g_\psi)} > 0 \\ \implies & \sqrt{(\text{Tr } \mathcal{J} - Dk^2)^2 - 4(\det \mathcal{J} - Dk^2 g_\psi)} > -(\text{Tr } \mathcal{J} - Dk^2) \\ \implies & -4(\det \mathcal{J} - Dk^2 g_\psi) > 0 \\ \implies & Dk^2 g_\psi > \det \mathcal{J}. \end{aligned} \quad (3.9)$$

The right hand side contribution in equation (3.9) is positive as the homogeneous fixed point is supposed to be stable. If  $g_\psi < 0$  it is clear that (3.9) does not admit solutions, the left hand side of the equation being negative. At variance, when  $g_\psi > 0$  we have:

$$k^2 > \frac{\det \mathcal{J}}{Dg_\psi} \implies k < -\sqrt{\frac{\det \mathcal{J}}{Dg_\psi}} \quad \text{and} \quad k > \sqrt{\frac{\det \mathcal{J}}{Dg_\psi}}. \quad (3.10)$$

Equation (3.10) implies that the relation of dispersion  $\lambda(k)$  is positive for all values of  $k \in \sigma$  above a critical threshold  $k_c = \sqrt{\det \mathcal{J}/(Dg_\psi)}$ . The quantity  $\lambda(k)$  grows as  $k$  does, the instability involving smaller and smaller spatial scales. It is therefore not possible to delimit a finite window in  $k$  for which  $\lambda(k)$  is found to be positive, and, hence, the Turing instability cannot take place. In conclusion, we have here confirmed a well establish fact: a two species systems where only one species can migrate, cannot undergo Turing instability [52].

Let us now turn to considering the case where the spatial support is supposed to be discrete. In practice, this amounts to assume the physical space, in any dimension, to be partitioned in a large collection of mesoscopic patches, where the constituents are assumed to be uniformly mixed. The diffusion can take place between adjacent patches. The differential equations that govern the evolution of the concentration are therefore discrete in space, a setting that is for instance of interest when reaction-diffusion models are applied to ecology [55].



For simplicity, and without losing generality, we will hereafter consider the problem in one dimension, assuming the physical space to be segmented in  $\Omega$  cells, each of finite linear size  $a$ . We label  $\phi_i$  and  $\psi_i$ , with  $i = 1, \dots, \Omega$ , the discrete concentrations, that respectively replace their continuum analogues  $\phi$  and  $\psi$ .

The discrete Laplacian operator  $\Delta$  is defined as:

$$\Delta\phi_i = \frac{1}{a^2} \sum_{j=i\pm 1} (\phi_j - \phi_i), \tag{3.11}$$

and periodic boundary conditions at  $i = 1$  and  $i = \Omega$  will be assumed throughout the rest of the chapter. Let  $\delta$  denote the transition probability per unit of time that control the migration between neighbors mesoscopic patches. In the continuum limit  $\delta a^2 \rightarrow D$ , when  $a \rightarrow 0$ . The discrete reaction diffusion system can be therefore written as:

$$\begin{cases} \frac{\partial\phi_i}{\partial t} = f(\phi_i, \psi_i) + (\delta a^2) \Delta\phi_i \\ \frac{\partial\psi_i}{\partial t} = g(\phi_i, \psi_i). \end{cases} \tag{3.12}$$

To study the onset of the instability, we operate in analogy with what has been done above and perform a spatio-temporal Fourier transform of eqs. (3.12). The transform of the discrete Laplacian  $\Delta$  reads  $\tilde{\Delta}_k = (2/a^2)(\cos(ak) - 1)$ . Proceeding in the analysis, one ends up with the following relation of dispersion:

$$\lambda(k) = \frac{h(k) + \sqrt{h(k)^2 - 4(\det \mathcal{J} + 2\delta(\cos(ak) - 1))g_\psi}}{2}, \tag{3.13}$$

where  $h(k) = \text{Tr } \mathcal{J} + 2\delta(\cos(ak) - 1)$ . By imposing  $\lambda(k) > 0$  one obtains, after a simple algebraic manipulation, the following condition:

$$\delta(1 - \cos(ak))g_\psi > 2 \det \mathcal{J}. \tag{3.14}$$

As it happens for the case of the continuum, no solution of (3.14) are possible when  $g_\psi < 0$ , namely when the non diffusing species has a self-inhibitory effect. At variance, if  $g_\psi > 0$  a finite interval in  $k$  can be found where  $\lambda(k)$  is different from zero, and the system can therefore experience a Turing instability which is indeed seeded by the discreteness of the spatial support. The most unstable mode  $k_M$  is however found to be  $k_M = \pi/(2a)$ , a trivial solution which stems from having assumed a discrete spatial support. It is worth emphasizing that, as expected,  $k_M$  diverges to infinity when the size of the patch  $a$  goes to zero <sup>1</sup>.

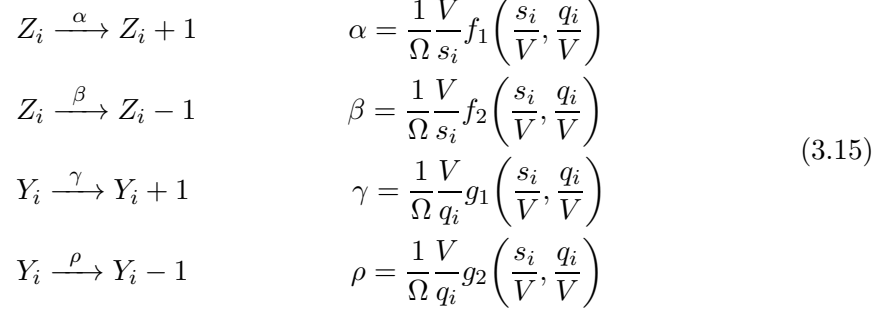
Starting from this setting, we will work in the context of a stochastic formulation of the generic reaction diffusion system considered above and show that finite size corrections can eventually drive the emergence of Turing like patterns. We will in particular specialize on the case of a model defined on a discrete lattice and assume  $g_\psi < 0$ . Under this condition the Turing patterns cannot develop in the mean-field approximation.

---

<sup>1</sup>The fact a discretised domain can produce wave modes to appears that do not exist in the continuum case was also noticed in [54].

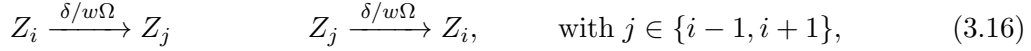
### 3.3 The Model and its Master Equation

The system that we are going to study is a general two species birth-death model, in which one of the species diffuses. As already mentioned, we assume the physical space to be partitioned in  $\Omega$  patches <sup>2</sup>, and label with  $V$  their carrying capacity. The integer index  $i$  runs from 1 to  $\Omega$  and identifies the cell to which the species belong. Label the two species  $Z$  and  $Y$  and assume the following chemical reaction scheme:



We indicated as  $s_i$  the number of elements of species  $Z$  and with  $q_i$  the number of elements of species  $Y$  in the cell  $i$ . Moreover, we require that  $f_1, f_2, g_1, g_2$  are sufficiently regular functions of the discrete number concentrations  $s_i/V$  and  $q_i/V$ .

We assume that only  $Z$  diffuses and therefore write



where, in general,  $w$  is the number of neighboring cells of a given cell  $i$  and, therefore,  $w = 2$  in the present one-dimensional case. A state of the system is characterized by two vectors, respectively  $\vec{s} = (s_1, s_2, \dots, s_\Omega)$  and  $\vec{q} = (q_1, q_2, \dots, q_\Omega)$ . It is worth emphasizing that the model is completely general: virtually any system composed by two species, one of each diffusing, can be cast in the form introduced above, upon a proper choice of the functions  $f_1, f_2, g_1, g_2$ .

We then turn to write down the master equation that governs the dynamics of the system. To this end we need to calculate the transition probability associated with each reaction:

$$\begin{aligned}
 T(s_i + 1, q_i | s_i, q_i) &= \alpha \frac{s_i}{V} \\
 T(s_i - 1, q_i | s_i, q_i) &= \beta \frac{s_i}{V} \\
 T(s_i, q_i + 1 | s_i, q_i) &= \gamma \frac{q_i}{V} \\
 T(s_i, q_i - 1 | s_i, q_i) &= \rho \frac{q_i}{V} \\
 T(s_i + 1, s_j - 1 | s_i, s_j) &= \frac{\delta}{\Omega} \frac{s_j}{bV} \\
 T(s_i - 1, s_j + 1 | s_i, s_j) &= \frac{\delta}{\Omega} \frac{s_i}{bV}.
 \end{aligned}$$

By introducing the following ‘‘step operators’’:

$$\varepsilon_{s_i}^\pm f(\vec{s}, \vec{q}) = f(\dots, s_i \pm 1, \dots, \vec{q}), \quad \varepsilon_{q_i}^\pm f(\vec{s}, \vec{q}) = f(\vec{s}, \dots, q_i \pm 1, \dots),$$

<sup>2</sup>For the sake of simplicity, and without losing generality we will set  $a = 1$  in the following.

the master equation reads:

$$\begin{aligned}
\frac{d}{dt}P(\vec{s}, \vec{q}, t) &= \sum_{i=1}^{\Omega} \left[ (\varepsilon_{s_i}^+ - 1) T(s_i - 1, q_i | s_i, q_i) + (\varepsilon_{s_i}^- - 1) T(s_i + 1, q_i | s_i, q_i) \right. \\
&\quad \left. + (\varepsilon_{q_i}^+ - 1) T(s_i, q_i - 1 | s_i, q_i) + (\varepsilon_{q_i}^- - 1) T(s_i, q_i + 1 | s_i, q_i) \right] P(\vec{s}, \vec{q}, t) \\
&\quad + \sum_{i=1}^{\Omega} \sum_{j \in \{i-1, i+1\}} \left[ (\varepsilon_{s_i}^+ \varepsilon_{s_j}^- - 1) T(s_i - 1, s_j + 1 | s_i, s_j) \right. \\
&\quad \left. + (\varepsilon_{s_i}^- \varepsilon_{s_j}^+ - 1) T(s_i + 1, s_j - 1 | s_i, s_j) \right] P(\vec{s}, \vec{q}, t),
\end{aligned} \tag{3.17}$$

where, in accordance with our assumption of periodic boundary conditions, we adopt a periodic convention for the indices out of the set  $\{1, \dots, \Omega\}$ .

The master equation is difficult to handle analytically and we perform a van Kampen system size expansion, putting forward the ansatz:

$$\frac{s_i}{V} = \phi_i + \frac{\xi_i}{\sqrt{V}}, \quad \frac{q_i}{V} = \psi_i + \frac{\eta_i}{\sqrt{V}}. \tag{3.18}$$

The number density  $s_i/V$  splits into two independent contributions:  $\phi_i$  stands for the deterministic (mean-field) concentration as measured in correspondence of the site  $i$ , and  $\xi_i$  is a stochastic variable that quantifies the fluctuation that perturbs the mean-field solution  $\phi_i$ . Similar considerations apply to  $q_i/V$ . The factor  $1/\sqrt{V}$  takes into account the finite volume of the system. In the limit for infinite systems size, the fluctuations can be neglected and the stochastic system as formulated above converges to its deterministic analogue. When working at finite  $V$ , stochastic fluctuations are important. The role of fluctuations can be quantitatively studied by implementing the aforementioned perturbative analysis, the van Kampen expansion [29], which assumes the amplitude factor  $1/\sqrt{V}$  to act as a small parameter. To this end we introduce the van Kampen hypothesis into the master equation and split the contributions of order  $1/\sqrt{V}$  and  $1/V$ , to respectively obtain the mean field equation and Fokker-Planck equation. To carry out the calculation explicitly one needs to expand the functions  $f_1, f_2, g_1, g_2$  with respect to the small parameter  $1/\sqrt{V}$ . As a representative example, we consider  $f_1$  and obtain:

$$f_1 \left( \phi_i + \frac{\xi_i}{\sqrt{V}}, \psi_i + \frac{\eta_i}{\sqrt{V}} \right) \approx f_1(\phi_i, \psi_i) + \frac{1}{\sqrt{V}} \frac{\partial f_1}{\partial \phi_i}(\phi_i, \psi_i) \xi_i + \frac{1}{\sqrt{V}} \frac{\partial f_1}{\partial \psi_i}(\phi_i, \psi_i) \eta_i + \dots \tag{3.19}$$

where the derivatives are evaluated at  $\xi_i = 0, \eta_i = 0$ . Similar results hold for  $f_2, g_1$  and  $g_2$ .

Let us introduce the new distribution

$$\Pi(\xi_i, \eta_i, t) = P(s_i(\phi_i(t), \xi_i), q_i(\psi_i(t), \eta_i), t), \tag{3.20}$$

where  $s_i(\phi_i(t), \xi_i)$  and  $q_i(\psi_i(t), \eta_i)$  are given by (3.18). Inserting into the master equation, and expanding the step operators to second order, one eventually obtains

$$\sum_{i=1}^{\Omega} \frac{\partial \Pi}{\partial t} - \frac{\partial \Pi}{\partial \xi_i} \sqrt{V} \dot{\phi}_i - \frac{\partial \Pi}{\partial \eta_i} \sqrt{V} \dot{\psi}_i = [A + B + C] \Pi, \tag{3.21}$$

where the contributions  $A, B, C$  take the following form:

$$\begin{aligned}
A &= \frac{1}{\Omega} \sum_{i=1}^{\Omega} \left\{ \frac{1}{\sqrt{V}} \left[ (f_2 - f_1) \frac{\partial}{\partial \xi_i} \right] + \right. \\
&\quad \left. + \frac{1}{V} \left[ \frac{\partial}{\partial \xi_i} \left( \frac{\partial f_2}{\partial \phi_i} - \frac{\partial f_1}{\partial \phi_i} \right) \xi_i + \frac{\partial}{\partial \xi_i} \left( \frac{\partial f_2}{\partial \psi_i} - \frac{\partial f_1}{\partial \psi_i} \right) \eta_i + \frac{1}{2} (f_1 + f_2) \frac{\partial^2}{\partial \xi_i^2} \right] \right\}, \\
B &= \frac{1}{\Omega} \sum_{i=1}^{\Omega} \left\{ \frac{1}{\sqrt{V}} \left[ (g_2 - g_1) \frac{\partial}{\partial \eta_i} \right] + \right. \\
&\quad \left. + \frac{1}{V} \left[ \frac{\partial}{\partial \eta_i} \left( \frac{\partial g_2}{\partial \phi_i} - \frac{\partial g_1}{\partial \phi_i} \right) \xi_i + \frac{\partial}{\partial \eta_i} \left( \frac{\partial g_2}{\partial \psi_i} - \frac{\partial g_1}{\partial \psi_i} \right) \eta_i + \frac{1}{2} (g_1 + g_2) \frac{\partial^2}{\partial \eta_i^2} \right] \right\}, \\
C &= \frac{\delta}{b\Omega} \sum_{i=1}^{\Omega} \sum_{j \in \{i-1, i+1\}} \left\{ \frac{1}{\sqrt{V}} \left[ \left( \frac{\partial}{\partial \xi_i} - \frac{\partial}{\partial \xi_j} \right) \phi_i + \left( \frac{\partial}{\partial \xi_j} - \frac{\partial}{\partial \xi_i} \right) \phi_j \right] + \right. \\
&\quad \left. + \frac{1}{V} \left[ \left( \frac{\partial}{\partial \xi_i} - \frac{\partial}{\partial \xi_j} \right) \xi_i + \left( \frac{\partial}{\partial \xi_j} - \frac{\partial}{\partial \xi_i} \right) \xi_j + \frac{1}{2} \left( \frac{\partial^2}{\partial \xi_i^2} + \frac{\partial^2}{\partial \xi_j^2} - 2 \frac{\partial}{\partial \xi_i} \frac{\partial}{\partial \xi_j} \right) (\phi_i + \phi_j) \right] \right\}.
\end{aligned}$$

### 3.4 Equations for the mean-field and the fluctuations

Introducing the rescaled time variable  $\tau \rightarrow t/\Omega V$ , we obtain from (3.21) at the order  $1/\sqrt{V}$  the following system of ordinary differential equations for the mean field concentrations  $\phi_i$  and  $\psi_i$ :

$$\begin{cases} \dot{\phi}_i = f_1(\phi_i, \psi_i) - f_2(\phi_i, \psi_i) + \delta \Delta \phi_i \\ \dot{\psi}_i = g_1(\phi_i, \psi_i) - g_2(\phi_i, \psi_i), \end{cases} \quad (3.22)$$

where  $\Delta = (\phi_{i+1} - 2\phi_i + \phi_{i-1})$ , the discrete Laplacian for  $a = 1$ . To proceed in the analysis we suppose that the homogeneous system:

$$\begin{cases} \dot{\phi}_i = f_1(\phi_i, \psi_i) - f_2(\phi_i, \psi_i) \equiv f(\phi_i, \psi_i) \\ \dot{\psi}_i = g_1(\phi_i, \psi_i) - g_2(\phi_i, \psi_i) \equiv g(\phi_i, \psi_i), \end{cases} \quad (3.23)$$

admits a fixed stable point  $(\hat{\phi}, \hat{\psi})$ . Notice that system (3.22), derived from a microscopic stochastic formulation, coincides with the general mean-field model (3.12) considered in Section 3.2.

The Fokker Planck equation that describes the dynamics of the fluctuations is obtained by considering the terms proportional to  $1/V$  in the master equation and reads as follows:

$$\frac{\partial}{\partial \tau} \Pi = \sum_{i=1}^{\Omega} \left( - \sum_{r=1}^2 \frac{\partial}{\partial \zeta_{r,i}} \left( \sum_{m=1}^2 \mathcal{J}_{rm,i} \zeta_{m,i} \Pi \right) + \frac{1}{2} \sum_{r,l=1}^2 \sum_{j=i-1}^{i+1} \frac{\partial}{\partial \zeta_{l,i}} \frac{\partial}{\partial \zeta_{r,j}} \left( \mathcal{B}_{rl,j}^{(i)} \Pi \right) \right). \quad (3.24)$$

Let us indicate as  $\vec{\zeta}_i = (\zeta_{1,i}, \zeta_{2,i})$  the vector  $(\xi_i, \eta_i)$  in (3.24). The  $2 \times 2$  matrices  $\mathcal{J}_i = \mathcal{J}_{rm,i}$  are given by

$$\mathcal{J}_i = \begin{pmatrix} \frac{\partial f_1}{\partial \phi_i} - \frac{\partial f_2}{\partial \phi_i} + \delta\Delta & \frac{\partial f_1}{\partial \psi_i} - \frac{\partial f_2}{\partial \psi_i} \\ \frac{\partial g_1}{\partial \phi_i} - \frac{\partial g_2}{\partial \phi_i} & \frac{\partial g_1}{\partial \psi_i} - \frac{\partial g_2}{\partial \psi_i} \end{pmatrix}, \quad (3.25)$$

and the three-vectors  $\mathcal{B}_{rl}^{(i)}$  are given by

$$\begin{aligned} \mathcal{B}_{11}^{(i)} &= (-\delta(\phi_i + \phi_{i-1}), \delta(\phi_{i-1} + 2\phi_i + \phi_{i+1}) + f_1(\phi_i, \psi_i) + f_2(\phi_i, \psi_i), -\delta(\phi_i + \phi_{i+1})), \\ \mathcal{B}_{12}^{(i)} = \mathcal{B}_{21}^{(i)} &= (0, 0, 0), \quad \mathcal{B}_{22}^{(i)} = (0, g_1(\phi_i, \psi_i) + g_2(\phi_i, \psi_i), 0). \end{aligned} \quad (3.26)$$

Note that, in the above expressions, the indices  $r$  and  $l$  label the species while the indices  $i$  and  $j$  refer to the cells. The matrix  $\mathcal{J}_i$  is the Jacobian matrix of  $(\phi_i, \psi_i) \mapsto (f_1 - f_2, g_1 - g_2)$ , modified with the inclusion of the spatial contribution represented by the discrete Laplacian.

Matrix  $\mathcal{B}$  can be cast in the more compact form:

$$\mathcal{B}_{rl,j}^{(i)} = (b_{rl}^{(0)} \delta_{i-j,0} + b_{rl}^{(1)} \delta_{|i-j|,1}) + b_{rl}^{(1)} \Delta, \quad (3.27)$$

where:

$$\begin{aligned} b^{(0)} &= \begin{pmatrix} 2\delta\hat{\phi} + f_1(\phi_i, \psi_i) + f_2(\phi_i, \psi_i) & 0 \\ 0 & g_1(\phi_i, \psi_i) + g_2(\phi_i, \psi_i) \end{pmatrix} \\ b^{(1)} &= \begin{pmatrix} -\delta\phi_i & 0 \\ 0 & 0 \end{pmatrix}. \end{aligned}$$

We are interested in studying the fluctuations around the fixed point, when the deterministic system is in a steady state, i.e. when  $(\phi_i, \psi_i) \equiv (\hat{\phi}, \hat{\psi}), \forall i$ . A powerful mean of investigation is the power spectrum of fluctuations, that allows us to resolve the typical spatio-temporal frequencies that are represented in the recorded signal. The analysis of the power spectrum is carried out in the next section.

### 3.5 Power Spectrum of fluctuations

The above Fokker-Planck equation is equivalent [29] to the Langevin equation:

$$\frac{d}{dt} \zeta_{r,i}(t) = \sum_{l=1}^2 \mathcal{J}_{rl,i} \zeta_{l,i}(t) + \lambda_{r,i}(t), \quad (3.28)$$

where  $\lambda_{r,i}(t)$  is a stochastic contribution which satisfies the following relations:

$$\langle \lambda_{l,i}(t), \lambda_{r,i'}(t') \rangle = \mathcal{B}_{lr,|i-i'|} \delta(t - t'), \quad (3.29)$$

$$\langle \lambda_{l,i}(t) \rangle = 0. \quad (3.30)$$

and  $\langle \cdot \rangle$  denotes expectation. Upon Fourier transform one gets:

$$-i\omega\tilde{\zeta}_{r,k}(\omega) = \sum_{l=1}^2 \tilde{\mathcal{J}}_{rl,k} \tilde{\zeta}_{l,k}(\omega) + \tilde{\lambda}_{r,k}(\omega), \quad (3.31)$$

where  $\tilde{(\cdot)}$  stands for the Fourier transform both in space and time. Notice that matrix  $\tilde{\mathcal{J}}_i$  coincides with the matrix  $\mathcal{J}_i$  given in (3.25) where the discrete Laplacian  $\Delta$ , is replaced by its Fourier transform  $\tilde{\Delta}_k$ . As previously remarked, and recalling that  $a = 1$ , one gets:

$$\tilde{\Delta}_k = 2(\cos(k) - 1). \quad (3.32)$$

Define

$$\Phi_{rl,k}(\omega) = -i\omega\delta_{rl} - \tilde{\mathcal{J}}_{rl,k},$$

then the solution of (3.31) reads:

$$\tilde{\zeta}_{r,k}(\omega) = \sum_{l=1}^2 \Phi_{rl,k}^{-1}(\omega) \tilde{\lambda}_{r,k}(\omega). \quad (3.33)$$

The power spectrum of the stochastic variable  $\zeta_{r,i}(t)$  is defined as:

$$P_r(k, \omega) = \left\langle |\tilde{\zeta}_{r,k}(\omega)|^2 \right\rangle. \quad (3.34)$$

Making use of condition (3.29) one gets:

$$P_r(k, \omega) = \left\langle |\tilde{\zeta}_{r,k}(\omega)|^2 \right\rangle = \sum_{l,p=1}^2 \Phi_{rl,k}^{-1}(\omega) \tilde{\mathcal{B}}_{lp,k} (\Phi^\dagger)_{rp,k}^{-1}(\omega). \quad (3.35)$$

By recalling expression (3.27) one gets:

$$\tilde{\mathcal{B}}_{lp,k} = (b_{lp}^{(0)} + 2b_{lp}^{(1)}) + b_{lp}^{(1)} \tilde{\Delta}_k, \quad (3.36)$$

which allows us to rewrite the power spectra in the form  $P_r(k, \omega)$  [24, 3]:

$$P_Z(k, \omega) \equiv P_1(k, \omega) = \frac{C_{Z,k} + \tilde{\mathcal{B}}_{11,k}\omega^2}{(\omega^2 - \Omega_0^2)^2 + \Gamma^2\omega^2}, \quad (3.37)$$

$$P_Y(k, \omega) \equiv P_2(k, \omega) = \frac{C_{Y,k} + \tilde{\mathcal{B}}_{22,k}\omega^2}{(\omega^2 - \Omega_0^2)^2 + \Gamma^2\omega^2}. \quad (3.38)$$

where the functions  $C_{Z,k}$  and  $C_{Y,k}$  are respectively defined:

$$C_{Z,k} = \tilde{\mathcal{B}}_{11,k}(\tilde{\mathcal{J}}_{22,k})^2 + \tilde{\mathcal{B}}_{22,k}(\tilde{\mathcal{J}}_{12,k})^2 - 2\tilde{\mathcal{B}}_{12,k}\tilde{\mathcal{J}}_{12,k}\tilde{\mathcal{J}}_{22,k}, \quad (3.39)$$

$$C_{Y,k} = \tilde{\mathcal{B}}_{22,k}(\tilde{\mathcal{J}}_{11,k})^2 + \tilde{\mathcal{B}}_{11,k}(\tilde{\mathcal{J}}_{21,k})^2 - 2\tilde{\mathcal{B}}_{12,k}\tilde{\mathcal{J}}_{21,k}\tilde{\mathcal{J}}_{11,k},$$

and

$$\Omega_0 = \sqrt{\det \hat{\mathcal{J}}_{rl,k}}, \quad (3.40)$$

$$\Gamma = -\text{Tr} \hat{\mathcal{J}}_{rl,k}. \quad (3.41)$$

In the above expression, the symbol  $(\hat{\cdot})$  indicates that from hereon the matrices are evaluated at the fixed point  $(\hat{\phi}, \hat{\psi})$ ;  $(\tilde{\cdot})$  stands instead for the spatial Fourier transform.

As anticipated, we are interested in studying the presence of stochastic stationary patterns. We remember that stochastic Turing patterns [53, 10] are signaled by the presence of at least a peak for the power spectrum in the direction of  $k$ , the spatial wavenumber, for  $\omega = 0$ , where  $\omega$  stands for the time frequency. We are therefore going to analyze the functions  $P_Z(k, 0) \equiv P_1(k, 0)$  and  $P_Y(k, 0) \equiv P_2(k, 0)$ , which respectively reads:

$$P_Z(k, 0) = \frac{C_{Z,k}}{\Omega_0^4} = \frac{b_{22}(\mathcal{J}_{11} + \delta\tilde{\Delta})^2 + (b_{11} - 2\hat{\phi}\delta\tilde{\Delta})\mathcal{J}_{21}^2}{(\det \mathcal{J} + \mathcal{J}_{22}\delta\tilde{\Delta})^2}, \quad (3.42)$$

$$P_Y(k, 0) = \frac{C_{Y,k}}{\Omega_0^4} = \frac{(b_{11} - 2\hat{\phi}\delta\tilde{\Delta})\mathcal{J}_{22}^2 + b_{22}\mathcal{J}_{12}^2}{(\det \mathcal{J} + \mathcal{J}_{22}\delta\tilde{\Delta})^2}, \quad (3.43)$$

where we have introduced:

$$b_{11} = f_1(\hat{\phi}, \hat{\psi}) + f_2(\hat{\phi}, \hat{\psi}), \quad (3.44)$$

$$b_{22} = g_1(\hat{\phi}, \hat{\psi}) + g_2(\hat{\phi}, \hat{\psi}). \quad (3.45)$$

To study the conditions that yield to one or more peaks, we need to calculate the power spectrum derivative. We make use of the notation  $g(k) \equiv \delta\tilde{\Delta} = 2\delta(\cos k - 1)$  and obtain the following general expression:

$$\frac{dP_j(k, 0)}{dk} = \frac{g'(k)}{(\det \mathcal{J} + \mathcal{J}_{22}g(k))^3} \{B_j g(k) + C_j\} \quad \text{for } j \in \{Z, Y\}, \quad (3.46)$$

where  $B_j$  and  $C_j$  are defined as:

$$B_Z = 2\hat{\phi}\mathcal{J}_{22}^3, \quad (3.47)$$

$$C_Z = -2\mathcal{J}_{22} \left( b_{11}\mathcal{J}_{22}^2 + b_{22}\mathcal{J}_{12}^2 + \hat{\phi}\mathcal{J}_{22} \det \mathcal{J} \right), \quad (3.48)$$

$$B_Y = 2\mathcal{J}_{21}(-b_{22}\mathcal{J}_{12} + \hat{\phi}\mathcal{J}_{21}\mathcal{J}_{22}), \quad (3.49)$$

$$C_Y = -2\mathcal{J}_{21}(b_{22}\mathcal{J}_{11}\mathcal{J}_{12} + \hat{\phi}\mathcal{J}_{21} \det \mathcal{J} + b_{11}\mathcal{J}_{22}\mathcal{J}_{21}). \quad (3.50)$$

Recall that  $J_{ij}$  are the entries of the Jacobian matrix of system  $(\phi_i, \psi_i) \mapsto (f_1 - f_2, g_1 - g_2)$  and  $b_{ij}$  are given by eqs. (3.45).

We observe that  $k = 0$  and  $k = \pi$  are always stationary points of  $P_j$ . In fact  $g'(k) = -2\delta \sin(k)$  is null if  $k = 0, \pi$ . To have additional stationary points of  $P_j$ , one should require the quantity  $B_j g(k) + C_j$  to vanish. This implies:

$$\cos(k) = 1 - \frac{C_j}{2\delta B_j}.$$

As  $\cos(k) \in [-1, 1]$ , it is necessarily the case that:

$$0 \leq \frac{C_j}{2\delta B_j} \leq 2. \quad (3.51)$$

Then, the derivative of  $P_j$  can be zero in  $k$  if  $B_j$  and  $C_j$  have the same sign. We indicate as  $k_1$  and  $k_2$ , the stationary wavenumbers different from  $\pi$ .

There are only two possible cases for the existence of  $k_1$  and  $k_2$ :

**(i) Existence condition of  $k_1, k_2$**

(a)  $B_j, C_j > 0$  and  $\delta \geq \frac{C_j}{4B_j}$ ,

(b)  $B_j, C_j < 0$  and  $\delta \geq \frac{|C_j|}{4|B_j|}$ .

We are interested to know whether  $k_1$  and  $k_2$  correspond to maxima or minima of  $P_j(k, 0)$ . To achieve this goal we calculate the second derivative of  $P_j(k, 0)$ :

$$\frac{d^2}{dk^2}P_j(k, 0) = \frac{g''(k)(B_jg(k) + C_j) + B_jg'(k)^2}{(\det \mathcal{J} + \mathcal{J}_{22}g(k))^3} - \frac{3\mathcal{J}_{22}g'(k)^2(B_jg(k) + C_j)}{(\det \mathcal{J} + \mathcal{J}_{22}g(k))^4}. \quad (3.52)$$

Remember that  $k_1$  and  $k_2$  are solution of  $B_jg(k) + C_j = 0$ . The expression of the second order derivative is therefore cast into the form:

$$\left. \frac{d^2}{dk^2}P_j(k, 0) \right|_{k=k_1, k_2} = \frac{B_jg'(k)^2}{(\det \mathcal{J} + \mathcal{J}_{22}g(k))^3}. \quad (3.53)$$

The nature of the stationary points  $k_1$  and  $k_2$  depends on the sign of both the denominator and  $B_j$  in (3.53). In particular, if we require that the points are maxima, or equivalently the second derivative in  $k_1$  and  $k_2$  has a negative sign, we must check one of the two following conditions:

**(ii) Maximum conditions for points  $k_1, k_2$**

(a)  $B_j < 0$  and  $\left. \det \mathcal{J} + \mathcal{J}_{22}g(k) \right|_{k=k_1, k_2} > 0$ ,

(b)  $B_j > 0$  and  $\left. \det \mathcal{J} + \mathcal{J}_{22}g(k) \right|_{k=k_1, k_2} < 0$ .

As anticipated we shall consider the case of a self-inhibitory non mobile species, which corresponds to requiring  $\mathcal{J}_{22} < 0$ . The denominator in (3.53) is then always positive, while  $g(k)$  is by definition negative. Accordingly, the kind of stationary points  $k_1$  and  $k_2$  depend on the sign of  $B_j$ . In particular, for the condition of maximum **(ii)**,  $B_j$  must be negative.

To characterize whether the other stationary points  $0, \pi$  are maxima or minima, we should again turn to evaluating the second derivatives for such choices of  $k$ . As  $g'(0) = 0$ , then equation (3.52) is:

$$\left. \frac{d^2}{dk^2}P_j(k, 0) \right|_{k=0} = \frac{g''(0)(B_jg(0) + C_j)}{(\det \mathcal{J} + \mathcal{J}_{22}g(\pi))^3} = \frac{-2\delta C_j}{(\det \mathcal{J} - 4\delta \mathcal{J}_{22})^3}. \quad (3.54)$$

Therefore  $k = 0$  is a maximum, if one of the following conditions is true:



**(iii) Maximum condition for  $k = 0$** 

$$(a) \begin{cases} -2\delta C_j < 0 \\ (\det \mathcal{J} - 4\delta \mathcal{J}_{22}) > 0. \end{cases} \quad (b) \begin{cases} -2\delta C_j > 0 \\ (\det \mathcal{J} - 4\delta \mathcal{J}_{22}) < 0. \end{cases}$$

Since by assumption  $\mathcal{J}_{22} < 0$ , condition **(iii)**(b) cannot be met. This is because the quantity  $\det \mathcal{J} - 4\delta \mathcal{J}_{22}$  is positive, as  $\det \mathcal{J} > 0$  since we have assumed that  $(\hat{\phi}, \hat{\psi})$  is a stationary stable fixed point. The nature of the stationary point  $k = 0$  ultimately depends on the sign of  $C_j$ . If  $C_j > 0$ , it is a maximum point, while, if  $C_j < 0$ , it is a minimum.

Consider now  $k = \pi$  and observe that  $g'(\pi) = 0$ . Equation (3.52) reads:

$$\frac{d^2}{dk^2} P_j(k, 0) \Big|_{k=\pi} = \frac{g''(\pi)(B_j g(\pi) + C_j)}{(\det \mathcal{J} + \mathcal{J}_{22} g(\pi))^3} = \frac{2\delta(-4\delta B_j + C_j)}{(\det \mathcal{J} - 4\delta \mathcal{J}_{22})^3}. \quad (3.55)$$

For having a maximum in  $k = \pi$  one of the following conditions must be satisfied:

**(iv) Maximum condition for  $k = \pi$** 

$$(a) \begin{cases} -4\delta B_j + C_j < 0 \\ (\det \mathcal{J} - 4\delta \mathcal{J}_{22}) > 0. \end{cases} \quad (b) \begin{cases} -4\delta B_j + C_j > 0 \\ (\det \mathcal{J} - 4\delta \mathcal{J}_{22}) < 0. \end{cases}$$

Since  $\mathcal{J}_{22} < 0$ , the condition **(iii)**(b) is never satisfied: as already remarked, the term  $\det \mathcal{J} - 4\delta \mathcal{J}_{22}$  is in fact always positive.

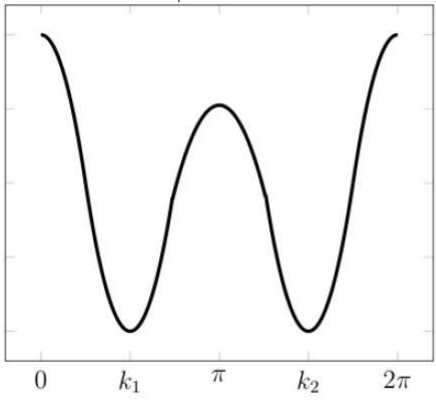
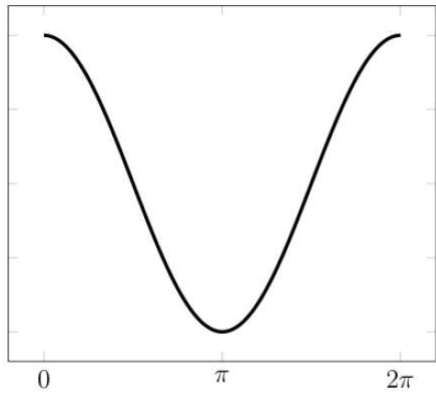
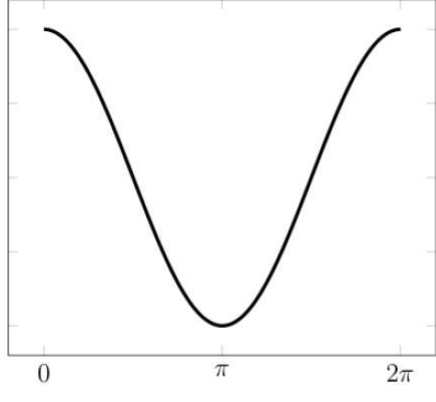
Notice that, if  $k = \pi$  is a maximum the values  $k = k_1$  and  $k = k_2$  are minima. Otherwise if  $k_1$  and  $k_2$  are maxima,  $k = \pi$  is a minimum. To show this, let us consider two different cases, respectively  $B_j < 0$  and  $B_j > 0$ .

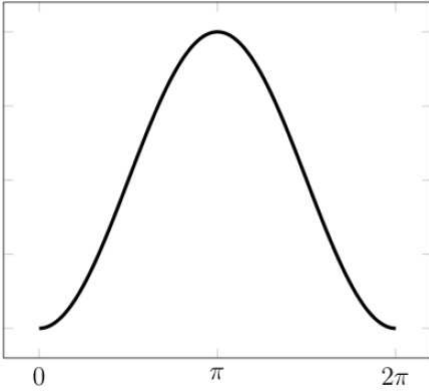
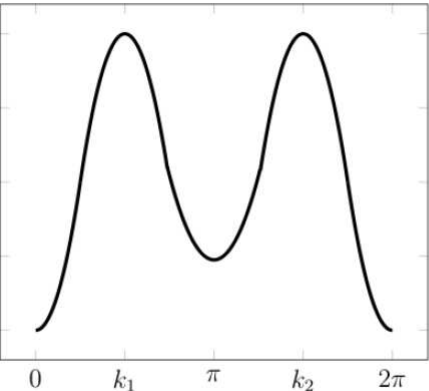
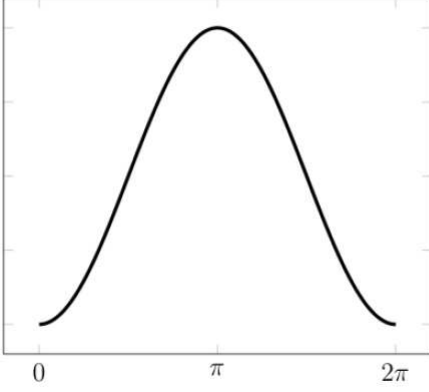
If  $B_j < 0$  and, at the same time, condition **(i)** is satisfied, then  $k_1$  e  $k_2$  exist. In this case, the condition **(ii)**(a) guarantees that the stationary points else than  $\pi$  are maxima. Indeed,  $B_j < 0$  and  $(\det \mathcal{J} + \mathcal{J}_{22} g(k)) \Big|_{k=k_1, k_2}$  is positive. The condition for having a maximum in  $k = \pi$ , namely  $-4\delta B_j + C_j < 0$ , is in contradiction with **(i)**. If  $B_j, C_j < 0$ , in fact, we can write  $-4\delta B_j + C_j < 0$ . Taking into account the signs of the quantities involved, it results  $4\delta|B_j| - |C_j| < 0$ , which implies  $\delta < \frac{|C_j|}{4|B_j|}$ , in disagreement with the condition **(i)**. In conclusion  $k = \pi$  is necessarily a minimum.

Let us now turn to considering the case  $B_j > 0$ . To have the existence of  $k_1$  and  $k_2$  one must impose  $C_j > 0$  and  $\delta > \frac{C_j}{4B_j}$ . Clearly, condition **(ii)** cannot be then satisfied and the two stationary points are minima. A maximum is instead found in  $k = \pi$ , as dictated by condition **(iv)**(b).

A summary of the above results is given in the Tables annexed below, where the different scenarios are highlighted depending on the sign of the reference quantities. We recall that our results have been derived under the hypothesis of discrete lattice spacing  $a$  (set to one in the calculations). Similar Tables can be in principle obtained for the case of a spatially continuum lattice, i.e. when  $a \rightarrow 0$  and  $g(k) \equiv -\delta k^2$ . It can be however shown [24, 3] that the power spectrum of fluctuations scales with an amplitude prefactor proportional to  $a^d$ ,  $d$  being the dimension of the embedding space ( $d = 1$ , in our case). Hence, in the limit  $a \rightarrow 0$ , fluctuations fade away and the stochastic pattering is not

detectable. However, as remarked in [53], another continuum limit can be performed, starting from the same microscopic discrete formulation. One could in fact imagine to keep patch dimension to a constant, while sending to infinity both  $\omega$  and the linear size of the physical space which hosts the system under scrutiny. This is indeed the case considered in [56]: working under this alternative scenario, fluctuations, and so the triggered patterns, are persistent also in the continuum limit. The choice of operating with patches of finite size, where microscopic constituents are supposed well mixed, and accounting for the possibility of jumping towards neighbor patches of a finite lattice, proves useful when modeling ecological systems [55], or in cellular biology, the space inside the membrane being partitioned in macro compartments and organelles [19], but also for studying chemical systems as e.g. the device introduced in [57].

$\mathcal{I}_{22} < 0$	$C_j > 0$
$B_j > 0$	<p data-bbox="435 220 1177 262"><math>\delta \geq \frac{C_j}{4B_j} \quad \exists \quad k_1 \text{ and } k_2 \text{ and are minima. Maxima are found in } k = 0, \pi, 2\pi</math></p> <div data-bbox="406 315 933 714" style="text-align: center;">  <p data-bbox="406 451 446 546" style="transform: rotate(-90deg);"><math>P_j(k, 0)</math></p> </div> <p data-bbox="365 787 1242 829"><math>\delta &lt; \frac{C_j}{4B_j} \quad \nexists \quad k_1 \text{ and } k_2. \quad k = 0 \text{ and } k = 2\pi \text{ are maxima. A minimum is found in } k = \pi.</math></p> <div data-bbox="406 892 933 1291" style="text-align: center;">  <p data-bbox="406 1029 446 1123" style="transform: rotate(-90deg);"><math>P_j(k, 0)</math></p> </div>
$B_j < 0$	<p data-bbox="422 1375 1193 1407"><math>\nexists \quad k_1 \text{ and } k_2. \quad k = 0 \text{ and } k = 2\pi \text{ are maxima. A minimum is found in } k = \pi.</math></p> <div data-bbox="406 1470 933 1869" style="text-align: center;">  <p data-bbox="406 1606 446 1701" style="transform: rotate(-90deg);"><math>P_j(k, 0)</math></p> </div>

$\mathcal{J}_{22} < 0$	$C_j < 0$
$B_j > 0$	<p data-bbox="345 216 1222 243"><math>\exists k_1</math> and <math>k_2</math>. <math>k = \pi</math> is always a maximum. Two minima are found in <math>k = 0</math> and <math>k = 2\pi</math></p> <div data-bbox="386 310 906 699">  <p data-bbox="386 447 418 531"><math>P_j(k, 0)</math></p> <p data-bbox="508 674 889 699">0                      <math>\pi</math>                      <math>2\pi</math></p> </div>
$B_j < 0$	<p data-bbox="451 768 1109 810"><math>\delta &gt; \frac{C_j}{4B_j} \quad \exists k_1</math> and <math>k_2</math> and are maxima. <math>k = 0, \pi, 2\pi</math> are minima.</p> <div data-bbox="386 863 906 1251">  <p data-bbox="386 999 418 1083"><math>P_j(k, 0)</math></p> <p data-bbox="508 1226 889 1251">0                      <math>k_1</math>                      <math>\pi</math>                      <math>k_2</math>                      <math>2\pi</math></p> </div> <p data-bbox="345 1346 1222 1388"><math>\delta &lt; \frac{C_j}{4B_j} \quad \exists k_1</math> and <math>k_2</math>. <math>k = 0</math> and <math>k = 2\pi</math> are minima. A maximum is found in <math>k = \pi</math>.</p> <div data-bbox="386 1461 906 1850">  <p data-bbox="386 1598 418 1682"><math>P_j(k, 0)</math></p> <p data-bbox="508 1824 889 1850">0                      <math>\pi</math>                      <math>2\pi</math></p> </div>

### 3.6 A simple stochastic reaction–diffusion model

We have so far demonstrated that stochastic Turing patterns exist for reaction-diffusion models, defined on a discrete lattice, in which only one species diffuses. Working in a general context, we elaborated on the conditions which lead to Turing pattern, mediated by demographic noise.

As an application of the results discussed above, we consider a specific stochastic reaction-diffusion model, which can be cast in the form specified by (3.15) and (3.16). We choose in particular:

$$f_1\left(\frac{s_i}{V}, \frac{q_i}{V}\right) = \eta_1 \quad (3.56)$$

$$f_2\left(\frac{s_i}{V}, \frac{q_i}{V}\right) = \eta_2 \left(\frac{s_i}{V}\right)^p + \eta_3 \left(\frac{q_i}{V}\right)^n \quad (3.57)$$

$$g_1\left(\frac{s_i}{V}, \frac{q_i}{V}\right) = \eta_4 \quad (3.58)$$

$$g_2\left(\frac{s_i}{V}, \frac{q_i}{V}\right) = \eta_5 \left(\frac{s_i}{V}\right)^p + \eta_6 \left(\frac{q_i}{V}\right)^n, \quad (3.59)$$

to define the microscopic reaction rates implicated in chemical equations (3.15). Here  $\eta_i$  are positive real numbers, while  $p$  and  $t$  are integers. We will set  $p = 4$  and  $n = 1$ . Note that the proposed model has no specific applied interest: it is solely introduced for demonstrative purposes, aiming at testing the validity of the mathematical analysis developed above.

In the mean-field approximation, one gets:

$$\begin{cases} \frac{\partial \phi_i}{\partial t} = -\eta_2 \phi_i^p - \eta_3 \psi_i^n + \eta_1 + \delta \Delta \phi_i \\ \frac{\partial \psi_i}{\partial t} = -\eta_5 \phi_i^p - \eta_6 \psi_i^n + \eta_4. \end{cases} \quad (3.60)$$

To calculate homogeneous fixed point  $(\hat{\phi}, \hat{\psi})$  of system (3.60) one needs to solve the following equations:

$$\begin{cases} -\eta_2 \hat{\phi}^p - \eta_3 \hat{\psi}^n + \eta_1 = 0 \\ -\eta_5 \hat{\phi}^p - \eta_6 \hat{\psi}^n + \eta_4 = 0. \end{cases} \quad (3.61)$$

which immediately yield:

$$\hat{\phi} = \left( \frac{\eta_1 \eta_6 - \eta_3 \eta_4}{\eta_2 \eta_6 - \eta_3 \eta_5} \right)^{1/p} \quad (3.62)$$

$$\hat{\psi} = \left( \frac{\eta_2 \eta_4 - \eta_1 \eta_5}{\eta_2 \eta_6 - \eta_3 \eta_5} \right)^{1/n}. \quad (3.63)$$

The parameters are to be in turn assigned so that the above fixed point is real and positive, a condition on which we shall return in the following. Furthermore, we require  $(\hat{\phi}, \hat{\psi})$  to be a stable fixed point, so to match the theory prescriptions. The trace of the Jacobian matrix  $\mathcal{J}$  associated to the homogeneous (a-spatial) version of system (3.60) reads:

$$\text{Tr}(\mathcal{J}) = - \left( \eta_2 p \hat{\phi}^{p-1} + \eta_6 n \hat{\psi}^{n-1} \right). \quad (3.64)$$

The trace is therefore always negative, for any choice of the parameters which returns a physically sound ( $\hat{\phi}, \hat{\psi} > 0$ ) homogeneous fixed point. For the fixed point to be stable, one should further impose:

$$\det(\mathcal{J}) = (\eta_2 \eta_6 - \eta_3 \eta_5) p n \hat{\phi}^{p-1} \hat{\psi}^{n-1} > 0. \quad (3.65)$$

This latter condition translates in:

$$\eta_3 < \left( \frac{\eta_2}{\eta_5} \right) \eta_6 \equiv \gamma_1 \eta_6, \quad (3.66)$$

where we brought into evidence the dependence on  $\eta_6$  and  $\eta_3$ , since they will later on act as control parameters. By using the above condition (3.66) into equations (3.62) the condition for positive concentrations  $\hat{\phi}, \hat{\psi} > 0$  gives:

$$\eta_2 \quad \eta_4 - \eta_1 \eta_5 \equiv \gamma_2 > 0, \quad (3.67)$$

$$\eta_3 < \left( \frac{\eta_1}{\eta_4} \right) \eta_6 \equiv \gamma_3 \eta_6. \quad (3.68)$$

The homogeneous fixed point ( $\hat{\phi}, \hat{\psi}$ ) determined above exists and it is stable, provided conditions (3.66) and (3.67) are simultaneously met. Moreover, and as discussed in the first part of the chapter, the spatially extended system (3.60) cannot experience a (deterministic) Turing instability since  $g_{\psi} = -n \eta_6 \hat{\psi}^{n-1}$  is by definition negative. The homogeneous fixed point is hence a stable, although trivial attractor of the spatial deterministic model.

A different scenario holds instead when the stochastic version of the deterministic model (3.60) is considered. As we will show, it is in fact possible to assign the model parameters so as to generate a power spectrum of the stochastic fluctuations with two maxima for non trivial values of  $k_1$  and  $k_2$ , for  $\omega = 0$ . These maxima are interpreted as the signature of stochastic Turing patterns.

To this end we fix all parameters to nominal, arbitrarily chosen values, except for  $\eta_3$  and  $\eta_6$  which can be tuned. We will then adjust  $\eta_3$  and  $\eta_6$  so to match conditions **(i)** and **(ii)**, as outlined in the preceding section. This results in region II of the parameter plane, as depicted in Figure 3.1. Conversely, in region I the power spectrum of fluctuations is predicted to display an isolated maximum for  $k = 0$ .

In Figure 3.2(b) we plot a two dimensional view of the theoretical power spectrum for a choice of the parameters ( $\eta_6, \eta_3$ ) which falls in region II. The predicted profile is just displayed in the interval  $k \in [0, \pi]$ : a peak is present for a value of  $k$  smaller than  $\pi$ . A second, specular, peak is clearly found for  $k > \pi$ . The two maxima of the power spectrum occur for  $\omega = 0$ . They correspond therefore to stationary non homogeneous patterns. To validate the theory predictions we performed direct numerical simulations, by means of the Gillespie algorithm [28]. This is a Monte Carlo based scheme which produces realizations of the stochastic dynamics equivalent to those obtained from the governing master equation. The power spectrum calculated by averaging over a large collection of independent realizations of the stochastic dynamics is depicted in Figure 3.2(a), showing

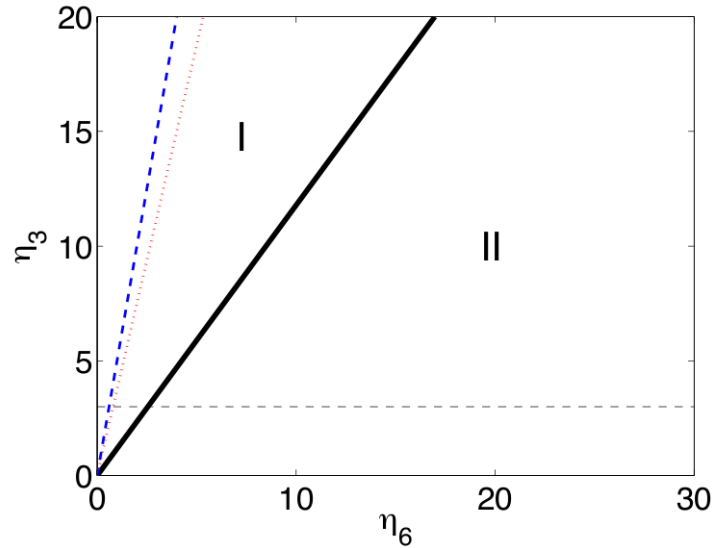


Figure 3.1: The plane  $(\eta_6, \eta_3)$  is partitioned into two regions. In region II, the power spectrum of fluctuations is predicted to display two peaks in, respectively,  $k_1$  and  $k_2$ . These are positions symmetric with respect to  $\pi$ . In region I the power spectrum has instead a maximum in  $k = 0$ . The parameters are  $\eta_1 = 15$ ;  $\eta_2 = 20$ ;  $\eta_4 = 4$ ;  $\eta_5 = 4$ ;  $\delta = 42.9473$ . With this choice,  $\gamma_1 = 4$ ;  $\gamma_3 = 20 > 0$ ;  $\gamma_3 = 3.75$ . The two lines which cross the origin represent respectively the two conditions  $\eta_3 = \gamma_1 \eta_6$  (blue online) and  $\eta_3 = \gamma_3 \eta_6$  (red online). Region I is delimited by this latter and the thick solid line which marks the transition to the adjacent region II. The horizontal dashed lines is drawn at  $\eta_3 = 3$ : the data reported in the following figures (3.2) and (3.3) refer to choices of the parameters that fall on such a line.

a good agreement with the corresponding theoretical profile. This confirms the validity of the analysis developed above, and summarized in the Tables presented above.

In figure 3.3, the position of the maxima of the power spectrum of species  $Z$  is plotted as a function of the control parameter  $\eta_6$ , while  $\eta_3$  is set to the value that corresponds to the dashed horizontal line in figure 3.1. This results in a bifurcation diagram from zone I to zone II. A similar plot can be obtained for the co-evolving species  $Y$ . The solid line stands for the theoretical predictions, which follows the results summarized in the Tables annexed above. A transition from zone I (one isolated peak) to zone II (two symmetric peaks) is predicted to occur at  $\eta_6 \simeq 2.5$ . The symbols in figure 3.1 refer to the position of the power spectrum as obtained via direct simulations and confirms the correctness of the theoretical scenario.

A final comment is mandatory at this point. Fluctuations driven patterns are stochastic in nature: as such they are not stationary, unlike their deterministic analogue. Stochastic patterns continuously decay, while they are recreated by the effect of the noise [58]. In general, the noisy nature of the patterns makes them hard to detect by visual inspection. The emergence of a length scale become often clear only via a Fourier analysis. This is the case for the simple model here investigated for demonstrative reasons: the patterns emerging from one single realization are indeed masked by a large amount of noise (data not shown). Similar conclusion are reached in [59] where stochastic simulations for the

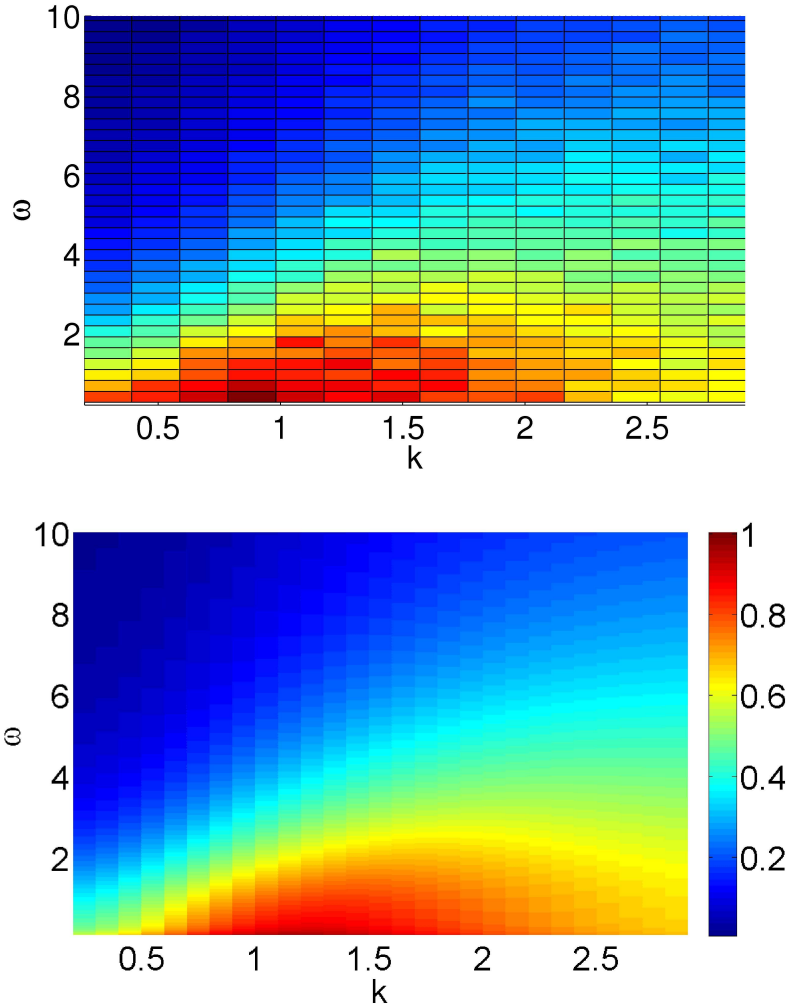


Figure 3.2: In the above panel, the numerical power spectrum of the fluctuations for species  $Z$  is represented, with an appropriate color code, in the plane  $(\omega, k)$ , for a choice of the parameters that fall in region I of Figure 3.1. Specifically, we have set  $\eta_6 = 25$ ,  $\eta_3 = 3$ . The other parameters are set to the values specified in the caption of Figure 3.1. Here  $V = 5000$  and  $\Omega = 32$ . The numerical power spectrum is obtained by averaging over 200 independent realizations based on the Gillespie algorithm. A peak is found in the interval  $[0, \pi]$ . A symmetric maximum exists in  $[\pi, 2\pi]$  (non displayed). In the below panel the power spectrum calculated analytically is plotted and shown to agree with the numerical result. The power spectra are normalized so to have maximum equal to unit. The color bar applies to both panels.

Schnakenberg kinetics [60] are carried out just outside the (deterministic) region of Turing order. On the other hand, patterns can possibly become more distinct depending on the simulated model, the dimensionality of the system ( $1D$  vs.  $2D$ ) and the structure (lattice vs. network) of the embedding space. For the Levin-Segel model [61] studied in two dimension [53], stochastic patterns are quite visible at the naked eye. Similarly, robust



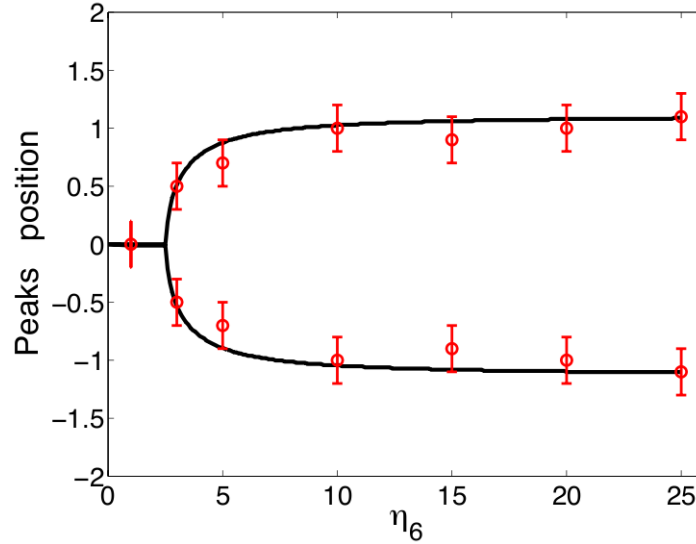


Figure 3.3: A bifurcation diagram is displayed, which exemplifies the transition from zone I to zone II. More specifically, the position of the peaks of the power spectrum of species  $Z$  is plotted as a function of the control parameter  $\eta_6$ . Here,  $\eta_3 = 3$ , a value that corresponds to the horizontal dashed line in figure 3.2. The solid line stands for the theory prediction, while the symbols refer to direct simulations of the stochastic dynamics. The simulations are averaged over 150 independent realizations. The error in the location of the peak is assumed as twice the spacing of the imposed wavelength mesh.

and rather distinct patterns are found when a stochastic reaction model of the Brusselator type [62] is defined on a network topology [63]. Also, quasi-waves patterns found in [56] for a modified version of the Brusselator model with long range couplings, stand out rather clearly from one single realization of the stochastic dynamics. The search for the necessary ingredients that make stochastic pattern accessible at visual inspection, remains however an important and still open question that deserves to be further addressed.

### 3.7 Conclusion

Pattern formation is an important domain of study which finds many applications in distinct contexts of interest, including ecology, biology and chemistry. The Turing instability is one of the mechanisms that can be invoked to explain the emergence of stationary stable, spatially ordered patterns in reaction-diffusion models. These latter are systems of coupled partial differential equations which govern the time and space evolution of the continuum concentrations of constituents. As such, reaction diffusion models are deterministic in nature. They omit the stochastic contributions that need to be included when dealing with finite populations and, in this respect, represent an idealized approach to the modeling of the inspected phenomena. The classical, deterministic theory for the Turing instability requires that at least two species diffuse in a domain in which they are confined: the diffusion potentially leads to an instability in following a perturbation of a stable equilibrium of the homogeneous system. Conversely, if just one species is allowed to diffuse the Turing instability is always precluded, when the system is defined on a

continuum support. Working on a discrete lattice, Turing patterns in principle develop, but just for a trivial choice of the most unstable wave number and limited to models that assume the non diffusing species to operate as a self-activator.

Beyond the deterministic viewpoint, in the last few years the concept of stochastic Turing instability has been introduced in the literature [53, 10]: discrete systems, made of a large though finite number of constitutive entities, can generate stochastic order on a macroscopic scale, as follows a resonant mechanism which self-consistently amplifies the intrinsic demographic noise. Elaborating on this concept, we have considered a general stochastic reaction diffusion model, with just one diffusing species, and showed that stochastic Turing patterns are indeed possible also when the non mobile species has a self-inhibitory capability, i.e. a condition for which deterministic patterns are a priori excluded. General analytical conditions for the existence of the stochastically driven patterns are given. The predictions are tested numerically working with a simplified model that falls in the general class of systems for which the theory has been developed. The quantitative agreement observed between theory and simulations points to the validity of our analysis, which, we believe, could open up novel perspectives to tackle the problem of pattern formation beyond the classical deterministic picture.

## Chapter 4

# The effect of crowding in Brussellator-type models

In the previous chapter we have introduced the classical concept of Turing instability in the mean-field context. Then we have characterized in details, the emergence of stochastic Turing pattern, as signalled by the power spectrum of fluctuations. Making explicit reference to a particularly simple setting when only one species is allowed to diffuse. In this final chapter we will elaborate on the role of molecular crowding, in relation to the problem of pattern formation. The effect of crowding result in cross terms in the diffusion operator. The presence of these terms can modify the classical Turing picture and as well as the corresponding stochastic analogue. In particular, the Turing instability can set in for all ratios of the diffusivities, also when the activator diffuses faster than the inhibitor. This conclusion, here demonstrated for the Brussellator model, is at odds with the classical Turing paradigm. Stochastic patterns are also studied for a generalized version of the Brussellator model with long-range coupling.

### 4.1 Turing instabilities in reaction-diffusion systems with cross diffusion

According to the classical viewpoint, in order to observe Turing patterns, the diffusion coefficient of the inhibitor species has to be larger than that of the activator, for the patterns to eventually develop. This is a strict mathematical constraint which is not always met in e.g. contexts of biological relevance [64, 65], and which limits the possibility of establishing a quantitative match between theory and empirical data. Spatially extended systems made of interacting species sharing similar diffusivities can indeed display self-organized patched patterns, an observation that still calls for a sound interpretative scenario, beyond the classical Turing mechanisms [9].

One viable strategy to possibly reconcile theory and observations has been explored in [53] and [10]. In these studies, the authors considered the spontaneous emergence of persistent spatial patterns as mediated by the demographic endogenous noise, stemming from the intimate discreteness of the scrutinized system. The intrinsic noise translates into a systematic enlargement of the parameter region yielding the Turing order, when compared to the corresponding domain predicted within the deterministic linear stability analysis. It is however unclear at present whether experimentally recorded patterns bear

the imprint of the stochasticity, a possibility that deserves to be further challenged in the future.

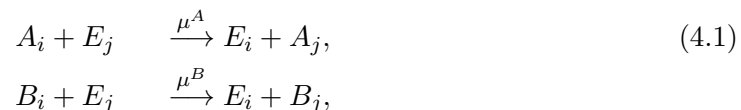
Alternatively, and to bridge the gap with the experiments, the Turing instability concept has been applied to generalized reaction–diffusion equations. These latter account for cross diffusion terms which are hypothesized to exist on purely heuristic grounds or by invoking the phenomenological theory of linear non–equilibrium thermodynamics [66, 67, 68]. Diagonal and off–diagonal coefficients of the diffusion matrix are not linked to any microscopic representation of the examined dynamics and are hence treated as free parameters of the model. In [69] the authors quantify the impact of cross terms on the Turing bifurcation, showing e.g. that spatial order can materialize also if the inhibitor’s diffusion ability is less pronounced than the activator’s one.

Starting from this setting, the aims of this chapter are twofold. On the one side, we shall elaborate on a microscopic theory of multispecies diffusion, fully justified from first principles. The theory here derived is specifically targeted to the two species case study and extends beyond the formulation of [70]. On the other side, and with reference to the Brusselator model, we will show that Turing patterns can take place for any ratio of the main diffusivities. In doing so we will cast the conclusions of [69] into a descriptive framework of broad applied and fundamental interest, where the key cross diffusion ingredients are not simply guessed a priori but rigorously obtained via a self–consistent derivation anchored to the microscopic world. Working in the context of a reference case study, the Brusselator model, we shall also perform numerical simulations based on both the underlying stochastic picture and the idealized mean–field formulation to elaborate on the robustness of the observed patterns.

In the following we briefly discuss the derivation of the model, focusing on the specific case where two species are supposed to diffuse, sharing the same spatial reservoir.

#### 4.1.1 The Diffusion model

Consider a generic microscopic system bound to occupy a given volume of a  $d$ –dimensional space. Assume the volume to be partitioned into a large number  $\Omega$  of small hypercubic patches, each of linear size  $l$ . Each mesoscopic cell, labelled by  $i$ , is characterized by a finite carrying capacity: it can host up to  $N$  particles, namely  $n_i^A$  of type  $A$ ,  $n_i^B$  of type  $B$ , and  $e_i = N - n_i^A - n_i^B$  vacancies, hereafter denoted by  $E$ . In general, the species will also interact, as dictated by specific reaction terms. Let us start by solely focusing on the diffusion part, silencing any direct interaction among elementary constituents. As we shall remark, there exists an indirect degree of coupling that results from the competition for the available spatial resources. In practice, the mobility of the particles is balked if the neighbouring patches have no vacancies. Particles may jump into a nearest–neighbour patch, only if there is a vacancy to be eventually filled. This mechanism translates into the following chemical equation



where  $i$  and  $j$  label nearest–neighbour patches. Here,  $A_i$  and  $B_i$  identify the particles that belong to cell  $i$ .  $E_i$  labels instead the empties that are hosted in patch  $i$ . The parameters  $\mu^A$  and  $\mu^B$  stand for the associated reaction rates. Similar reactions control the migration from cell  $j$  towards cell  $i$ .

In addition, and extending beyond the scheme proposed in [70], we imagine the following reactions to hold:



which in practice account for the possibility that elements  $A_i$  (resp.  $A_j$ ) and  $B_j$  (resp.  $B_i$ ) swap their actual positions.

The state of the system is then specified by the number of  $A$  and  $B$  particles in each patch, the number of vacancies following from a straightforward normalization condition. Introduce the vector  $\mathbf{n} = (\mathbf{n}_1, \dots, \mathbf{n}_\Omega)$ , where  $\mathbf{n}_i = (n_i^A, n_i^B)$ . The quantity  $T(\mathbf{n}'|\mathbf{n})$  represents the rate of transition from state  $\mathbf{n}$ , to another state  $\mathbf{n}'$ , compatible with the former. The transition rates associated with the migration between nearest-neighbour, see Eqs. (4.1), take the form

$$T(n_i^{(a)} - 1, n_j^{(a)} + 1 | n_i^{(a)}, n_j^{(a)}) = \frac{\mu^{(a)}}{z\Omega} \frac{n_i^{(a)}}{N} \frac{N - n_j^A - n_j^B}{N}, \quad (4.3)$$

with  $a = A, B$  and where we have made explicit in  $T(\cdot|\cdot)$  the components that are affected by the reactions. As discussed in [70], the factor  $N - n_j^A - n_j^B$ , reflects the natural request of a finite capacity, and will eventually yield a macroscopic modification of the Fick's law of diffusion. Moreover, chemical equations (4.2) result in the following transition rates:

$$\begin{aligned} T(n_i^A - 1, n_j^A + 1, n_i^B + 1, n_j^B - 1 | n_i^A, n_j^A, n_i^B, n_j^B) &= \frac{\alpha}{z\Omega} \frac{n_i^A}{N} \frac{n_j^B}{N}, \\ T(n_i^A + 1, n_j^A - 1, n_i^B - 1, n_j^B + 1 | n_i^A, n_j^A, n_i^B, n_j^B) &= \frac{\alpha}{z\Omega} \frac{n_j^A}{N} \frac{n_i^B}{N}. \end{aligned}$$

The process here imagined is Markov, and the probability  $P(\mathbf{n}, t)$  to observe the system in state  $\mathbf{n}$  at time  $t$  is ruled by the master equation

$$\frac{dP(\mathbf{n}, t)}{dt} = \sum_{\mathbf{n}' \neq \mathbf{n}} [T(\mathbf{n}|\mathbf{n}')P(\mathbf{n}', t) - T(\mathbf{n}'|\mathbf{n})P(\mathbf{n}, t)], \quad (4.4)$$

where the allowed transitions depend on the state of the system via the above relations. Starting from this microscopic, hence inherently stochastic picture, one can derive a self-consistent deterministic formulation, which exactly holds in the continuum limit. Mathematically, one needs to obtain the dynamical equations that govern the time evolution of the ensemble averages  $\langle n_i^A \rangle$  and  $\langle n_i^B \rangle$ . To this end, multiply first the master Eq. (4.23) by  $n_i^a$ , with  $a = A, B$ , and sum over all  $\mathbf{n}$ . After an algebraic manipulation which necessitates shifting some of the sums by  $\pm 1$ , one eventually gets

$$\begin{aligned} \frac{d}{dt} \langle n_i^{(a)} \rangle &= \sum_{j \in i} \left[ \langle T(n_i^{(a)} + 1, n_j^{(a)} - 1 | n_i^{(a)}, n_j^{(a)}) \rangle - \langle T(n_i^{(a)} - 1, n_j^{(a)} + 1 | n_i^{(a)}, n_j^{(a)}) \rangle \right. \\ &\quad + \langle T(n_i^A + 1, n_j^A - 1, n_i^B - 1, n_j^B + 1 | n_i^A, n_j^A, n_i^B, n_j^B) \rangle \\ &\quad \left. - \langle T(n_i^A - 1, n_j^A + 1, n_i^B + 1, n_j^B - 1 | n_i^A, n_j^A, n_i^B, n_j^B) \rangle \right], \end{aligned} \quad (4.5)$$

where the notation  $\sum_{j \in i}$  means that we are summing over all patches  $j$  which are nearest-neighbours of patch  $i$ . The averages in Eq. (4.5) are performed explicitly by recalling

the expression for the transition rates as given in Eqs. (4.3) and (4.4). Replace then the averages of products by the products of averages, an operation that proves exact in the continuum limit  $N \rightarrow \infty$ . By introducing the continuum concentration  $(\phi_{A,B})_i = \lim_{N \rightarrow \infty} \frac{\langle n_i^{A,B} \rangle}{N}$ , rescaling time by a factor of  $N\Omega$  and taking the size of the patches to zero one finally gets<sup>1</sup>

$$\begin{aligned} \frac{\partial \phi_A}{\partial t} &= D_{11} \nabla^2 \phi_A + D_{12} [\phi_A \nabla^2 \phi_B - \phi_B \nabla^2 \phi_A], \\ \frac{\partial \phi_B}{\partial t} &= D_{22} \nabla^2 \phi_B + D_{21} [\phi_B \nabla^2 \phi_A - \phi_A \nabla^2 \phi_B], \end{aligned} \quad (4.6)$$

where<sup>2</sup>  $D_{11,22} \rightarrow l^2 \mu_{A,B}$  and  $D_{12,21} \rightarrow l^2 (\mu_{A,B} - \alpha)$ . The above system of partial differential equations for the concentration  $\phi_A$  and  $\phi_B$  is a slightly modified version of the one derived in [70], this latter being formally recovered when setting  $\alpha$  to zero. In the generalized context here considered, the cross diffusion coefficients  $D_{12}$  and  $D_{21}$  are different, specifically smaller, than the corresponding mean diffusivities  $D_{11}$  and  $D_{22}$ . We emphasize again that the crossed, nonlinear contributions  $\pm(\phi_{A,B} \nabla^2 \phi_{B,A} - \phi_{B,A} \nabla^2 \phi_{A,B})$  stem directly from the imposed finite carrying capacity and, as such, have a specific, fully justified, microscopic origin. The diffusive fluxes that drive the changes in the concentrations  $\phi_A$  and  $\phi_B$  can be written as:

$$\begin{aligned} \mathbf{J}_{\phi_A} &= -D_{11} \left( 1 - \frac{D_{12}}{D_{11}} \phi_B \right) \nabla \phi_A - D_{12} \phi_A \nabla \phi_B, \\ \mathbf{J}_{\phi_B} &= -D_{21} \phi_B \nabla \phi_A - D_{22} \left( 1 - \frac{D_{21}}{D_{22}} \phi_A \right) \nabla \phi_B. \end{aligned} \quad (4.7)$$

It is interesting to notice that relations (4.7) enable us to make contact with the field of linear non-equilibrium thermodynamics (LNET), a branch of statistical physics which defines the general framework for the macroscopic description of e.g. transport processes. One of the central features of LNET is the relation between the forces, which cause the state of the system to change, and the fluxes, which are the result of these changes [66]. Within the formalism of LNET the fluxes  $\mathbf{J}_{\phi_A}$  and  $\mathbf{J}_{\phi_B}$  that rule the diffusion of the two species  $\phi_A$  and  $\phi_B$  are linearly related to the forces, the gradients of the respective concentrations. The quantities that establish the formal link between forces and fluxes are the celebrated Onsager coefficients, postulated on pure heuristic grounds. Interestingly, Eqs. (4.7) provide a self-consistent derivation for the Onsager coefficients, that enters the generalized Fick's scenario here depicted.

Define  $\Phi = (\phi_A, \phi_B)$  and  $\mathbf{J} = (J_{\phi_A}, J_{\phi_B})$ . Then Eqs. (4.6) can be written in the compact form:

$$\frac{\partial \Phi}{\partial t} = -\nabla \mathbf{J} = \nabla \mathbf{D}(\Phi) \nabla \Phi, \quad (4.8)$$

where the  $2 \times 2$  matrix  $\mathbf{D}$  reads:

$$\mathbf{D}(\Phi) = \begin{pmatrix} D_{11} \left( 1 - \frac{D_{12}}{D_{11}} \phi_B \right) & D_{12} \phi_A \\ D_{21} \phi_B & D_{22} \left( 1 - \frac{D_{21}}{D_{22}} \phi_A \right) \end{pmatrix}.$$

<sup>1</sup>Use has been made of the discrete Laplacian operator  $\Delta f_i = (2/z) \sum_{j \in i} (f_j - f_i)$ , which then turns into the continuum operator  $\nabla$  when sending to zero the size of the patch and scaling the rates  $\mu^{A,B}$  and  $\alpha$  appropriately.

<sup>2</sup>From the above expressions, one derives the consistency conditions  $\mu_A > \alpha$  and  $\mu_B > \alpha$ .

A stringent constraint from thermodynamics is that all eigenvalues of the diffusion matrix  $\mathbf{D}$  are real and positive. This in turn corresponds to requiring  $\text{tr}(\mathbf{D}) > 0$  and  $\det(\mathbf{D}) > 0$ . A straightforward calculation yields:

$$\begin{aligned}\text{tr}(\mathbf{D}) &= D_{11}(1 - \phi_B) + D_{22}(1 - \phi_A) + \Delta D(\phi_A + \phi_B), \\ \det(\mathbf{D}) &= D_{11}D_{22}(1 - \phi_A - \phi_B) + \Delta D(D_{11}\phi_A + D_{22}\phi_B),\end{aligned}$$

where  $\Delta D \equiv D_{11} - D_{12} = D_{22} - D_{21}$ . By definition  $\Delta D > 0$ . Moreover,  $\phi_A$  and  $\phi_B$  are both positive and smaller than one. Hence,  $\text{tr}(\mathbf{D}) > 0$  and  $\det(\mathbf{D}) > 0$ , a result that points to the consistency of the proposed formulation.

### 4.1.2 The region of Turing order

Having derived a plausible macroscopic description for the two components diffusion process, we can now move on by allowing the involved species to interact and consequently consider in the mathematical model the corresponding reaction terms. As an important remark, we notice that these latter can be also obtained as follows the above, rather general, approach that bridges micro and macro realms. First, one need to resolve the interactions among individual constituents, by translating into chemical equations the microscopic processes implicated. These include cooperation and competition effects, as well as the indirect interferences stemming from the finite carrying capacity that we have imposed in each mesoscopic patch. Then, one can recover the deterministic equations for the global concentrations, by operating in the continuum system size limit. In general, Eq. (4.8) is modified into:

$$\frac{\partial \Phi}{\partial t} = \mathbf{F}(\Phi) + \nabla \mathbf{D} \nabla \Phi, \quad (4.9)$$

where  $\mathbf{F} = (f_A(\phi_A, \phi_B), f_B(\phi_A, \phi_B))$ . As we have anticipated, the interest of this generalized formulation, resides in that it allows for Turing like patterns in a region of the parameter space that is instead forbidden when conventional reaction–diffusion systems are considered. The novelty of the proposed formulation has to do with the presence of specific cross diffusion terms, which follow a sound physical request, and add to the classical Laplacians, signature of Fickian diffusion.

Let  $\hat{\phi}_A, \hat{\phi}_B$  be the steady state solution of the homogeneous (aspatial) system, namely  $f_A(\hat{\phi}_A, \hat{\phi}_B) = f_B(\hat{\phi}_A, \hat{\phi}_B) = 0$ . The fixed point is linearly stable if the Jacobian matrix  $\mathbf{A}$

$$\mathbf{A} = \begin{pmatrix} \frac{\partial f_A}{\partial \phi_A} & \frac{\partial f_A}{\partial \phi_B} \\ \frac{\partial f_B}{\partial \phi_A} & \frac{\partial f_B}{\partial \phi_B} \end{pmatrix},$$

has positive determinant and negative trace. It is worth stressing that the derivatives in matrix  $\mathbf{A}$  are evaluated at the homogeneous fixed point. Back to the complete model, a spatial perturbation superposed to the homogeneous fixed point can get unstable if specific conditions are met. Such conditions, inspired to the seminal work by Turing, are hereafter derived via a linear stability analysis. Define  $\eta = \Phi - \hat{\Phi}$  and proceed with a linearization of Eq. (4.9) to eventually obtain:

$$\frac{\partial \eta}{\partial t} = \mathbf{A}(\hat{\Phi})\eta + \mathbf{D}(\hat{\Phi})\nabla^2 \eta.$$

Going to Fourier space one gets:

$$\frac{d\tilde{\eta}}{dt} = \mathbf{A}^*(k)\tilde{\eta}, \quad (4.10)$$

where  $\mathbf{A}^*(k) = \mathbf{A}(\hat{\Phi}) - k^2 \mathbf{D}(\hat{\Phi})$ . By characterizing the eigenvalues of the matrix  $\mathbf{A}^*$ , one can determine whether a perturbation to the homogeneous solution can yield patterns formation. In particular, if one of the eigenvalues admits a positive real part for some values of  $k$ , then a spatially modulated instability develops. The growth of the perturbation as seeded by the linear instability will saturate due to the non linearities and eventually results in a characteristic pattern associated to the unstable mode  $k$ . Steady patterns of the Turing type require in addition that the imaginary part of the eigenvalues associated to the unstable mode are zero. In formulae, the Turing instability sets in if there exists a  $k$  such that  $\text{tr}(\mathbf{A}^*(k)) < 0$  and  $\det(\mathbf{A}^*(k)) < 0$ . These latter conditions are to be imposed, jointly with the request of a stable homogeneous fixed point ( $\text{tr}(\mathbf{A}) < 0$ ,  $\det(\mathbf{A}) > 0$ ), to identify the parameters' values that drive the instability. Alternatively, one can obtain a set of explicit conditions following the procedure outlined below, and adapted from [10]. The eigenfunctions of the Laplacian operator are:

$$(\nabla^2 + k^2) \mathbf{W}_k(\mathbf{r}) = 0,$$

and we write the solution to Eq. (4.10) in the form:

$$\mathbf{x}(t, \mathbf{r}) = \sum_k e^{\lambda t} a_k \mathbf{W}_k(\mathbf{r}). \quad (4.11)$$

By substituting the ansatz (4.11) into Eq. (4.10) yields:

$$e^{\lambda t} [\mathbf{A} - k^2 \mathbf{D} - \lambda \mathbf{1}] \mathbf{W}_k = 0.$$

The above system admits a solution if the matrix  $\mathbf{A} - k^2 \mathbf{D} - \lambda \mathbf{1}$  is singular, i.e.:

$$\det(\mathbf{A} - k^2 \mathbf{D} - \lambda \mathbf{1}) = 0. \quad (4.12)$$

The solutions  $\lambda(k)$  of (4.12) can be interpreted as dispersion relations. If at least one of the two solutions displays a positive real part, the mode is unstable, and the dynamics drives the system towards a non-homogeneous configuration in response to the initial perturbation. Introduce the auxiliary quantity  $\Gamma$  defined as:

$$\Gamma = D_{11} \frac{\partial f_B}{\partial \phi_B} + D_{22} \frac{\partial f_A}{\partial \phi_A} - \hat{\phi}_A \left[ D_{21} \frac{\partial f_A}{\partial \phi_A} + D_{12} \frac{\partial f_B}{\partial \phi_A} \right] - \hat{\phi}_B \left[ D_{12} \frac{\partial f_B}{\partial \phi_B} + D_{21} \frac{\partial f_A}{\partial \phi_B} \right], \quad (4.13)$$

Then a straightforward calculation results in the following compact conditions for the instability to occur:

$$\begin{aligned} \Gamma &> 0, \\ \Gamma^2 &> 4D_{11}D_{22} \left( 1 - \frac{D_{12}}{D_{11}} \phi_A - \frac{D_{21}}{D_{22}} \phi_B \right) \det(\mathbf{A}), \end{aligned} \quad (4.14)$$

together with  $\text{tr}(\mathbf{A}) < 0$  and  $\det(\mathbf{A}) > 0$ .

For demonstrative purposes we now specialize on a particular case study and trace out in the parameters' plane, the domain that corresponds to the Turing instability. Our choice is to work with the Brusselator model<sup>3</sup> which implies setting  $f_A = -(b+d)\phi_A +$

<sup>3</sup>The term  $a(1 - \phi_A - \phi_B)$  reflects the presence of the finite carrying capacity, as discussed in [10]. Similar conclusions hold however if the diluted limit is performed, *just* in the reaction terms, hence replacing  $a(1 - \phi_A - \phi_B)$  with  $a$ .



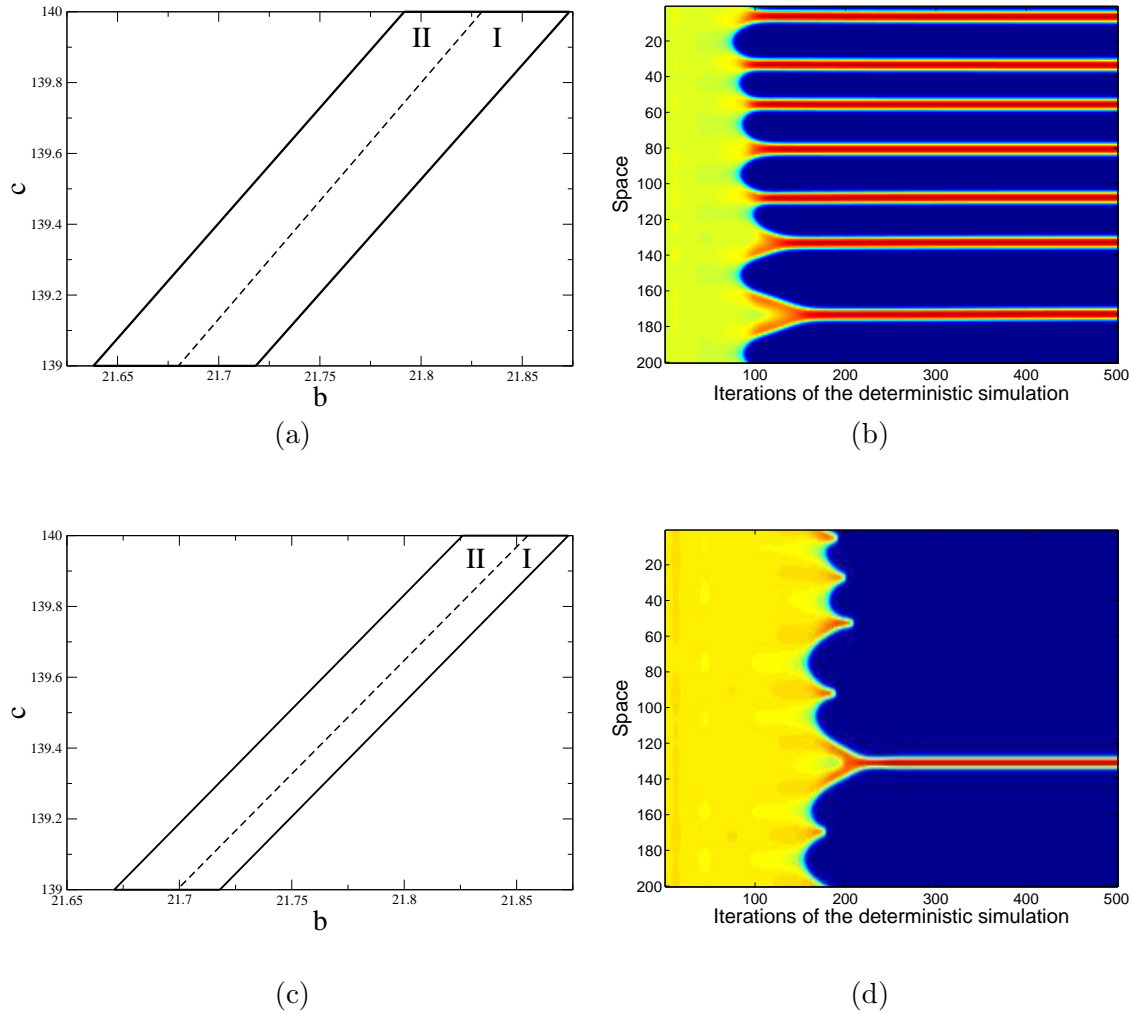


Figure 4.1: Panels (a) and (c): the boundaries of the region of Turing instability are traced in the plane  $(b, c)$ , for  $D_{22}/D_{11} = 1$  (panel (a)) and  $D_{22}/D_{11} = 0.7$  (panel (c)). The calculated domains refer to the Brusselator model with non Fickian diffusion, as explained in the main text. The solid line, which encloses regions I and II, stands for  $\Delta D = 0$ , while the dashed line delimits region I, where the condition  $\Delta D = 0.1$  applies. The other parameters are set as  $a = 5$ ,  $d = 3$ . Panels (b) and (d): the time evolution of the concentration  $\phi_A$ , as revealed by direct numerical simulations. In both cases, a small perturbation is superposed at  $t = 0$  to the (non trivial) stable homogeneous fixed point of the Brussellator, namely  $\hat{\phi}_A = (a + \sqrt{a^2 - 4ab(a+d)/c})/2/(a+d)$ ,  $\hat{\phi}_B = b/c/\hat{\phi}_A$ . Here,  $D_{11} = 1.0$ ,  $D_{22} = 0.7$ ,  $b = 21.71$ ,  $c = 139$ ,  $a = 5$ ,  $d = 3$ . The upper right figure, panel (b), refers to  $\Delta D = 0$ , the lower right, panel (d), to  $\Delta D = 0.1$ . In the simulations we have assumed a symmetric box  $[-L, L]$ , with  $L = 10$ . The box is discretized in 200, uniformly spaced, mesh points. The simulations are run by employing an explicit Euler scheme with time step equal to 0.0001. The density in each cell of the mesh is displayed in the vertical axis, while the horizontal axis refers to the number of iterations.

$a(1 - \phi_A - \phi_B) + c\phi_A^2\phi_B$  and  $f_B = b\phi_A - c\phi_A^2\phi_B$ . Species  $A$  plays now the role of the activator, while  $B$  stands for the inhibitor. Results of the analysis are reported in left panels of Fig. 4.1, where the region of interest is singled out in the plane  $(b, c)$ , for different choices of  $\Delta D$ . Turing patterns are predicted to occur for  $D_{22}/D_{11} \leq 1$ , at odd with what happens in the conventional scenario where standard Fick's diffusion is assumed to hold (see below). The right panels report the results of direct simulations and confirm the presence of macroscopically organized patterns in a region of the parameters space that is made classically inaccessible by the aforementioned, stringent condition  $D_{22} > D_{11}$ . The simulations refers to the choice  $D_{22}/D_{11} = 0.7$ . These observations are general and similar conclusions can be drawn assuming other reactions schemes of the inhibitor/activator type, different from the Brusselator model.

It is now instructive to elaborate on a simple interpretation of the above result. Let us start by briefly revisiting the necessary conditions for the classical Turing instability to occur, namely:

$$\begin{aligned} \text{tr}(\mathbf{A}) = \partial f_A / \partial \phi_A + \partial f_B / \partial \phi_B &< 0, \\ D_{11} \partial f_B / \partial \phi_B + D_{22} \partial f_A / \partial \phi_A &> 0. \end{aligned} \quad (4.15)$$

Both conditions can be simultaneously matched, only if the diagonal elements of the Jacobian matrix  $\mathbf{A}$  have opposite signs. For the sake of clarity, let us assume<sup>4</sup> that:

$$\frac{\partial f_A}{\partial \phi_A} > 0 \quad \frac{\partial f_B}{\partial \phi_B} < 0.$$

Hence, species  $A$  activates its own production, while species  $B$  has a self-inhibitory feedback. Requiring  $\text{tr}(\mathbf{A}) < 0$  implies imposing  $|\frac{\partial f_B}{\partial \phi_B}| > \frac{\partial f_A}{\partial \phi_A}$  which, by making use of the second of (4.15), readily translates into the necessary condition

$$\frac{D_{22}}{D_{11}} > \frac{|\partial f_B / \partial \phi_B|}{\partial f_A / \partial \phi_A} > 1. \quad (4.16)$$

As already mentioned, the inhibitor must diffuse faster than the activator (when the two species are evolved in separate containers) for the conventional Turing pattern to occur: the system has to accommodate for two competing processes, a short-range activation and long-range inhibition. Starting from this setting we can adapt the above reasoning to the generalized case study where cross diffusion terms are also present. To this end, and to keep the notation light, we shall solely consider the limiting case with  $\Delta D = 0$ . Similar conclusions hold when  $\Delta D \neq 0$ . The second of relations (4.15) is now replaced by the condition  $\Gamma > 0$  (see Eq. (4.13)), which can be cast in the form:

$$D_{11} \left[ \frac{\partial f_B}{\partial \phi_B} (1 - \hat{\phi}_B) - \hat{\phi}_A \frac{\partial f_B}{\partial \phi_A} \right] + D_{22} \left[ \frac{\partial f_A}{\partial \phi_A} (1 - \hat{\phi}_A) - \hat{\phi}_B \frac{\partial f_A}{\partial \phi_B} \right] > 0$$

when  $D_{11} = D_{12}$  and  $D_{22} = D_{21}$ . To proceed in the discussion we note that the elements that enter the square brackets have dimension of the inverse of time. Assume  $\frac{\partial f_B}{\partial \phi_B} (1 - \hat{\phi}_B) - \hat{\phi}_A \frac{\partial f_B}{\partial \phi_A}$  to be negative as it is reasonable to hypothesize if (i) the correction term that scales to the number densities  $\hat{\phi}_A$  is sufficiently small, or conversely if (ii)

<sup>4</sup>This is indeed the case for the Brusselator model. For  $c$  sufficiently large, see also panels (a) and (c) of Fig. 4.1, we have in fact  $\frac{\partial f_A}{\partial \phi_A} \simeq 2c\hat{\phi}_A\hat{\phi}_B > 0$  and  $\frac{\partial f_B}{\partial \phi_B} = -c\hat{\phi}_A^2 < 0$ .

we require  $\partial f_B/\partial\phi_A > 0$  (i.e. the first species stimulates with a positive feedback the other). Under these conditions, one can then introduce the characteristic time scale  $\tau_B$  associated to the reaction dynamics of species  $B$ , defined as:

$$\tau_B = \left[ \left| \frac{\partial f_B}{\partial\phi_B} \right| (1 - \hat{\phi}_B) + \hat{\phi}_A \frac{\partial f_B}{\partial\phi_A} \right]^{-1}. \quad (4.17)$$

Similarly, for species  $A$ , we have:

$$\tau_A = \left[ \frac{\partial f_A}{\partial\phi_A} (1 - \hat{\phi}_A) - \hat{\phi}_B \frac{\partial f_A}{\partial\phi_B} \right]^{-1}, \quad (4.18)$$

assuming  $\partial f_A/\partial\phi_A$  to control the sign in the above expression, or alternatively imposing  $\partial f_A/\partial\phi_B < 0$  (i.e. the second species acts with a negative feedback on the first one). The necessary condition (4.17) for the generalized Turing instability to occur takes the form:

$$l_A^2 = \tau_A D_{11} < \tau_B D_{22} = l_B^2.$$

where we have introduced two characteristic length scales, respectively  $l_A$ ,  $l_B$ , associated to the reactive dynamics of species  $A$  and  $B$ . In practice, also when  $D_{22} < D_{11}$ , spatially organized patterns can develop in the generalized reaction diffusion scheme provided the activator has a shorter life time, than the inhibitor. In formulae,  $\tau_A = \tau_B D_{22}/D_{11} < \tau_B$ . In practical terms, the competition for the microscopic spatial resources modifies the time scales associated to the reactions processes and induces a self-consistent long-range effect that enlarges the region of influence of the (isolated) inhibitors, also when the microscopic diffusion of the (isolated) activator is assumed to be faster. The crossed terms in the diffusion matrix determine a non trivial modification of the underlying characteristic times, which are now also sensitive to the off-diagonal elements of the Jacobian matrix. In the diluted limit in fact,  $\tau_A \rightarrow \tau_A^{dil} = (\partial f_A/\partial\phi_A)^{-1}$  and  $\tau_B \rightarrow \tau_B^{dil} = |\partial f_B/\partial\phi_B|^{-1}$  and one is brought back to the standard, stringent condition (4.16). In Fig. 4.2 the ratio  $\tau_B/\tau_A$  is displayed for the Brusselator model, inside the Turing region, as a function of the chemical parameter  $b$ . Different curves refer to distinct choices of  $c$ , while the other parameters are set to the values of Fig. 4.1a, with  $\Delta D = 0$ . As expected,  $\tau_B/\tau_A > 1$  a condition that eventually yields the generalized Turing patterns as described above. Conversely, and as pictured in the small inset,  $\tau_B^{dil}/\tau_A^{dil} < 1$ . Hence, since  $D_{22} < D_{11}$ , Turing patterns cannot manifest via the classical pathway, which applies to diluted conditions.

The remaining part of this section is devoted to discussing the robustness of the patterns depicted in Fig. 4.1 (panels (b) and (d)), and obtained upon integration of the governing system of partial differential equations. It should be emphasized however that the model of multispecies diffusion here considered is stochastic in nature. It is therefore interesting to further elaborate on the contributions played by finite size effects, associated to the graininess of the system, and hence deliberately neglected under the idealized deterministic representation of the dynamics. To this aim, one can carry out stochastic simulations, based on the Gillespie algorithm [28], which produces realizations of the dynamics formally equivalent to those obtained from the governing master equation (4.23). We have here chosen to operate for the parameter setting of Fig. 4.1b and the results of our analysis are reported in Fig. 4.3. If the number of elements  $N$  is sufficiently large ( $N = 3000$ , in the left panel of Fig. 4.3) the patterns appear robust and resemble those recorded when operating in the framework of the deterministic picture. However, if

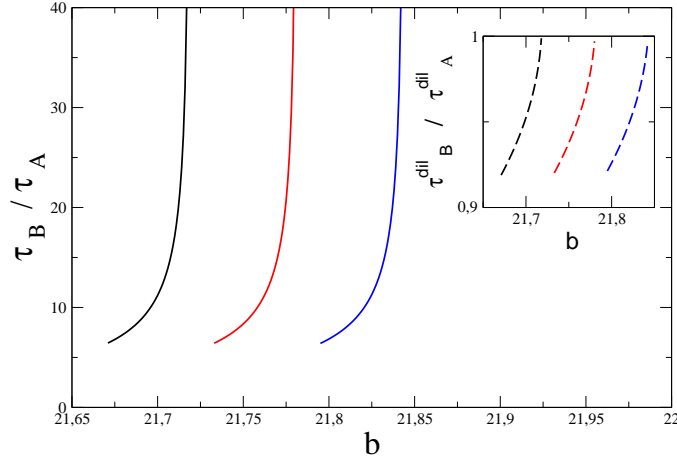


Figure 4.2: Main figure: the ratio  $\tau_B/\tau_A$  is plotted for the Brusselator model, inside the Turing region, as a function of the chemical parameter  $b$ , for different choices of  $c$ . From left to right,  $c = 139, 139.4, 139.8$ . The other parameters are set as in Fig. 4.1a, with  $\Delta D = 0$ .  $\tau_B$  and  $\tau_A$  follow respectively Eqs. (4.17) and (4.18) and quantify the time scales of the reactive processes, within the framework of the generalized reaction diffusion scheme. As expected, the existence of a region of Turing order, as revealed in Fig 4.1a, implies  $\tau_B > \tau_A$ . In the inset, the ratio of the time scales  $\tau_B^{dil}/\tau_A^{dil}$  obtained in the diluted limit is reported and proven to be smaller than unit.

the total number of microscopic individuals is reduced ( $N = 300$ , in the right panel of Fig. 4.3) the patterns are less distinct and eventually fade away. Demographic fluctuations ultimately destroy the self-organized spatial patterns, relic of Turing instability, and the system evolves towards an asymptotically stable homogeneous solution. The lifetime of the metastable non homogeneous patterns increases with the system size and formally diverges in the thermodynamic limit  $N \rightarrow \infty$ . Waiting for a sufficiently large time, also the apparently stable density structures as displayed in Fig. 4.3a are expected to coalesce and smear out. In other words, and intriguingly enough, the two limits for  $N \rightarrow \infty$  and  $t \rightarrow \infty$  do not commute. If the system size limit is taken before the infinite time limit, the dynamics is permanently frozen into a stationary non homogeneous configuration, the spatially ordered Turing patterns. Conversely, the system is attracted towards a stable homogeneous equilibrium, due of the microscopic mixing that is seeded by the finite size fluctuations. Clearly the time of homogeneization can be extremely long, when compared to the finite time window of the experimental observation. In this respect, the metastable spatially extended patterns are possibly the solely regimes to be accessible to direct measures. This observation shares many similarities with the phenomenon of Quasi-Stationary States, so far associated to the long range nature of the two-body interaction [71, 72]. These findings, as well as the analysis of [73], can possibly shed new light onto the emergence of the Quasi-Stationary States, beyond the domain of applications for which they have been reported to occur. As a side remark, it is worth emphasising that similar conclusions hold when considering the diluted limit, i.e. when neglecting the role of a finite carrying capacity and the competition for the finite spatial resources that eventually yield the generalized cross diffusion terms here considered.

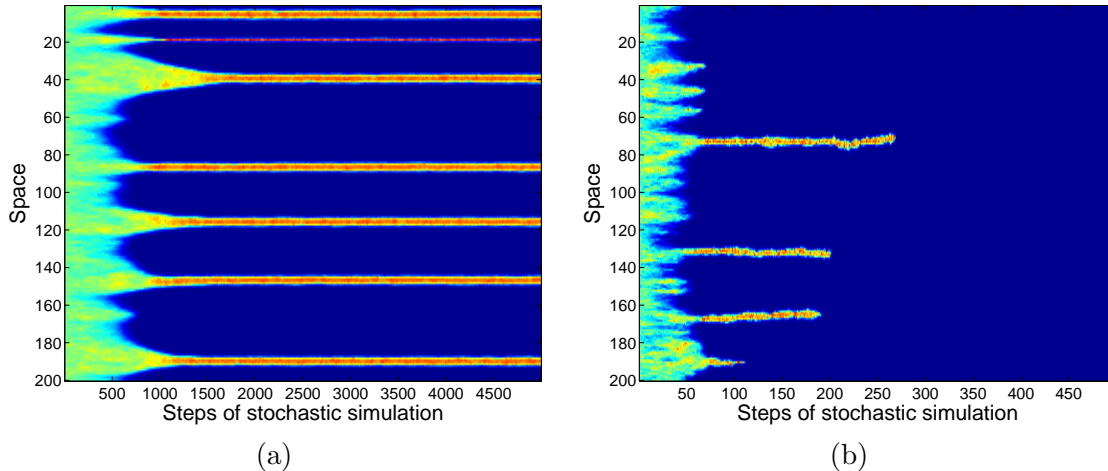


Figure 4.3: Time evolution of the discrete concentration  $n_A/N$ , as it results from a direct integration of the stochastic Brussellator model. The simulations follow the Gillespie algorithm [28]. Parameters refer to region II of Fig. 4.1b, namely  $D_{11} = 1.0$ ,  $D_{22} = 0.7$ ,  $\Delta D = 0$ ,  $a = 5$ ,  $d = 3$ ,  $b = 21.71$ ,  $c = 139$ . In panel (a):  $N = 3000$ , while in panel (b)  $N = 300$ . Demographic fluctuations destroy the deterministic patterns which are hence interpreted as a metastable regime of the finite  $N$  stochastic dynamics.

In the next section we turn to considering a generalized version of the Brussellator model with long range coupling and excluded volume effect. We will further elaborate on the condition that yield Turing pattern, but also discuss the interesting regime where travelling waves set in. The role of finite size correction will be also elucidated and shown to drive stochastic waves and Turing patterns.

## 4.2 The modified Brussellator model

Travelling waves are examples of spatio-temporal self-organized patterns [48, 9], which can spontaneously emerge in a reaction-diffusion scheme. A stable homogeneous fixed point can be destabilized by imposing an external, supposedly small, perturbation. Diffusion seeds a linear instability which enhances the aforementioned perturbation. Depending on the specific non-linear contributions, and as follows the initial instability, the system under scrutiny can eventually evolve towards distinct asymptotic configurations. Beautiful stationary patterns can for instance materialize, which display rather peculiar topologies, from spirals to stripes. These are the celebrated Turing patterns, recurrently invoked in chemistry [49, 50] and biology [48]. Alternatively, and among other possibilities, the density of the constituents can travel through space-time, a phenomenon that is encountered in many contexts of broad applied and fundamental interest.

The diffusion of species sharing the same spatial reservoir is customarily assumed to be modelled with classical Laplacian terms, as dictated by Fick's law of diffusion. However, when the hosting volume is densely populated, the so-called crowding conditions, mutual interferences are present, reflecting excluded volume effects and the competition for spatial microscopic resources. Starting from a correct formulation of the microscopic dynamics and accounting for the finite carrying capacity of the embedding volume, one

obtains in fact a modified diffusive behaviour [70], different from that postulated a priori on the basis of a phenomenological ansatz. Cross diffusive terms appear which links multiple diffusing communities and which can contribute to explain the deviation from the conventional Fick's law as seen in crowded molecular diffusion experiments [69]. The interplay between molecular crowding of the type derived in [70] and the Turing instability has been discussed in [70]. According to the conventional Turing scenario, which applies to the diluted limit, the diffusion coefficient of the inhibitor has to be larger than the diffusion coefficient associated to the activator. In short, the system has to accommodate for two competing processes, a short-range activation and long-range inhibition, for the Turing patterns to eventually occur and because of the constraints on the reaction terms, i.e. the stability of the homogeneous, a-spatial, fixed point. At variance, the competition for the available space that materializes in the cross diffusion terms, impacts on the time scales associated to the reactions processes and induces a self-consistent long-range effect that enlarges the region of influence of the inhibitors, also when the diffusion coefficient of the activator is assumed to be faster [70].

Our work is positioned in this context. We will in particular consider a Brusselator model, with a nonlocal interaction term as hypothesized in [56]. This latter term can be tuned as sought and controls the appearance of travelling wave solutions. Turing instabilities can also develop, for specific parameters setting. At variance with the formulation introduced in [56], we will here impose a finite carrying capacity at the microscopic level, which builds on the general idea of [70], and extends the limit of validity of the model to ideally embrace the regime of crowded conditions. By operating within this setting, we will continue to elaborate on the conditions that yield to the deterministic Turing order, quantifying the role of cross diffusion. Further, the concept of stochastic waves will be revisited working in such a generalized descriptive scenario.

This last section is organized as follows: in the next subsection the stochastic model is presented and the necessary mathematical concepts introduced. Then, we turn to discussing the mean-field deterministic limit. Under specific conditions, and studying the system in a sub-manifold of reduced dimensionality, a 2-codimensional bifurcation is found that separates the region of deterministic Turing and wave instability. The point of bifurcation is determined analytically, a result that casts on solid grounds the observation that Turing order is possible when the activator diffuses faster than the inhibitor, for a generalized reaction-diffusion scheme where cross diffusion terms are accommodated for. Then, we turn to discussing the stochastic dynamics. By calculating the power spectrum of fluctuations, we will show that intrinsic noise can trigger time independent Turing patterns and travelling waves, a conclusion that naturally follows from [10, 56] and that we here revisit, by including the effects of exclusive interference due to crowding into the model. Finally, we sum up and conclude.

#### 4.2.1 The stochastic model and its master equation

The system that we are going to study is a modified version of the Brusselator model, with the inclusion of a non local interaction term. This latter contribution was postulated in [56], inspired to previous work [74], and drives a long range correlation in the reaction scheme, which is eventually responsible for the emergence of travelling wave solutions. As compared to the original formulation [56], we will here introduce an additional complication into the model by constraining the number of molecules that can be eventually hosted in a given mesoscopic patch. In doing so, we will force a degree of spatial interfer-

ence between diffusing species, which indirectly reflects the competition for the available resources.

Imagine the physical space in which the system is embedded to be partitioned in  $\Omega$  cells (or patch), whose linear size is set to one. Each cell is denoted with a progressive index  $i$  which runs from 1 to  $\Omega$ . Label with  $X_i$  (resp.  $y_i$ ) a molecule of type  $X$  (resp.  $Y$ ) hosted inside cell  $i$ . Moreover, let us call  $E_i$  the vacancies, or empty spaces, that are available in patch  $i$ . Label with  $n_i$  the number of molecules of type  $X$  in cell  $i$ . Similarly, quantities  $m_i$  and  $q_i$  refer to species  $Y$  and  $E$ , respectively. Each cell can then host a maximum of  $N$  elements, including the empties, a physical constraint on the local maximal density, which translates into the following mathematical relation:

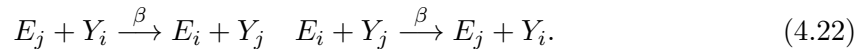
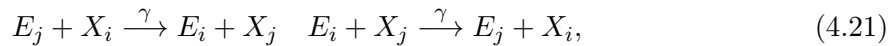
$$n_i + m_i + q_i = N. \quad (4.19)$$

$N$  is therefore an invariant quantity of the dynamics which will prove crucial in the forthcoming discussion. The reactions that define the backbone of the models read [56]:



The quantities  $a, b, d$  are scalar parameters and stand for the rates of the associated reactions. The third reaction assumes instead a non local interaction of the type introduced in [56]. More specifically, one imposes a non local coupling which decays exponentially with the distance among sites, an effect that we will make explicit in the following when characterizing the associated transition rate.

In addition to the above reactions (4.20) we here consider the possibility for any selected molecule to diffuse from cell  $i$  towards an adjacent cells  $j$ . This latter migration can occur only if space allows, namely if cell  $j$  has at least one empty case  $E_j$  that can be eventually filled. As discussed earlier, This process can be translated in the following chemical equations [70]:



where  $\gamma$  and  $\beta$  quantify the ability to diffuse of species  $X$  and  $Y$ , respectively. We here omit the equivalent of reaction 4.2 as introduced in the earlier part of this chapter. The above set of chemical equations define a stochastic model which can be mathematically investigated through the associated master equation. Let us introduce, as in the previous section, the  $\Omega$  components vectors  $\mathbf{n} = (n_1, \dots, n_i, \dots, n_\Omega)$  and  $\mathbf{m} = (m_1, \dots, m_i, \dots, m_\Omega)$ . The state of the system is therefore specified by the vector  $(\mathbf{n}, \mathbf{m})$ , since the number of empties  $q_i$  inside each compartment  $i$  can be readily deduced by making use of the conserved quantity (4.19). The master equation governs the evolution of the probability  $P_{\mathbf{n}, \mathbf{m}}(t)$  of seeing the system in the state  $(\mathbf{n}, \mathbf{m})$  at time  $t$ . To write down explicitly the master equation, one needs to specify the transition rates associated to the above chemical equations. The transition rate is customarily indicated with the symbol  $T(\mathbf{n}_F, \mathbf{m}_F | \mathbf{n}_I, \mathbf{m}_I)$ , where

the index  $I$  stands for the initial state and  $F$  refers to the final state, compatible with the selected chemical equation. The transition rates that follows reactions (4.20) can be cast in the form:

$$\begin{aligned} T(n_i + 1, m_i | n_i, m_i) &= a \frac{N - n_i - m_i}{N}, \\ T(n_i - 1, m_i + 1 | n_i, m_i) &= b \frac{n_i}{N}, \\ T(n_i + 1, m_i - 1 | n_i, m_i) &= c \frac{n_i^2}{N^2} \Lambda \sum_{j=1}^{\Omega} e^{(-\sigma|i-j|)} \frac{m_j}{N}, \\ T(n_i - 1, m_i | n_i, m_i) &= d \frac{n_i}{N}. \end{aligned}$$

where we have assumed that the molecules are uniformly distributed inside each mesoscopic cell  $i$ . To keep the notation light, we solely keep track of the entries in  $\mathbf{n}$  and  $\mathbf{m}$  that get affected by the inspected reaction. The third transition rate encapsulates the long-range coupling to which we alluded above and follows the scheme hypothesized in [56]. The constant  $\sigma$  controls the range of interaction and  $\Lambda$  is a proper normalization constant, to which we will return in the following.

Similarly, the transition rates associated to the diffusion equations (4.22) yield to the following transition rates:

$$\begin{aligned} T(n_i + 1, n_j - 1 | n_i, n_j) &= \frac{\gamma n_j}{z N} \frac{N - n_i - m_i}{N}, \\ T(n_i - 1, n_j + 1 | n_i, n_j) &= \frac{\gamma n_i}{z N} \frac{N - n_j - m_j}{N}, \\ T(m_i + 1, m_j - 1 | m_i, m_j) &= \frac{\beta m_i}{z N} \frac{N - n_j - m_j}{N}, \\ T(m_i - 1, m_j + 1 | m_i, m_j) &= \frac{\beta m_j}{z N} \frac{N - n_i - m_i}{N}. \end{aligned}$$

The pair of integers  $i$  and  $j$  refer to neighbors cells. The factor  $z$  stands for the number of nearest neighbors cells: when dealing with a one dimensional system, the case to which we are bound in the forthcoming discussion,  $z = 2$ . Given the above expression for the transition rates, the governing master equation reads:

$$\begin{aligned} \frac{d}{dt} P_{\mathbf{n}, \mathbf{m}}(t) &= \sum_{i=1}^{\Omega} \left[ (\varepsilon_{X,i}^+ \varepsilon_{Y,i}^- - 1) T(n_i - 1, m_i + 1 | n_i, m_i) \right. \\ &+ (\varepsilon_{X,i}^- \varepsilon_{Y,i}^+ - 1) T(n_i + 1, m_i - 1 | n_i, m_i) + (\varepsilon_{X,i}^- - 1) T(n_i + 1, m_i | n_i, m_i) \\ &+ (\varepsilon_{X,i}^+ - 1) T(n_i - 1, m_i | n_i, m_i) + \sum_{j \in i-1, i+1} \left( (\varepsilon_{X,j}^+ \varepsilon_{X,i}^- - 1) T(n_i + 1, n_j - 1 | n_i, n_j) \right. \\ &+ (\varepsilon_{X,i}^+ \varepsilon_{X,j}^- - 1) T(n_i - 1, n_j + 1 | n_i, n_j) + (\varepsilon_{Y,i}^+ \varepsilon_{Y,j}^- - 1) T(m_i - 1, m_j + 1 | m_i, m_j) \\ &\left. \left. + (\varepsilon_{Y,j}^+ \varepsilon_{Y,i}^- - 1) T(m_i + 1, m_j - 1 | m_i, m_j) \right) \right] P_{\mathbf{n}, \mathbf{m}}(t). \end{aligned} \tag{4.23}$$



where  $\varepsilon_{X,i}^{\pm}$  and  $\varepsilon_{Y,i}^{\pm}$  are the step operators. Assume a generic function  $f(\mathbf{n}, \mathbf{m})$ . The action of the operator  $\varepsilon_{X,i}^{\pm}$  on  $f(\cdot, \cdot)$  is explicated as:

$$\varepsilon_{X,i}^{\pm} f(\mathbf{n}, \mathbf{m}) = f(n_1, \dots, n_i \pm 1, \dots, n_{\Omega}, \mathbf{m}). \quad (4.24)$$

In practical terms  $\varepsilon_{X,i}^{\pm}$  increments or decrements by a unit the population of type  $X$  in site  $i$ . Similarly,  $\varepsilon_{Y,i}^{\pm}$  acts as specified by the following relation:

$$\varepsilon_{Y,i}^{\pm} f(\mathbf{n}, \mathbf{m}) = f(\mathbf{n}, m_1, \dots, m_i \pm 1, \dots, m_{\Omega}, ). \quad (4.25)$$

The master equation is difficult to handle analytically and one has to resort to approximate techniques of manipulation to progress in the analysis. One viable alternative is the celebrated van Kampen system size expansion, by setting:

$$\frac{n_i}{N} = \phi_i + \frac{\xi_i}{\sqrt{N}} \quad \frac{m_i}{N} = \psi_i + \frac{\eta_i}{\sqrt{N}}. \quad (4.26)$$

In the following sections, we shall discuss the results of the analysis, being in particular interested in highlighting the peculiar features that relate to the imposed finite carrying capacity. Next section is entirely devoted to discussing the mean-field limit of model (4.23).

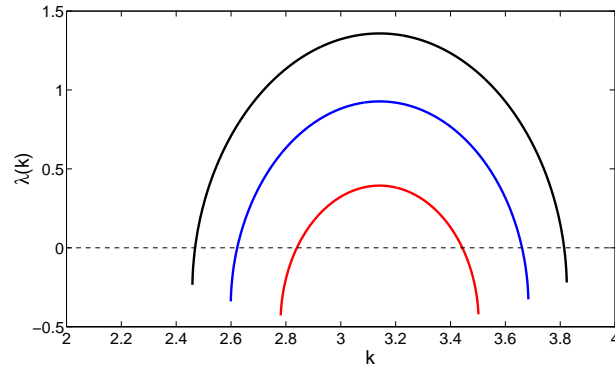


Figure 4.4: The dispersion relation  $\lambda(k)$  is plotted as a function of the scalar wave number  $k$ . The figure refers to  $a = d = 1$ ;  $\sigma = 2$ ;  $\gamma = 1$ ;  $b=15$ ;  $\beta = 0.6$ . Different curves refer to different values of  $c$ : from top to bottom  $c = 138, 139, 140$ . A finite range of  $k$  exists that yield to  $\lambda(k) > 0$ , so signaling an instability. Notice that the most unstable mode, i.e. the peak of the profile  $\lambda(k)$  is located in  $k = \pi$ .

### 4.2.2 The mean field limit

By truncating the van Kampen system size expansion at the leading order  $1/\sqrt{N}$ , one eventually obtains the following system of partial differential equations for the deterministic concentrations  $\phi_i$  and  $\psi_i$ :

$$\begin{cases} \frac{\partial \phi_i}{\partial \tau} = a - a(\phi_i + \psi_i) - (b + d)\phi_i + c\Lambda\phi_i^2 \sum_j \exp(-\sigma|i - j|)\psi_j \\ \quad + \gamma(\Delta\phi_i - \psi_i\Delta\phi_i + \phi_i\Delta\psi_i) \\ \frac{\partial \psi_i}{\partial \tau} = b\phi_i - c\Lambda\phi_i^2 \sum_j \exp(-\sigma|i - j|)\psi_j + \beta(\Delta\psi_i - \phi_i\Delta\psi_i + \psi_i\Delta\phi_i), \end{cases} \quad (4.27)$$

where  $\Delta f_i = f_{i+1} - 2f_i + f_{i-1}$  is the discrete one dimensional Laplacian and where  $\tau = t/N$ . Some details of the technicalities involved in the calculation can be found in 4.2.4.  $\Lambda$  is a normalization constant. Following [56] we assign it to match the condition

$$\Lambda \sum_j \exp(-\sigma|j|) = 1,$$

which in turn implies:

$$\Lambda = \frac{e^\sigma - 1}{e^\sigma + 1}.$$

A comment is mandatory at this point. The deterministic model (4.27) follows from the microscopic stochastic reaction scheme, discussed in the preceding section and it is formally recovered when operating in the thermodynamic limit  $N \rightarrow \infty$ . The effect of the finite carrying capacity imposed in (4.22), reflects in the mean-field equations through the cross diffusion terms  $(-\phi_i \Delta \psi_i + \psi_i \Delta \phi_i)$  which appear to modify the conventional Fickian behaviour. These are second order contributions in the concentrations and are therefore important in the regime of high densities. For this reason, and following the analysis in [70], we believe that eqs (4.27) enables us to extend the analysis of [56] to the interesting regime of crowding conditions. In the remaining part of this paragraph, we will elaborate on the mean field instabilities that can eventually destabilize the homogeneous solution of system (4.27). In doing so we will adapt the calculation of [56] to the present setting and so identify the peculiarities that can be eventually traced back to the diffusive transport here assumed.

The homogeneous fixed point  $(\phi^*, \psi^*)$  of system (4.27) is:

$$\phi^* = (a + \sqrt{a^2 - 4ab(a+d)/c})/2/(a+d) \quad \psi^* = b/c/\phi^*. \quad (4.28)$$

Impose now a small spatially inhomogeneous perturbation  $(\delta\phi_i(t), \delta\psi_i(t))$  to perturb the homogeneous fixed point as:

$$\delta\phi_i(t) = \phi_i(t) - \phi^*, \quad \delta\psi_i(t) = \psi_i(t) - \psi^*.$$

We are then interested to identifying the conditions that can yield to a spontaneous amplification of the perturbation and eventually translate in the emergence of Turing or wave like patterns, to which we alluded in the introduction. To this end, and following the standard approach, we solely focus on the linear contributions in  $\delta\phi_i$  and  $\delta\psi_i$ , dropping out higher order corrections. In formulae:

$$\begin{aligned} \frac{\partial \delta\phi_i}{\partial \tau} &= -a(\delta\phi_i + \delta\psi_i) - (b+d)\delta\phi_i + c\Lambda\phi_i^2 \sum_j \exp(-\sigma|i-j|)\delta\psi_j \\ &\quad + 2c\Lambda\psi^*\phi^*\delta\phi_i + \gamma(\Delta\delta\phi_i - \psi^*\Delta\delta\phi_i + \phi^*\Delta\delta\psi_i), \end{aligned} \quad (4.29)$$

$$\begin{aligned} \frac{\partial \delta\psi_i}{\partial \tau} &= b\delta\phi_i - c\Lambda\phi_i^2 \sum_j \exp(-\sigma|i-j|)\delta\psi_j + 2c\Lambda\psi^*\phi^*\delta\phi_i \\ &\quad + \beta(\Delta\delta\psi_i - \phi^*\Delta\delta\psi_i + \psi^*\Delta\delta\phi_i). \end{aligned} \quad (4.30)$$

Operate now the spatial Fourier transform of the above system:

$$\begin{aligned} \frac{\partial \tilde{\phi}}{\partial \tau} = & -a(\tilde{\delta\phi} + \tilde{\delta\psi}) - (b+d)\tilde{\delta\phi} + c\Lambda\tilde{\phi}^2\tilde{e}(k)\tilde{\delta\psi} + 2c\Lambda\psi^*\phi^*\tilde{\delta\phi} \\ & + \gamma \left( \tilde{\Delta}\tilde{\delta\phi} - \psi^*\tilde{\Delta}\tilde{\delta\phi} + \phi^*\tilde{\Delta}\tilde{\delta\psi} \right), \end{aligned} \quad (4.31)$$

$$\frac{\partial \tilde{\psi}}{\partial \tau} = b\tilde{\delta\phi} - c\Lambda\tilde{\phi}^2\tilde{e}(k)\tilde{\delta\psi} + 2c\Lambda\psi^*\phi^*\tilde{\delta\phi} + \beta \left( \tilde{\Delta}\tilde{\delta\psi} - \phi^*\tilde{\Delta}\tilde{\delta\psi} + \psi^* + \tilde{\Delta}\tilde{\delta\phi} \right), \quad (4.32)$$

where  $(\tilde{\cdot})$  denotes the Fourier transform and  $\tilde{\phi} = \tilde{\phi}(k, \tau)$ . The two symbols  $\tilde{e}(k)$  and  $\tilde{\Delta}$  respectively refer to the Fourier transform of the exponential factor in eqs. (4.32) and of the discrete Laplacian operator  $\Delta$  and read:

$$\tilde{\Delta}f(k) = 2[\cos(k) - 1] \quad \tilde{e}(k) = \frac{\sinh(\sigma)}{\cosh(\sigma) - \cos(k)}.$$

System (4.32) can be written in a compact form as:

$$\frac{\partial \Psi}{\partial \tau} = J^*(k)\Psi,$$

where  $\Psi = (\tilde{\delta\phi}, \tilde{\delta\psi})$  and

$$J^*(k) = \begin{pmatrix} -(b+d) + 2c\phi^*\psi^* - a + \gamma(\tilde{\Delta} - \psi^*\tilde{\Delta}) & c\Lambda(\phi^*)^2\tilde{e}(k) - a + \gamma\phi^*\tilde{\Delta} \\ b - 2c\phi^*\psi^* + \beta\psi^*\tilde{\Delta} & -c\Lambda(\phi^*)^2\tilde{e}(k) + \beta(\tilde{\Delta} - \psi^*\tilde{\Delta}) \end{pmatrix}.$$

The eigenvalues  $\lambda_1(k)$  and  $\lambda_2(k)$  of matrix  $J^*(k)$  provide us with the information concerning the stability of the fixed point to the externally imposed perturbation. Eigenvalues  $\lambda_{1,2}$  take the following explicit expression:

$$\lambda_{1,2} = \frac{1}{2} \left( tr J^* \pm \sqrt{(tr J^*)^2 - 4det J^*} \right). \quad (4.33)$$

where  $tr J^*$  and  $det J^*$  stand for the trace and determinant of matrix  $J^*$ .

If the real part of both the eigenvalues is negative, for all values of  $k$ , the homogeneous state is stable, and the external perturbation gets damped. At variance, if one eigenvalue admits a positive real part, within a compact, finite range of non-zero  $k$ , then the perturbation is destabilized and the system undergoes the so-called Turing instability. Beyond the linear regime, non linear terms do matter. Because of the complex and highly non-linear interplay between reaction and diffusion contributions, the system can eventually freeze in asymptotically stationary, non homogeneous configurations. Steady patterns require in addition a null imaginary part of the eigenvalues  $\lambda_{1,2}(k)$ , for all unstable  $k$  values. These are the celebrated Turing patterns, beautiful extended motifs that are revealed when inspecting the spatial distribution of the interacting elements. Beyond the prototypical Turing solution, waves can also manifest when the imaginary part of the eigenvalues is different from zero inside the region of unstable  $k$ . In the following, we refer to the dispersion relation  $\lambda(k)$  as to the eigenvalue with the largest real part. By studying the function  $\lambda(k)$ , when varying the parameters of the model, one can elaborate on the conditions that drive Turing and/or waves instabilities. As an example, for demonstrative

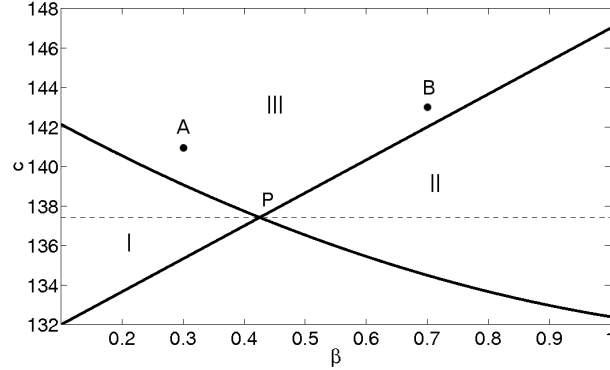


Figure 4.5: The regions of wave (labeled with I) and Turing (denoted with II) instabilities are traced in the parameters plane  $(\beta, c)$ . Region III identifies the domain of parameters that corresponds to a stable homogeneous fixed point. The other parameters are set as in figure 4.4 and, more specifically,  $a = d = 1$ ,  $\sigma = 2$ ,  $\gamma = 1$ ,  $b = 15$ . We notice in particular that the Turing instability can occur also when  $\beta$ , the diffusion of the inhibitor, is smaller than  $\gamma = 1$ , the diffusion of the activator. This observation is at odd with the conventional Turing paradigm and reflects the presence of the cross diffusion terms, in our reaction diffusion scheme.  $P$  is positioned in  $(\beta_P, c_P)$  and identifies the cusp like point where regions I and II touch. The dashed line is horizontal ( $c_P = 137.7$ ) and passes through  $P$ . The points  $A$  and  $B$  fall outside the domain of instability, where the homogeneous fixed point is believed to be stable. As we shall demonstrate later, ordered structures which are reminiscent of wave and Turing like instabilities can develop when the choice of parameters correspond respectively to points  $A$  and  $B$  in the reference plane  $(\beta, c)$ .

purposes, we plot in figure 4.4 the dispersion relation  $\lambda(k)$  vs.  $k$ , for distinct choices of the chemical rate  $c$ , having fixed the other parameters to a set of representative values. Interestingly, the profile of  $\lambda(k)$  is peaked in  $k = \pi$ , an important observation that will be extensively used in the following.

To discriminate the behaviour of the system, and so classify the possible type of instabilities as reviewed above, we make use of the following general strategy [75, 74, 56]. Clearly, when:

$$\det J^*(k) > 0 \quad \text{tr} J^*(k) < 0 \quad \forall k. \quad (4.34)$$

the fixed point is stable as it can be immediately appreciated by recalling expression (4.33). When (4.34) applies, in fact, the real part of  $\lambda_i(k)$  is necessarily negative  $\forall k$ . To abandon the region of stability, two different pathways are possible. The transition from stable to unstable solution takes for instance place when there exists a  $\bar{k}$  such that  $\det J^*(\bar{k}) = 0$  and  $\text{tr} J^*(\bar{k}) < 0$ ,  $\forall k$ . In this case the system enters a region where Turing instability is expected to occur. Another transition realizes when  $\text{tr} J^*(\bar{k}) = 0$  and  $\det J^*(\bar{k}) > 0$   $\forall k$ , which takes the system into the region of wave instability. Using the above criteria, we can delimit the boundaries of the regions respectively deputed to Turing and wave instability. To favour a pictorial representation of our findings and to make contact with the analysis of [56], we let the (positive) quantities  $c$  and  $\beta$  to change freely, and assign the other involved parameters to the values specified in the caption of figure 4.4. The result is displayed in figure 4.5 where three different regions are identified.

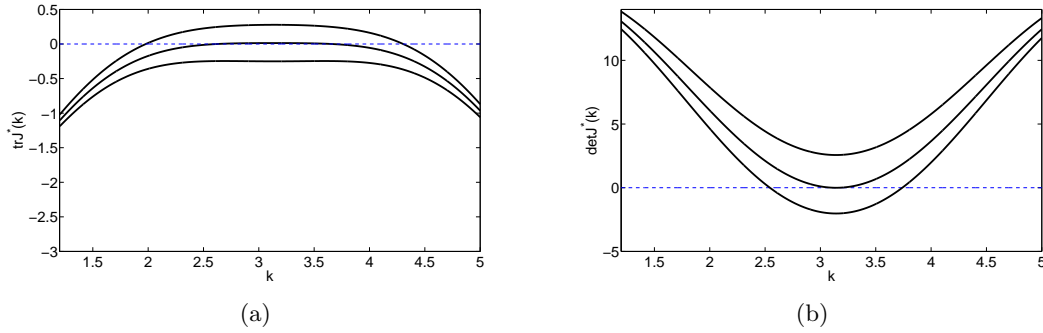


Figure 4.6: Right: The trace of  $J^*$  is plotted as a function of  $k$ , for different values of  $\beta = 0.3, 0.42, 0.5$  moving horizontally along the dashed line of figure 4.5, i.e. setting  $c = 137.7$ . The other parameters are assigned as specified in figure 4.5. Left: The determinant of  $J^*$  is plotted as a function of  $k$ , for different values of  $\beta = 0.3, 0.42, 0.5$ . The parameters are the same as in right panel.

In region I, waves are predicted to occur, while in region II Turing patterns are expected to develop. When the pair  $(\beta, c)$  falls inside region III, the perturbation fades away and the system relaxes back to the homogeneous solution. Notice that a cusp marks the transition from region II to region III. This bifurcation point (labeled  $P$  in figure 4.5) corresponds to the degenerate condition:

$$\det J^*(\bar{k}) = 0 \quad \text{tr} J^*(\bar{k}) = 0. \quad (4.35)$$

where the scalar  $\bar{k}$  identifies the critical wavelength. It is also very interesting to notice that the singular cusp like point occurs at  $\beta < 1$ , where  $\beta$  measures the diffusion ability of the inhibitor. Recalling, that  $\gamma$ , the diffusion coefficient of the activator, is equal to one (see caption of figure 4.5), we conclude that Turing patterns can possibly occur within the explored setting also if  $\beta < \gamma$ . This is at odd with the customarily agreed scenario, which, it is worth emphasizing, assumes a conventional scheme of diffusion. The cross diffusion terms included in the model here explored to account for the microscopic competition for the finite spatial resources, are responsible for the observed behaviour, as outlined in [12]. The position of the cusp that separates region II and region III can be used to pinpoint the presence of the Turing order in the classically prohibited region  $\beta < \gamma$ , or equivalently  $\beta < 1$  when  $\gamma = 1$ , as it is assumed in this work.

Based on the above, we aim at characterizing analytically, the point of transition from region I and II, by operating in the reference plane  $(\beta, c)$ . In this space of reduced dimensionality, two parameters, both  $\beta$  and  $c$ , must be varied to force a direct transition from zone I to zone II. For this reason we refer to point  $P$ , located in  $(\beta_P, c_P)$ , as to a codimension 2 bifurcation. In figures 4.6(a) and 4.6(b) we respectively plot the trace and the determinant of matrix  $J^*$  as a function of  $k$ , for distinct values of  $\beta$  and for  $c = c_P$ , a value that we have preliminarily computed numerically. In practice, we cross horizontally the plan  $(c, \beta)$ , moving along the dashed line of figure 4.5, which passes from  $P$ .

At first glance, from figure 4.6(a), one sees that the trace of  $J^*$  is negatively defined for  $\beta > \beta_P$  and, importantly, presents a global maximum in  $k_M$ , just before crossing the horizontal axis. The maximum is progressively moved upward when  $\beta$  approaches the

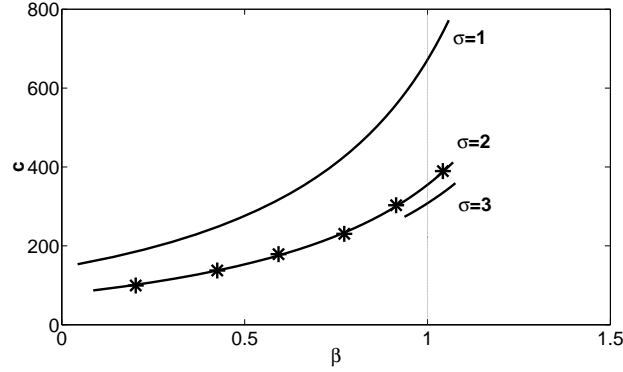


Figure 4.7: The bifurcation point  $(\beta_P, c_P)$  as determined by solving system (4.40) is plotted, for distinct values of  $\sigma$ , and by tuning the parameter  $b$ , inside a given interval. Here,  $a = d = 1$ ,  $\gamma = 1$  and  $\sigma = 1, 2, 3$ .  $b$  belongs to the interval  $[10, 40]$ . The symbols (star) refer to direct numerical estimates of the bifurcation points. The agreement between the analytical line and the locations of the bifurcation points as predicted by system (4.40), constitutes an a posteriori validation of the assumptions made.

critical value  $\beta_P$ . Therefore, it is in  $\bar{k} = k_M$  that the critical condition  $tr J^*(\bar{k}) = 0$  is first matched. Similarly, see figure 4.6(b), the determinant of  $J^*(k)$  is positive for  $\beta < \beta_P$  and displays a rather distinct minimum in  $k_m$ . By increasing  $\beta$ , the condition  $det J^*(\bar{k}) = 0$  is reached for the first time in  $\bar{k} = k_m$ . This empirical observation defines the starting point of our analysis. Based on the above, we hypothesize in fact that the degenerate condition yielding to the cusp like bifurcation can only occur if: (i) the maximum of the trace and the minimum of the determinant, occur for an identical value of  $\bar{k}$ ; (ii) system (4.35) admits a solution in  $\bar{k} = k_m \equiv k_M$ . This latter condition translates in:

$$D\tilde{e}(\bar{k}) - E\tilde{e}(\bar{k})\tilde{\Delta} + \tilde{\Delta}^2 F + \tilde{\Delta} G + H = 0 \quad A + \tilde{\Delta} B - c\Lambda(\phi^*)^2 \tilde{e}(\bar{k}) = 0, \quad (4.36)$$

where:

$$\begin{cases} A = -b - d + 2c\phi^*\psi^* - a \\ B = \gamma(1 - \psi^*) + \beta(1 - \phi^*) \\ D = c\lambda(\phi^*)^2(d + a) \\ E = c\lambda(\phi^*)^2(\gamma(1 - \psi^*) + \beta\psi^*) \\ F = \gamma\beta(1 - \psi^*)(1 - \phi^*) - \gamma\beta\psi^*\phi^* \\ G = a\beta\psi^* - \gamma\phi^*(b - 2c\phi^*\psi^*) + \beta(1 - \phi^*)(-b - d - a + 2c\phi^*\psi^*) \\ H = a(b - 2c\phi^*\psi^*). \end{cases} \quad (4.37)$$

Condition (i) requires setting to zero the derivative of eqs. (4.35) so yielding to the following relations:

$$\begin{cases} \frac{d\tilde{\Delta}}{dk}|_{k=\bar{k}} B - c\Lambda(\phi^*)^2 \frac{d\tilde{e}}{dk}|_{k=\bar{k}} = 0 \\ \frac{d\tilde{e}}{dk}|_{k=\bar{k}} (D - E\tilde{\Delta}) - \frac{d\tilde{\Delta}}{dk}|_{k=\bar{k}} (E\tilde{e}(k) + 2F\tilde{\Delta} + G) = 0, \end{cases}$$

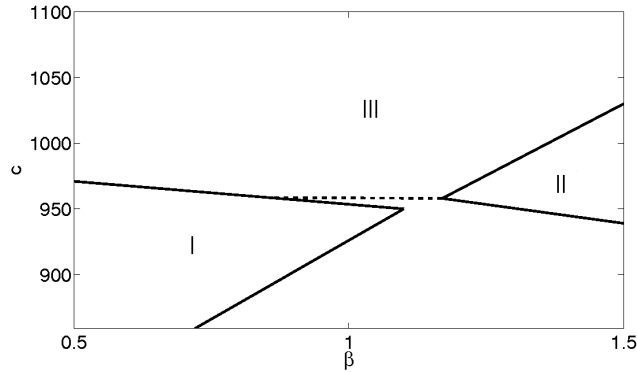


Figure 4.8: The regions of wave (I) and Turing (II) instabilities are traced in the parameters plane  $(\beta, c)$ , for a choice of  $b$  for which system (4.35) does not admit a solution. As expected the regions I and II appear to be disconnected. III refers to the region of stable homogeneous fixed point. Here,  $a = d = 1$ ,  $\gamma = 1$ ,  $\sigma = 2$  and  $b = 43$ . The dashed line sets the lower boundary of region III. No homogeneous fixed point exists in the portion of plane below the dashed line, and outside the region of Turing and wave instability.

where:

$$\left. \frac{d\tilde{\Delta}}{dk} \right|_{k=\bar{k}} = -2 \sin(\bar{k}) \quad (4.38)$$

$$\left. \frac{d\tilde{e}}{dk} \right|_{k=\bar{k}} = \frac{-\sinh(\sigma) \sin(\bar{k})}{(\cosh(\sigma) - \cos(\bar{k}))^2}. \quad (4.39)$$

Equations (4.38) admit a trivial solution when  $\bar{k} = n\pi$ , with  $n$  integer. In fact, both  $\left. \frac{d\tilde{\Delta}}{dk} \right|_{k=n\pi}$  and  $\left. \frac{d\tilde{e}}{dk} \right|_{k=n\pi}$  are identically equal to zero, as it follows from relations (4.39). For  $n$  even,  $\tilde{\Delta}(n\pi) = 0$ . Under this limiting condition the trace and the determinant collapse to their homologous expressions as obtained for the homogeneous case. Recall that the present calculation builds on a linear expansion around a stable homogeneous fixed point. Therefore, the associated trace and determinant are bound to respectively negative and positive values. In conclusion, conditions (4.35) cannot be met, if  $n$  is assumed to be an even integer.

Conversely, when  $n$  is odd, one always gets  $\tilde{\Delta}(n\pi) = -4$ . Hence, equations (4.36) reduce to:

$$\begin{cases} -4B + A - c\Lambda(\phi^*)^2 \frac{\sinh(\sigma)}{\cosh(\sigma)+1} = 0 \\ (D + 4E) \frac{\sinh(\sigma)}{\cosh(\sigma)+1} + 16F - 4G + H = 0. \end{cases} \quad (4.40)$$

System (4.40) can be solved numerically. It returns the coordinates  $c_P$  and  $\beta_P$  of the cusp like point  $P$ , as a function of the parameters of the model that enters the definitions of the coefficients implicates in the equations. To favour a pictorial representation of our result, we perform the analysis by tuning continuously  $b$  inside a finite interval. We therefore obtain a family of bifurcation points that define a line in the representative parameters plane  $(\beta, c)$ . The analysis is then repeated for different choices of  $\sigma$ , as illustrated in figure 4.7.

Our analysis rests on speculative grounds: the mathematical development follows in fact the intuitive idea that the degenerate condition (4.35) is eventually attained when the stationary points of trace and determinant touch, simultaneously, the horizontal axis. Although reasonable, this working assumption needs to be carefully evaluated. To this end, we turned to computing the exact location of the transition point  $(\beta_P, c_P)$ , by delineating for each choice of  $b$  the boundaries of the regions respectively deputed to Turing and wave instabilities. The analysis is carried out by setting  $\sigma = 1$ , for  $b$  sampling the aforementioned interval. The results are plotted, with symbols in figures 4.7. The agreement between the (discrete) direct estimates and the (continuous) line based on the analytical strategy implemented above returns an excellent agreement, thus providing an a posteriori validation of the approximations made. In figure 4.7, we also plot, as a reference, the vertical line  $\beta = 1$ . When the bifurcation points fall on the left of such line, Turing instability can set in also if the inhibitor diffuses slower than the activator, at odd with the classical scenario which, however, applies to conventional reaction diffusion schemes, where the cross diffusion terms are omitted. If system (4.40) admits no solutions, then the domains of wave and Turing instabilities appear to be disconnected, as displayed in figure 4.9(b).

As a final remark, we wish to stress that two other stationary points of the dispersion relation can in principle exist, besides the trivial point  $k = \pi$ . More specifically, two maxima can materialize in  $k_{\pm}$ , positions symmetric with respect to  $k = \pi$ <sup>5</sup>.

We shall return on this interesting observation in the next section when aiming at exploring the impact on the dynamics of the finite size corrections to the idealized deterministic dynamics. As discussed in [10] and [56] Turing patterns and wave can emerge outside the region of mean field order, as follows a self-consistent resonant mechanism that amplifies the endogenous demographic noise. This observation is made quantitative by inspecting analytically the power spectrum of fluctuations and looking for localized peaks both in time and space. These latter peaks testify in fact on the degree of macroscopic organization of the system, as mediated by its granular, hence stochastic, microscopic component.

### 4.2.3 The Stochastic analysis: power spectrum of fluctuations

To the next to leading order in the van Kampen system size expansion, one characterizes the distribution of fluctuations. This latter, labeled  $\Pi(\xi, \eta, t)$ , obeys to a Fokker Planck equation, which can be equivalently represented in terms of its associated Langevin stochastic equation. Working in this framework, one obtains a close analytical expression for the power spectra of fluctuations  $P_i(\omega, k)$ , where the index  $i = 1, 2$  identifies the selected species and  $k$  and  $\omega$  refer to the Fourier time and space frequencies. The details of the calculation are confined into the 4.2.5, where the expressions for the power spectra are explicitly given, see equations (4.46). In this section, we exploit this result to represent

---

<sup>5</sup>Consider equations (4.38) and focus on the condition  $d(\text{tr}J^*)/dk = 0$ , more easy to handle. It can be straightforwardly seen that, under specific conditions, two other stationary points  $k_{\pm}$  of the trace  $J^*$  exist provided  $\left| \cosh(\sigma) - \sqrt{\frac{c\lambda\phi^* \sinh(\sigma)}{2\gamma(1-\phi^*)+2\beta(1-\phi^*)}} \right| < 1$ . It can be analytically shown however that  $d(\det J(k)^*)/dk|_{k_{\pm}} \neq 0$ . This implies that the trace maximum and the determinant minimum can simultaneously cross the horizontal axis for the same value of  $k$  *only* at  $k = \pi$ , the value that we considered in the our analysis. In practice, when the above condition is met, and the trace has a maximum in  $k_{\pm}$ , the cusp like bifurcation, between Turing and wave regions, cannot realize point and a gap opens between those regions in the parameter plane.



the computed power spectrum outside the regions of deterministic order. Our aim is to look for the signatures of a spatio-temporal organization, that should ultimately reflect the graininess of the investigated stochastic model. More concretely, we will operate close to the regions of mean field, wave and Turing instabilities, and assign the parameters so to have the system initialized in points A and B, as highlighted in figure 4.5.

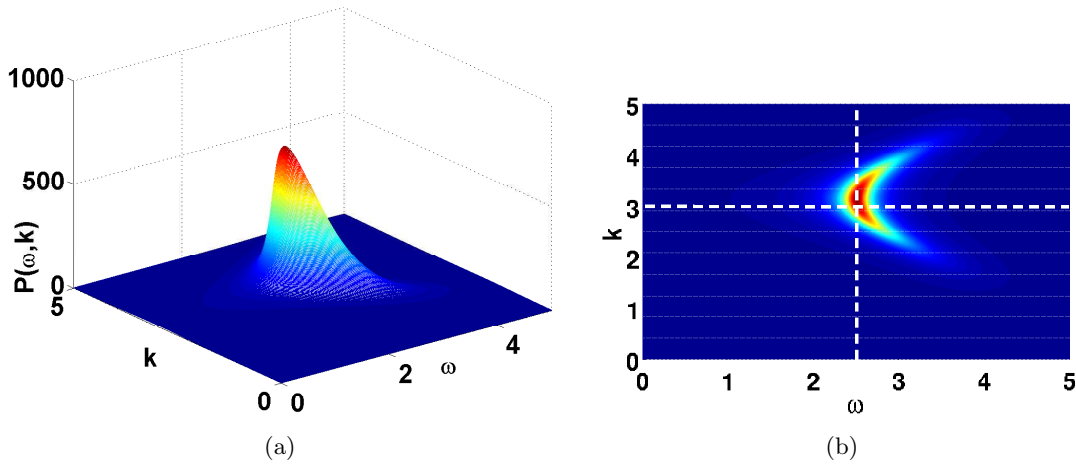


Figure 4.9: Right: The power spectrum of fluctuations for species 1, near the region of mean field wave instability, see point A in figure 4.5. Point A corresponds to the following choice of parameters:  $a = d = 1$ ,  $\sigma = 2$ ,  $\gamma = 1$ ,  $b = 15$ ,  $\beta = 0.27$ ,  $c = 141$ . Left: 2D projection of the power spectrum in the plan  $(k, \omega)$ . A clear peak is displayed, implying that a quasi-wave sets in outside the region of deterministic wave like instability. The dashed line are traced in correspondence of (i)  $k = \pi$  the value that maximizes the (negative) real part of the dispersion relation (horizontal line); (ii) the value of the imaginary part of the dispersion relation as measured in  $k = \pi$  (vertical dashed line).

The power spectrum relative to position A in the reference plane  $(\beta, c)$  is reported in figures 4.9(a) and 4.9(b). A clear peak is displayed for values of  $k$  and  $\omega$  different from zero. The maximum of the power spectrum is approximately located at  $k = \pi$ , where the real part of the dispersion has its maximum. Notice that this latter is negative, implying that no instability can develop in the mean field limit. The value that  $\omega$  takes in correspondence of the peak is very similar to the value that the imaginary part of the dispersion relation has for  $k = \pi$ , see vertical dashed line in figure 4.9(b). Stochastic corrections can hence drive the emergence of a quasi-wave, an observation which agrees with the conclusion of [56]. The phase velocity  $\omega/k$  of the wave can be approximately predicted by working with the linearized mean field equations for the continuum concentration amount. As a simple rule of the thumb, quasi-waves manifest when the system is sufficiently close to region I, i.e. the region of deterministic wave instability, while still being confined in region III, where the homogeneous fixed point is stable.

Conversely, when the parameters are assigned so to fall in the vicinity of region II, stochastic Turing patterns [10] are expected to occur. This intuitive picture finds its justification in figure 4.10(a) and 4.10(b). A localized peak in the power spectrum is in fact seen at  $k = \pi$  (the maximum of the real part of the distribution function), along the  $\omega = 0$  direction, when the parameters of the system are set to the values corresponding

to point B of figure 4.5, just outside the boundaries of the classical Turing region II. Stochastic fluctuations will materialize in a asymptotically stable pattern ( $\omega = 0$ , namely  $t \rightarrow \infty$ ) with a characteristic wavelength that is controlled by the dominant  $k$  number. This latter value can be correctly anticipated based on a straightforward linear stability analysis of the underlying deterministic equations.

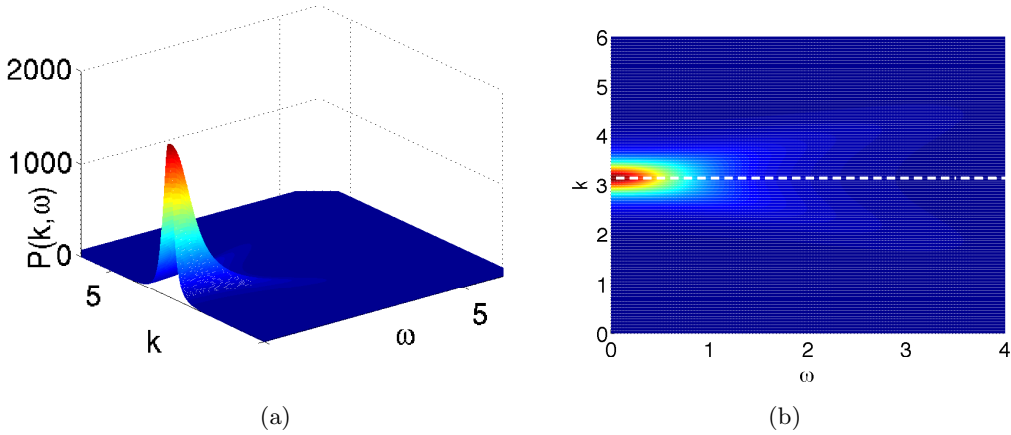


Figure 4.10: Right: The power spectrum of fluctuations for species 1, near the region of mean field Turing instability, see point B in figure 4.5. Point B corresponds to the following choice of parameters:  $a = d = 1$ ,  $\sigma = 2$ ,  $\gamma = 1$ ,  $b = 15$ ,  $\beta = 0.7$ ,  $c = 143$ . Left: 2D projection of the power spectrum in the plan  $(k, \omega)$ . A peak in  $k$  is found along the  $\omega = 0$  direction, implying that a stochastic Turing instability develops just outside the region of deterministic Turing like instability. The horizontal dashed line is located at  $k = \pi$ , the value that maximizes the (negative) real part of the dispersion relation.

Summing up, the maxima of the, negatively defined, relation of dispersion signals the spatial location of the peaks in the power spectrum of fluctuations. As we emphasized in the previous section, the dispersion relation can occasionally display two maxima, which in principle should yield to two distinct peaks in the corresponding power spectrum. This possibility is testified in figure 4.11, where the location of the peak(s) in  $k$  is plotted (stars) as a function of  $c$ , in a region where the homogeneous fixed point is stable, and close to the Turing domain of mean field order. The parameters are chosen so that the dispersion relation has two bumps inside, and immediately outside the region of deterministic instability. Then, by increasing the value of  $c$ , the two peaks in the power spectrum approach each other and eventually merge to give rise to a localized peak in  $\pi$ . This behaviour results in the bifurcation diagram reported in figure 4.11. The circles in figure 4.11 pinpoint to the positions of the maxima of the dispersion relation. An overall agreement is observed, thus confirming the intuition that the position of maxima of the power spectrum should reflect very closely the location of the maxima of the (real in this case) dispersion relation function. Discrepancies are instead detected in the vicinity of the transition point. Similar conclusions hold, when working close to the wave instability domain. In figures 4.12(a) and 4.12(b) the power spectrum is plotted for distinct values of  $c$ , yielding to, respectively, two or one peaks.

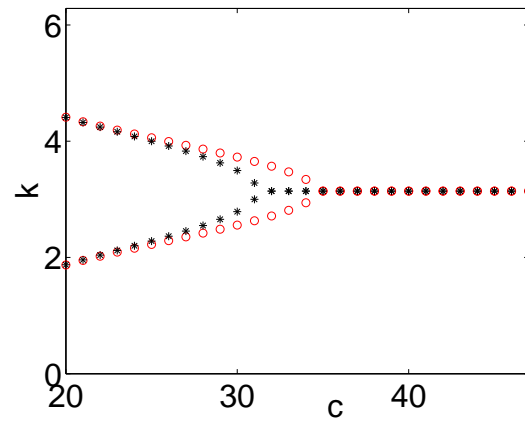


Figure 4.11: The location in  $k$  of the peaks in the power spectra as a function of  $c$ , the region when the homogeneous fixed point is stable to spatial perturbation (stars). The circles identify the position of the maxima of the dispersion relation. Parameters are set as  $a = d = 1$ ,  $\sigma = 1$ ,  $\gamma = 1$ ,  $b = 2$ ,  $\beta = 0.7$ .

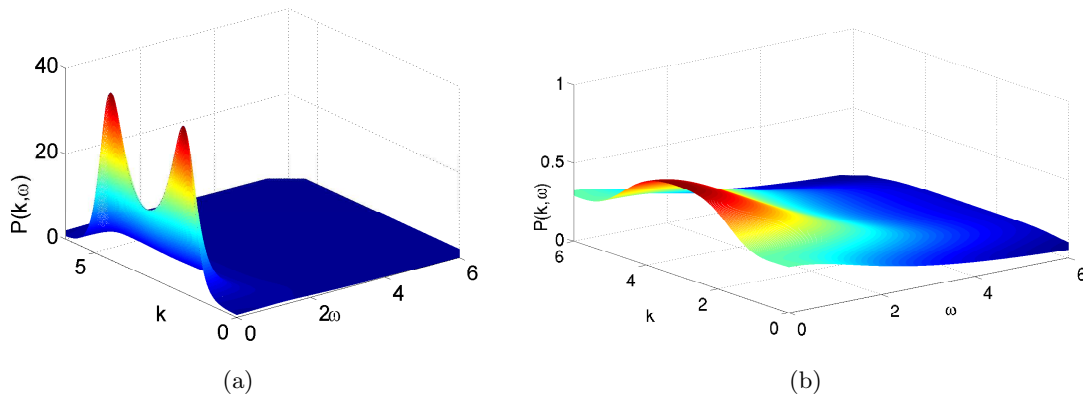


Figure 4.12: Right: The power spectrum of fluctuations relative to species 1 for  $a = d = 1$ ,  $\sigma = 1$ ,  $\gamma = 1$ ,  $b = 2$ ,  $\beta = 0.7$ ,  $c = 23$ , which corresponds to operate before the bifurcation point in figure.4.11. Two peaks are indeed observed. Left: The power spectrum of fluctuations relative to species 1 for  $a = d = 1$ ,  $\sigma = 1$ ,  $\gamma = 1$ ,  $b = 2$ ,  $\beta = 0.7$ ,  $c = 38$ , which corresponds to working after the bifurcation point in figure.4.11. One isolated peak in  $k = \pi$  is found.

#### 4.2.4 Details of the van Kampen expansion

In the following we briefly outline the main steps involved in the implementation of the van Kampen system size expansion, with reference to model (4.23). As already discussed in the main body of the chapter, the quantity  $1/\sqrt{N}$  serves as a small parameter in the development. First, one can expand the operator  $\varepsilon_{X,i}^\pm$   $\varepsilon_{Y,i}^\pm$  to get the approximate expressions:

$$\begin{aligned}\varepsilon_{X,i}^\pm &= 1 \pm \frac{1}{N^{1/2}} \frac{\partial}{\partial \xi_i} + \frac{1}{2N} \frac{\partial^2}{\partial \xi_i^2} \pm \frac{1}{3!N^{3/2}} \frac{\partial^3}{\partial \xi_i^3} + \dots \quad . \\ \varepsilon_{Y,i}^\pm &= 1 \pm \frac{1}{N^{1/2}} \frac{\partial}{\partial \eta_i} + \frac{1}{2N} \frac{\partial^2}{\partial \eta_i^2} \pm \frac{1}{3!N^{3/2}} \frac{\partial^3}{\partial \eta_i^3} + \dots \quad .\end{aligned}$$

Then we set:

$$\Pi(\boldsymbol{\xi}, \boldsymbol{\eta}, t) = P_{\mathbf{n}, \mathbf{m}}(t).$$

A simple manipulation yields to:

$$\frac{dP}{dt} = \frac{\partial P}{\partial t} - \sqrt{N} \left( \nabla_{\boldsymbol{\xi}} \Pi \frac{\partial \phi_i}{\partial t} + \nabla_{\boldsymbol{\eta}} \Pi \frac{\partial \psi_i}{\partial t} \right).$$

Similarly, one can act on the right hand side of Eq. (4.23) and hierarchically organize the resulting terms with respect to their respective  $N$ -dependence. Consider, as an example the term:

$$T(n_i + 1, m_i | n_i, m_i) = \left( -\frac{1}{\sqrt{N}} \frac{\partial}{\partial \xi_i} + \frac{1}{2N} \frac{\partial^2}{\partial \xi_i^2} \right) \left( 1 - \phi_i - \frac{\xi_i}{\sqrt{N}} - \psi_i - \frac{\eta_i}{\sqrt{N}} \right).$$

At order  $N^{-1/2}$ , one gets:

$$\frac{\partial}{\partial \xi_i} (-a + a\phi_i + \psi_i).$$

Then, at the order  $N^{-1}$ , we obtain:

$$\frac{1}{2} \left( \frac{\partial^2}{\partial \xi_i^2} (a(1 - \phi_i - \psi_i)) \right) + \frac{\partial}{\partial \xi_i} (\xi_i + \eta_i) a.$$

The other terms in the right hand side of the master equation, including the diffusion parts, can be treated in a completely analogous fashion. Combining together the leading contribution (order  $1/\sqrt{N}$ ), one eventually recovers the mean field equations (4.27), i.e. the partial differential equations for the local concentration amount  $\phi_i$  and  $\psi_i$ . Notice that in equations (4.27) the rescaled time  $\tau$  appears. This is defined as  $\tau = t/N$ .

At the next to leading order (order  $1/N$ ), one gets a Fokker-Planck equation for the evolution of the distribution of fluctuations  $\Pi$ :

$$\frac{\partial \Pi}{\partial \tau} = - \sum_{i=1}^{\Omega} \left( \sum_{r=1}^2 \frac{\partial}{\partial \xi_{r,i}} \left[ J_{r,i} \xi_{r,i} \Pi \right] + \frac{1}{2} \sum_{j \in i-1, i+1} \sum_{r,s=1}^2 \frac{\partial}{\partial \xi_{s,i}} \frac{\partial}{\partial \xi_{r,j}} \left[ K_{rs,ij} \Pi \right] \right), \quad (4.41)$$

where we have indicated with  $\xi_{1,i} = \xi$  and  $\xi_{2,i} = \eta$ . Here, the matrix  $J$  reads:

$$J = \begin{pmatrix} -a - d - b + 2c\phi_i\Lambda \sum_j e^{-\sigma|j|}\psi_{i-j} + \gamma(1 - \psi_i)\Delta_i & -a + c\phi_i^2 + \gamma\phi_i\Delta_i \\ b - 2c\phi_i\Lambda \sum_j e^{-\sigma|j|}\psi_{i-j} + \beta\psi_i\Delta_i & -c\phi_i^2 + \beta(1 - \phi_i)\Delta_i \end{pmatrix}.$$

Since we are interested in characterizing the fluctuations at equilibrium, we shall impose  $\phi = \phi^*$  and  $\psi = \psi^*$ ,  $\forall i$  and indicate with the symbol  $J^*$  the obtained matrix. To write in a compact form the the elements of matrix  $K$  we introduce the index  $h = |i - j|$ , which takes values 0, 1. Element  $K_{rs,ij}$  can be therefore mapped into  $K_{rs,h}$ , as hereafter specified:

$$\begin{cases} K_{11,0} = a - a\phi_i - a\psi_i + d\phi_i + b\psi_i + c(\phi_i)^2\Lambda \sum_j e^{-\sigma|j|}\psi_{i-j} + 4\gamma(\phi_i - (\phi_i)^2 - \phi_i\psi_i) \\ K_{11,1} = +2\gamma(-\phi_i + (\phi_i)^2 + \phi_i\psi_i) \\ K_{22,1} = +2\gamma(-\psi_i + (\psi_i)^2 + \phi_i\psi_i) \\ K_{22,0} = b\phi_i + c(\phi_i)^2\Lambda \sum_j e^{-\sigma|j|}\psi_j + 4\beta(\psi_i - (\psi_i)^2 - \psi_i\phi_i) \\ K_{12,1} = 0 \\ K_{12,0} = -b\phi_i - c(\phi_i)^2\Lambda \sum_j e^{-\sigma|j|}\psi_{i-j}. \end{cases}$$

Matrix  $K$  is also evaluated at the fixed point  $(\phi^*, \psi^*)$  and transforms into  $K^*$ .

#### 4.2.5 Details of the power spectrum calculation

The Fokker-Planck equation (4.41) yields to the following Langevin equation:

$$\dot{\xi}_{r,i}(t) = \sum_{s=1}^2 J_{rs,i}\eta_{r,i}(t), \quad (4.42)$$

which rules the evolution of the fluctuations  $\xi_{r,i}(t)$ . Here,  $\eta_{r,i}(t)$  is a random Gaussian variable, whose statistical properties are:

$$\langle \eta_{r,i} \rangle = 0 \quad \langle \eta_{r,i}(t)\eta_{s,j}(t') \rangle = K_{rs,|i-j|}^*\delta(t - t'). \quad (4.43)$$

Starting from this setting one can straightforwardly calculate the power spectrum of fluctuations following a procedure which is for example discussed in [24, 3]. Here, we shall detail the main steps of the derivation adapting it to the present setting. We first take the spatial and temporal Fourier transform of (4.42), here denoted with the symbol  $\tilde{\cdot}$ , to obtain:

$$-i\omega\tilde{\xi}_{r,k}(\omega) = \sum_{s=1}^2 \tilde{J}_{rs,k}\tilde{\xi}_{s,k}(\omega) + \tilde{\eta}_{s,k}(\omega), \quad (4.44)$$

where  $\Omega$  and  $k$  respectively stand for the Fourier time and space frequencies. In the above equation,  $\tilde{J}_{rs,k}$  are just the  $J_{rs,i}$  terms, where we have replaced the discrete Laplacian  $\Delta_i$  with the corresponding spatial Fourier transform  $\Delta_k = 2(\cos(k) - 1)$ .

By defining  $\tilde{M}_{rs,k}(\omega) = -i\omega\delta_{rs} - \tilde{J}_{rs,k}$ , equation (4.42) can be cast in the form:

$$\tilde{\xi}_{r,k}(\omega) = \sum_{s=1}^2 \tilde{M}_{rs,k}^{-1}(\omega)\tilde{\eta}_{s,k}(\omega).$$

The Power Spectrum of fluctuations of a given species  $s$  is defined as  $P_s(k, \omega) = \langle |\tilde{\xi}_s(k, \omega)|^2 \rangle$ . Making use of relation (4.43), after some calculations one eventually comes to the final expression:

$$P_s(k, \omega) = \sum_{r,u=1}^2 \tilde{M}_{sr,k}^{-1}(\omega) \tilde{W}_{ru,k} (\tilde{M}_{us,k}^\dagger)^{-1}(\omega), \quad (4.45)$$

where:

$$\tilde{W}_{ru,k} = \tilde{K}_{ru,0} + 2\tilde{K}_{ru,1} + \tilde{K}_{ru,1}\Delta_k.$$

Closed analytic expressions for the power spectra are also derived [24, 3] which read:

$$P_1(\omega, k) = \frac{C_{1,k} + \tilde{W}_{11,k}\omega^2}{(\omega^2 - \Omega_0^2)^2 + \Gamma^2\omega^2} \quad P_2(\omega, k) = \frac{C_{2,k} + \tilde{W}_{22,k}\omega^2}{(\omega^2 - \Omega_0^2)^2 + \Gamma^2\omega^2}, \quad (4.46)$$

where

$$\begin{cases} \Omega_0 = \sqrt{\det(J^*(k))} \\ \Gamma = -\text{tr}(J^*(k)) \\ \tilde{W}_{11,k} = a(1 - \phi^* - \psi^*) + \phi^*(d + b) + c(\phi^*)^2\psi^* + 2\Delta_k\gamma(-\phi^* + (\phi^*)^2 + \phi^*\psi^*) \\ \tilde{W}_{22,k} = b\phi^* + c(\phi^*)^2\psi^* + 2\Delta_k\beta(-\psi^* + (\psi^*)^2 + \phi^*\psi^*) \\ C_{1,k} = \tilde{W}_{22,k}(J_{11,k}^*)^2 - 2\tilde{W}_{12,k}J_{21,k}^*J_{11,k}^* + \tilde{W}_{11,k}(J_{21,k}^*)^2. \end{cases} \quad (4.47)$$

Spatio temporal self-organized patterns [76] can spontaneously emerge in a reaction-diffusion systems. A small perturbation of a homogeneous fixed point can for example amplify, as follows a symmetry breaking instability seeded by diffusion, and eventually yield to a steady state non homogeneous solution. These are the Turing patterns [9], recurrently investigated in chemistry [49, 50] and biology [76].

The majority of studies devoted to the Turing instability consider two, mutually interacting, species. More specifically, and following the customarily accepted paradigm, one species activates the production of the other, this latter acting through an inhibitor feedback. Systems of three [51] simultaneously diffusing species have been also considered and shown to display a rich zoology of possible patterns and instabilities. Patterns can also develop if only one species is allowed to diffuse in the embedding medium, provided the system is composed of at least three coupled species [52]. In contrast, it is well known [52] that two species systems where only one species can migrate, cannot undergo Turing instability. Models however exist which fall within this category [18]. For this reason, it is of general interest to theoretically explore the possibility of bifurcation patterns of such systems, beyond the classical Turing framework. This chapter aims at elaborating along these lines, by considering the generalized concept of stochastically driven patterns.

Reaction-diffusion systems are in fact generally studied by resorting to deterministic mathematical models. The continuum concentrations of the interacting species is hence monitored over space and in time. As opposed to this, one can develop an individual based description of the scrutinized dynamics, which effectively accounts for the inherent discreteness of the system. Stochastic contributions, stemming from finite size corrections, can thus modify the idealized mean field picture and occasionally return alternative scenarios to interpret available data.

In a series of recent publications, the effect of the intrinsic noise was indeed shown to create stochastic patterns, in a region of the parameters for which macroscopically ordered structures do not occur. When the deterministic dynamics predicts a stable homogeneous state, the stochastic component can amplify via a resonant mechanism, giving birth to stochastic Turing patterns [53, 10, 12]. The effect of finite size fluctuations can be characterized with numerical simulations, but also analytically with a mathematical technique, known as van Kampen system size expansion. This allows to expand the governing master equation, which accounts for the role of demographic fluctuations. At the first order of the expansion, the deterministic mean-field model is obtained, while the second order contributions form an equation for the stochastic fluctuations.

Working in this context, we will consider a simple birth and death model, with two species, of which one can diffuse. The reaction rates are assumed to be generic non linear functions of the concentration amount. Conditions for the emergence of stochastic Turing patterns are derived. More concretely, stochastic Turing patterns can materialize if the power spectrum of fluctuations has at least a peak for a non zero spatial wave number  $k$  for  $\omega$ , the Fourier time frequency, equal to zero. We will here prove that a non trivial maximum of the power spectrum exists, if the system matches specific conditions that we shall mathematically characterise. The validity of our conclusions are tested for a simple non linear model, which falls in the general class of models inspected. With reference to this specific case study, we perform stochastic simulations through the Gillespie's algorithm and confirm a posteriori the adequacy of the predictions.

### 4.3 Conclusion

In this chapter we have presented two Brusellator-type models with excluded volume competition. Particles can migrate from one site to a neighbouring patch only if there is at least one empty site, or vacancy, to be eventually filled. Because of this competition for the available space, a modified (deterministic) diffusive behaviour was recovered: cross diffusive terms appear which link multiple diffusing communities and which add to the standard Laplacian terms, relics of Fick's law. In the first model, we have seen that Turing patterns can develop for virtually any ratio of the main diffusivities in a multi-species setting. This striking effect originates from the generalized diffusion theory that has been here assumed to hold and that builds on the scheme discussed in [70]. The fact that Turing like patterns are possible for equal diffusivities of the species involved, as follows a sound dynamical mechanism, constitutes an intriguing observation that hold promises to eventually reconcile theory and experimental evidences. The investigated setting applies in particular to multi-species systems that evolve in a crowded environment, as happens for instance inside the cells where different families of proteins and other biomolecular actors are populating a densely packed medium. It is interesting to notice that the stochastic fluctuations, endogenous to the scrutinized system in its discrete version, eventually destroy the patterns, that are instead deemed to be stable according to the idealized deterministic viewpoint. The lifetime of the metastable patched patterns increases however with the size of the system, in striking analogy with what has been observed for the so called Quasi-Stationary States, out of equilibrium regimes observed in systems subject to long-range interactions. For large enough  $N$ , the homogenization as seeded by fluctuations is progressively delayed and eventually prevented in the continuum limit  $N \rightarrow \infty$ .

In the second part of this chapter we have further modified the model with the inclusion of a long range coupling between interacting species, following the scheme introduced in [56]. The proposed model is inherently stochastic and it was first studied in its mean field limit. The excluded volume effect that we have imposed at the mesoscopic scale, yields cross terms in the diffusion part, as mentioned before. These latter are believed to play a crucial role under crowding conditions [70]. In its deterministic version, the model admits both Turing like and wave instabilities, an observation that extends the analysis of [56] to the present setting, where cross diffusion terms are accommodated for. Interestingly, and as remarked in the first part of the chapter [12], the Turing instability can occur also if the activator diffuses faster than the inhibitor. A cusp-like transition was found between the Turing and waves instability zone. The location of the cusp was analytically characterized. Parameters can be eventually set so as to produce a region of Turing order which is disconnected by the domain of wave instability. In the end we have elaborated on the role of finite size corrections showing that these can drive the emergence of stochastic waves and Turing patterns, beyond the region of mean field instability. This observation makes contact with the analysis of [10, 56]. Furthermore, we have here discussed the specific form of the power spectra of fluctuations. One or two peaks are occasionally found, reflecting the peculiar specificity of the underlying dispersion relation.



# Conclusion

Microscopic systems are characterized by temporal oscillations and spatial organization that, in some cases, the standard deterministic approach fails to capture. In the last few years, this observation has stimulated researchers to develop new theoretical frameworks to understand better these systems. The discrete nature of the systems, not considered commonly in literature, can drive it to a stochastic resonance, resulting in spatio-temporal patterns.

In this thesis we have investigated crucial aspects of the dynamics of different systems due to the finite size effects. First we have studied a stochastic intracellular calcium oscillation model that gave us the opportunity to introduce the analytical and numerical techniques, that we used throughout the thesis. We demonstrated [77] that the stochastic component of the dynamics, which is generally not included in model of deterministic inspiration, resulted in the emergence of self-sustained oscillations, named quasi-cycles. The signature to the presence of cycles was represented by a peak in the power spectrum of temporal fluctuations. We have characterized analytically the frequency for which the power spectrum presents a maximum in dependence of the IP3 stimulation. IP3 in a cell was generated by an external signal that is possible to control in the experiment. As a possible future study along this direction, it could be interesting to verify, in direct experiments, the existence of quasi-cycles for intracellular calcium oscillation as mediated by finite size. In practice this amounts to verify that our theoretical prediction of the maximum of the power spectrum is reflected in the effective dynamics of real system and allow to see calcium oscillation also for some degree of stimulation of IP3 that are not predicted by a mean-field model.

In the second chapter we have introduced the Kaneko model [6], that involves a closed scheme of auto-catalytic reactions. From a numerical observation we revealed that, for low concentration, the distribution of fluctuations was no longer Gaussian. We wanted to characterize analytically this non-Gaussian behaviour. In order to achieve this goal, we used the van Kampen expansion beyond the classical Gaussian approximation and calculated the corresponding generalized Fokker-Planck equation. Then, it was possible to write a system of ordinary differential equation for the moments of the distribution. From the knowledge of the moments it was possible to rebuild the profile of the distribution of fluctuations.

Motivated by the good agreement between theoretical and numerical distributions, we wanted to extend this preliminary result. To this end we made use of a simple one dimensional model, known as the voter model [7]. For this model it became possible to derive explicitly all the moments for any order of the development. The ODE for the moments resulted in a closed system, that allowed us to rebuild the profile of distribution for any time and close to the absorbing barrier. The agreement between theory and

numerical simulations represented an a posteriori demonstration of the validity of the van Kampen expansion beyond the Gaussian approximation which was classically being employed. Expanding along this direction it could be interesting to test the generalized van Kampen expansion for spatially extended system.

At the end of this second chapter of the thesis we wanted to compare the accuracy of the van Kampen expansion and the WKB method, both used beyond the classical order of approximation, for a microscopic logistic model. The WKB techniques was developed to study rare events from one metastable state to another one. We focused on extinction phenomenon, and for this reason, we considered the van Kampen expansion beyond the classical order of approximation.

In the last two chapters we used the van Kampen expansion in order to study self-organized dynamics due to the intrinsic fluctuations in spatially extended systems. Working in this context, we were particularly interested in studying the Turing patterns formation, from a microscopic point of view.

First we presented a reaction diffusion model in one spatial dimension in which only one species could diffuse [11]. For such system, the classical Turing instability could not take place. However considering the finite size corrections, Turing like patterns could develop. General conditions were derived for the stochastic Turing patterns to occur. The observable that allowed us to conclude that stochastic Turing pattern occur in the system was a peak in the spatial Fourier variable  $k$  for the power spectrum of fluctuations.

In the fourth chapter we investigated the roles of crowding in relation to the Turing instability. Starting from a microscopic formulation of the dynamics and accounting for the finite carrying capacity of the hosting volume, we recovered a modified diffusive behaviour in the mean-field limit. Cross diffusive terms appeared, which could contribute to explain the deviation from the conventional Fick's law, as seen in crowded diffusion experiments. Working in this generalized setting of diffusion, the Turing instability could take place for some parameters for which in the classical approach is mathematically prohibited. We derived analytically the new conditions for having Turing instability in this generalized context. We concluded that Turing instability could set in for all ratios of the main diffusivities, also when the (isolated) activator diffuses faster then the (isolated) inhibitor. The numerical results, that supported our conclusion was carried out for the Brussellator model.

The second model, studied in the fourth chapter, was a modified version of the Brussellator model, that accounted for a long range coupling among constituents [13]. The mean-field limit of the model was studied and the condition for Turing and wave instability obtained. A degenerate, cusp-like transition, was found analytically, that separates the domains of Turing and wave order. We also elaborated on the role of stochastic corrections. Stochastic waves or Turing patterns could set in as signalled by the power spectrum of fluctuations. To complete our study about stochastic patterns it could be interesting to extend the previous results to a 2D model that presents spiral waves patterns in a mean-field context. In particular it could be interesting to look for the emergence of stochastic spiral waves and elaborate on their analytical description.

# Appendix A

## A technique to simulate the full stochastic process: The Gillespie algorithm

In 1976 Daniel T. Gillespie proposed an algorithm to exactly simulate the stochastic dynamics of chemical reactions [28],[39]. To describe this method, let us consider a volume  $V$  which contains molecules of  $N$  chemically active species  $S_i$  for  $i = 1, \dots, N$ , and denote by  $X_i$  the current number of molecules of species  $S_i$  in  $V$ . The molecules interact according to  $M$  chemical reactions  $R_\mu$  for  $\mu = 1, \dots, M$ , each characterized by a reaction parameter  $c_\mu$ . The quantity  $c_\mu \delta t$  represents the first order approximation<sup>1</sup> of the average probability that a particular combination of  $R_\mu$  reactant molecules will react accordingly in the next time interval  $\delta t$ , as it follows by a chemical kinetics theory derived into details in the original paper [28].

To illustrate the relationship between  $c_\mu$  and the more familiar “reaction rate constant”  $k_\mu$  used in the deterministic formulation of chemical kinetics, let us consider as example the reaction  $S_1 + S_2 \longrightarrow 2S_3$ . In this case,  $X_1 X_2 \cdot c_\mu dt$  is the probability that the reaction will occur inside  $V$  in the next time interval  $dt$ , where  $X_1 X_2$  represents the distinct combinations of reactant molecules in  $V$ . Averaging over a set of stochastically identical system, and diving by  $V$ , we obtain the average reaction rate per unit time  $\langle X_1 X_2 \rangle c_\mu / V$  or, in terms of molecular concentrations  $x_i = X_i / V$ ,  $\langle x_1 x_2 \rangle c_\mu V$ . If we divide this latter quantity by the product of the average densities of the reactants, we obtain the expression for  $k_\mu$ , namely

$$k_\mu = \frac{\langle x_1 x_2 \rangle c_\mu V}{\langle x_1 \rangle \langle x_2 \rangle} \quad (\text{A.1})$$

In the deterministic formulation the average of a product is equivalent to the product of the averages, thus  $\langle x_1 x_2 \rangle = \langle x_1 \rangle \langle x_2 \rangle$  and (A.1) simplifies to

$$k_\mu = V c_\mu$$

The factor  $V$  in this relation is due to the type of reaction considered. In reactions with only one reactant molecule, indeed, the factor  $V$  would be absent, while in those with three reactants, a  $V^2$  would instead appear.

---

<sup>1</sup>More precisely, the first order in  $\delta t$  means that the average probability is  $c_\mu \delta t + o(\delta t)$  with  $\lim_{\delta t \rightarrow 0} o(\delta t) / \delta t = 0$ .

The aim of the method is to simulate the time evolution of the  $N$  variables  $X_i$  knowing their initial values  $X_i(0)$ , the  $M$  reactions  $R_\mu$  and the associated reaction parameters  $c_\mu$ . The standard stochastic approach to this problem focuses on the master equation, namely the time evolution of the probability function  $P(X_1, \dots, X_N; t)$  to have  $X_i$  molecules of  $S_i$  (for  $i = 1, \dots, N$ ) at time  $t$ . In most cases this approach turns out to be intractable, both analytically and numerically. To overcome this problem, Gillespie proposed a method based on what he called the reaction probability density function  $P(\tau, \mu)$ . He defined this quantity as the probability at time  $t$  that the next reaction in  $V$  will occur in the time interval  $(t + \tau, t + \tau + \delta\tau)$  and that the selected reaction was of the type  $R_\mu$ .

The first step for deriving an analytical expression for  $P(\tau, \mu)$ , consists in associating to every chemical reaction, a state variable  $h_\mu$  defined as the distinct molecular reactant combinations for reaction  $R_\mu$  within the volume  $V$  at time  $t$ . Table ?? shows the state variables for a selection of reactions. In this way  $h_\mu c_\mu \delta t$  is the probability, to first order in  $\delta t$ , that an  $R_\mu$  reaction occurs in  $V$ , in the next time interval  $\delta t$ .

The second step requires decomposing  $P(\tau, \mu)$  as

$$P(\tau, \mu) d\tau = P_0(\tau) \cdot h_\mu c_\mu d\tau \quad (\text{A.2})$$

where  $P_0(\tau)$  is the probability at time  $t$  that no reaction will occur in the time interval  $(t, t + \tau)$ , and  $h_\mu c_\mu d\tau$  is the probability that an  $R_\mu$  reaction will occur in the next differential time interval  $(t + \tau, t + \tau + d\tau)$ .

To calculate  $P_0(\tau)$  one can divide the interval  $(t, t + \tau)$  in  $K$  subintervals of equal length  $\epsilon = \tau/K$ . In each subinterval, the probability that none of the reactions occurs is given by

$$\prod_{\nu=1}^M [1 - h_\nu c_\nu \epsilon + o(\epsilon)] = 1 - \sum_{\nu=1}^M h_\nu c_\nu \epsilon + o(\epsilon) \quad (\text{A.3})$$

In this way,  $P_0(\tau)$  is just the product of  $K$  times equation (A.3)

$$\begin{aligned} P_0(\tau) &= \left[ 1 - \sum_{\nu=1}^M h_\nu c_\nu \epsilon + o(\epsilon) \right]^K \\ &= \left[ 1 - \sum_{\nu=1}^M h_\nu c_\nu \frac{\tau}{K} + o(K^{-1}) \right]^K \end{aligned}$$

This relation holds for any  $K > 1$ , and therefore it is true for infinitely large value of  $K$ :

$$\begin{aligned} P_0(\tau) &= \lim_{K \rightarrow \infty} \left[ \frac{1 - \sum_{\nu=1}^M h_\nu c_\nu \tau + o(K^{-1})K}{K} \right]^K \\ &= \exp \left[ - \sum_{\nu=1}^M h_\nu c_\nu \tau \right] \end{aligned} \quad (\text{A.4})$$

Putting together equation (A.2) with equation (A.4) one obtains the exact expression for the probability density function

$$P(\tau, \mu) = h_\mu c_\mu \exp \left[ - \sum_{\nu=1}^M h_\nu c_\nu \tau \right] \quad (\text{A.5})$$

for  $0 \leq \tau < \infty$  and  $1 \leq \mu \leq M$  with  $\tau \in \mathbb{R}$  and  $\mu \in \mathbb{N}$ .

Before moving to the description of the algorithm, we recall the main ideas of a Monte Carlo method. This latter constitutes a crucial step in the Gillespie implementation, providing a method to generate two random numbers  $\tau$  (real) and  $\mu$  (integer) according to the joint probability density function in (A.5). The trick consists in splitting the probability density function  $P(\tau, \mu)$  into the product of two one-variable probability density functions. This procedure is called conditioning and leads to

$$P(\tau, \mu) = P_1(\tau) \cdot P_2(\mu|\tau) \quad (\text{A.6})$$

where  $P_1(\tau)d\tau$  is the probability that the next reaction will occur between times  $t + \tau$  and  $t + \tau + d\tau$ , and  $P_2(\mu|\tau)$  is the probability that the next reaction will be an  $R_\mu$  type, given that it happens at time  $t + \tau$ . Invoking the addition theorem for probabilities,  $P_1(\tau)d\tau$  is obtained by summing  $P(\tau, \mu)d\tau$  over all  $\mu$ , and thus

$$P_1(\tau) = \sum_{\mu=1}^M P(\tau, \mu)$$

Putting this into (A.6) and solving for  $P_2(\mu|\tau)$  it gives

$$P_2(\mu|\tau) = P(\tau, \mu) / \sum_{\nu=1}^M P(\tau, \nu)$$

Substituting  $P(\tau, \mu)$  with (A.5) in the previous two equations, we obtain

$$P_1(\tau) = \begin{cases} a \exp[-a\tau] & \text{for } 0 \leq \tau < \infty \\ 0 & \text{otherwise} \end{cases} \quad (\text{A.7})$$

and

$$P_2(\mu|\tau) = \begin{cases} a_\mu / \sum_{\nu=1}^M a_\nu & \text{for } \nu = 1, \dots, M \\ 0 & \text{otherwise} \end{cases} \quad (\text{A.8})$$

where

$$a = \sum_{\mu=1}^M a_\mu$$

with

$$a_\mu = h_\mu c_{mu} \quad \text{for } \mu = 1, \dots, M \quad (\text{A.9})$$

In this way the problem of finding two random numbers according to  $P(\tau, \mu)$  may be recast as the problem of drawing a real random number from the  $P_1$  distribution, and an integer random number according to  $P_2$ .

Let us first focus on the former case. We wish to generate a real number  $x$  according to a probability density function  $P(x)$ . The corresponding probability distribution function

$$F(x_0) = \int_{-\infty}^{x_0} P(x) dx \quad (\text{A.10})$$

quantifies the probability that  $x$  will be less than  $x_0$ . The inversion method for generating a random value  $x$  according to  $P(x)$  is to draw a random number  $r$  from the uniform distribution in the unit interval, and then take

$$x = F^{-1}(r) \quad (\text{A.11})$$

To prove that this procedure is correct, we have to show that the probability that the  $x$  value so generated will lie between  $x'$  and  $x' + dx'$ , is  $P(x')dx'$ . By construction, this is equivalent to calculating the probability that  $r$  will lie between  $F(x')$  and  $F(x' + dx')$ . Since  $r$  is a random number drawn from the uniform distribution in the unit interval, this probability is just the length of the interval  $[F(x'), F(x' + dx')]$ , namely  $F(x' + dx') - F(x') = F'(x')dx'$ . Applying the definition (A.10), we get

$$F(x' + dx') - F(x') = F'(x')dx' = P(x')dx'$$

and this prove that the probability density function for the random number  $x$  generated according to (A.11) is indeed  $P(x)$ .

For the specific case at hand, we wish to generate a random number  $\tau$  according to the probability density function (A.7). In this case  $F(\tau) = 1 - \exp[-a\tau]$ . Putting  $F(\tau) = r$  and inverting the function  $F$ , we obtain

$$\tau = \frac{1}{a} \ln \left( \frac{1}{r} \right) \quad (\text{A.12})$$

where, for simplicity, we have replaced the random variable  $1 - r$  by the statistically equivalent random variable  $r$ .

We have seen how to generate a random number according to a specific probability density distribution for a continuous variable. Now we consider the discrete case and we look for a method which enables us to obtain a random integer  $i$  according to the probability density function  $P(j)$ , where now  $P(j)$  is the probability that  $i = j$ . The corresponding distribution function  $F(i)$  is defined by

$$F(i) = \sum_{j=-\infty}^i P(j)$$

and  $F(i_0)$  represents the probability that  $i \leq i_0$ . With analogy to the continuous case, the inversion method consists in drawing a random number  $r$  from the uniform distribution in the unit interval and take for  $i$  that value which satisfies

$$F(i - 1) < r \leq F(i) \quad (\text{A.13})$$

To show that the procedure is correct also in this case, we use the fact the resulting integer  $i$  will equal  $j$  is equivalent to the probability that  $r$  will lie between  $F(j - 1)$  and  $F(j)$ . So we have

$$F(j) - F(j - 1) = \sum_{k=-\infty}^j P(k) - \sum_{k=-\infty}^{j-1} P(k) = P(j)$$

This proves that  $P(i)$  is indeed the probability density function for the random integer  $i$  generated according to (A.13).

As an example, we consider again our specific case, and make it explicit the expression of the random integer  $\mu$  with respect to the density function (A.8). Applying (A.13) we see that we have to select the integer  $\mu$  so that

$$\sum_{\nu=1}^{\mu-1} P_2(\nu|\tau) < r \leq \sum_{\nu=1}^{\mu} P_2(\nu|\tau)$$

or

$$\sum_{\nu=1}^{\mu-1} a_{\nu} < r \sum_{\nu=1}^M a_{\nu} \leq \sum_{\nu=1}^{\mu} a_{\nu} \quad (\text{A.14})$$

Now we have all the ingredients to describe the details of the simulation methods. The steps of the algorithm are the following:

**Step 0** Assign values to the  $M$  reaction constants  $c_1, \dots, c_M$  and initialize the  $N$  molecular population numbers  $X_1, \dots, X_N$ . Set the time variable  $t = 0$ , and specify a stopping time  $t_{stop}$ .

**Step 1** Calculate the quantities  $a_{\nu} = h_{\nu} c_{\nu}$  for  $\nu = 1, \dots, M$  for the current molecular population numbers, and the quantity  $a_0 = \sum_{\nu=1}^M a_{\nu}$ .

**Step 2** Use the Monte Carlo technique to generate a random pair  $(\tau, \mu)$  according to (A.12) and (A.14).

**Step 3** According to the numbers  $\tau$  and  $\mu$  generated in the previous step, advance time by  $\tau$  ( $t = t + \tau$ ) and update the values of  $X_i$  for every species involved in reaction  $R_{\mu}$ .

**Step 4** If  $t < t_{stop}$  go to step 1, otherwise terminate the calculation.

It is important to stress that the time series generated with this algorithm recover the exact probability distribution function given by the master equation. It can be shown, in fact, that the two approaches, the master equation and the Gillespie's method, are equivalent at the first order approximation grounded on the kinetic theory argument mentioned before.





# Bibliography

- [1] A. J. McKane and T. J. Newman. Predator-prey cycles from resonant amplification of demographic stochasticity. *Phys Rev Lett*, 94:218102, 2005.
- [2] T. Dauxois, F. Di Patti, D. Fanelli, and A. J. McKane. Enhanced stochastic oscillations in autocatalytic reactions. *Phys Rev E*, 79:036112, 2009.
- [3] P. de Anna, F. Di Patti, A. J. McKane, and T. Dauxois. Spatial model of autocatalytic reactions. *Phys Rev E*, 81:056110, 2010.
- [4] A. J. McKane, J. D. Nagy, T. J. Newman, and M. O. Stefanini. Amplified biochemical oscillations in cellular systems. *J Stat Phys*, 128:165–191, 2007.
- [5] A. J. McKane and T. J. Newman. Stochastic models in population biology and their deterministic analogs. *Phys Rev E*, 70:041902, 2004.
- [6] Y. Togashi and K. Kaneko. Transitions induced by the discreteness of molecules in a small autocatalytic system. *Phys Rev Lett*, 86:2459–2462, 2001.
- [7] C. Cianci, F. Di Patti, and D. Fanelli. Non-gaussian fluctuations in stochastic models with absorbing barriers. *EPL*, 96:50011, 2011.
- [8] C. Cianci, D. Fanelli, and A. J. McKane. Wkb versus generalized van kampen system size expansion: the stochastic logistic equation. page In preparation, 2013.
- [9] A. M. Turing. The chemical basis of morphogenesis. *Phils Trans R Soc London Ser B*, 237:37–72, 1952.
- [10] T. Biancalani, D. Fanelli, and F. Di Patti. Stochastic turing patterns in the brusselator model. *Phys Rev E*, 81:046215, 2010.
- [11] L. Cantini, C. Cianci, D. Fanelli, E. Massi, L. Barletti, and Malbor Aslani. Stochastic amplification of spatial modes in a system with one diffusing species. (*to appear*) *Journal of Mathematical Biology*.
- [12] D. Fanelli, C. Cianci, and F. Di Patti. Multispecies reaction diffusion models and the turing instability revisited. *Eur. Phys. J. B*, 86:142, 2013.
- [13] C. Cianci and D. Fanelli. Stochastic patterns and the role of crowding. *Discontinuity, Nonlinearity, and Complexity*, 2:301–319, 2013.
- [14] T. Reichenbach, M. Mobilia, and E. Frey. Mobility promotes and jeopardizes biodiversity in rockpapersissors games. *Nature*, 30:448, 2007.

- [15] A. J. Black and A. J. McKane. Stochastic amplification in an epidemic model with seasonal forcing. *J. Theor. Biol.*, 179:85–94, 2010.
- [16] H. Li, Z. Hou, and H. Xin. Internal noise stochastic resonance for intracellular calcium oscillations in a cell system. *Phys. Rev. E*, 71:061916, 2005.
- [17] G. Dupont and A. Goldbeter. Theoretical insights into the origin of signal-induced calcium oscillations. *Cell to Cell Signaling: from experiments to theoretical models*, pages 461–474, 1989.
- [18] A. Goldbeter, G. Dupont, and M. J. Berridge. *Biochemical oscillations and cellular rhythms*. 1996.
- [19] H. Lodish. *Molecular Cell Biology*. 2002.
- [20] R. W. Tsien and R. Y. Tsien. Calcium channels, stores and oscillations. *Annu. Rev. Cell. Bio.*, 6:715–760, 1990.
- [21] T. Meyer and L. Stryer. Molecular model for receptor-stimulated calcium spiking. *Proc. Natl. Acad. Sci. USA*, 85:5051–5055, 1988.
- [22] A. Goldbeter, G. Dupont, and M. J. Berridge. Minimal model for signal-induced  $ca_{2+}$  oscillations and for their frequency encoding through protein phosphorylation. *Proc. Natl. Acad. Sci. USA*, 87:1461–1465, 1990.
- [23] F. Di Patti, S. Azaele, J. R. Banavar, and A. Maritan. System size expansion for systems with an absorbing state. *Phys Rev E*, 83:010102(R), 2011.
- [24] C. A. Lugo and A. J. McKane. Quasicycles in a spatial predator–prey model. *Phys Rev E*, 78:051911, 2008.
- [25] J. Marchant and I. Parker. Role of elementary  $ca_{2+}$  in generating repetitive  $ca_{2+}$  oscillations. *EMBO J*, 20:65–71, 2001.
- [26] M. Falcke. On the role of stochastic channel behavior in intracellular  $ca_{2+}$  dynamics. *Biophys J*, 84:42–56, 2003.
- [27] A. Goldbeter. Computational approaches to cellular rhythms. *Nature*, 420:238, 2002.
- [28] D. T. Gillespie. A general method for numerically simulating the stochastic time evolution of coupled chemical reactions. *J. Comp. Phys.*, 22:403–434, 1976.
- [29] N. G. van Kampen. *Stochastic processes in Physics and Chemistry*. North Holland, Amsterdam, 1992.
- [30] B. Alberts et al. *Molecular Biology of the Cell*. Garland Science, fifth edition edition, 2007.
- [31] H. J. Morowitz, B. Heinz, and D. W. Deamer. Origin life evolution biosphysic. *Phys Rev E*, 18:281, 1988.
- [32] D. W. Deamer. Orig. life evol. biosph. *Phys Rev E*, 17:3, 1986.
- [33] P. L. Luisi. *The Emergence of Life*. Cambridge University Press, 2006.

- [34] M. Eigen. *Naturwissenschaften*, 58:465, 1971.
- [35] Y. Togashi and K. Kaneko. Alteration of chemical concentrations through discreteness-induced transitions in small autocatalytic systems. *J Phys Soc Jpn*, 72:62–68, 2003.
- [36] C. W. Gardiner. *Handbook of Stochastic Methods*. Springer, second edition, 1985.
- [37] R. Grima. Noise-induced breakdown of the Michaelis-Menten equation in steady-state conditions. *Phys Rev Lett*, 102:218103, 2009.
- [38] H. Risken and H. D. Vollmer. On the application of truncated generalized Fokker-Planck equations. *Z. Physik B*, 35:313, 1979.
- [39] D. T. Gillespie. Exact stochastic simulation of coupled chemical reactions. *J Phys Chem*, 81:2340–2361, 1977.
- [40] S. Zamuner. Tesi di laurea. Master’s thesis, Department of Physics, University of Padua, 2009.
- [41] R. F. Pawula. Approximation of the linear boltzmann equation by the Fokker Planck equation. *Physical Review*, 162:186–188, 1967.
- [42] R. F. Pawula. Generalizations and extensions of the Fokker Planck Kolmogorov equation. *IEEE Transaction on Information Theory*, 13:33–41, 1967.
- [43] C. Cianci, F. Di Patti, D. Fanelli, and L. Barletti. Analytical study of non gaussian fluctuations in a stochastic scheme of autocatalytic reactions. *Eur. Phys. J. Special Topics*, 212:5–22, 2012.
- [44] P. C. Bressloff. Metastable states and quasicycles in stochastic wilson-cowan model of neuronal population dynamics. *Phys. Rev. E*, 82:051903, 2010.
- [45] H. Touchette. The large deviation approach to statistical mechanics. *Physics Report*, 43(1):1–3, 2009.
- [46] M. I. Freidlin and A. D. Wentzell. *Random Perturbations of Dynamical systems*. 1984.
- [47] A. J. Black and A. J. McKane. Wkb calculation of an epidemic outbreak distribution. *J. Stat. Mech.*, page P12006, 2011.
- [48] J. D. Murray. *Mathematical Biology I: An Introduction*. Springer-Verlag, third edition, 2002.
- [49] B. P. Belousov. Periodically acting reaction and its mechanism. *Collection of Abstracts on Radiation Medicine*, 145:147, 1959.
- [50] S. Strogatz. *Non linear dynamics and chaos: with applications to Physics, Biology, Chemistry and Engineering*. Perseus Book Group, 2001.
- [51] R. A. Satnoianu, M. Menzinger, and P.K. Maini. Multispecies reaction diffusion models and the turing instability revisited. *Math. Biol.*, 41:493–512, 2000.

- [52] B. Ermentrout and M. Lewis. Pattern formation in systems with one spatially distributed species. *Bull. of Math. Biol.*, 59:533–549, 1997.
- [53] T. Butler and N. Goldenfeld. Robust ecological pattern formation induced by demographic noise. *Phys Rev E*, 80:030902(R), 2009.
- [54] E. A. Gaffney T. E. Woolley, R. E. Baker and K. Maini P. Stochastic reaction and diffusion on growing domains: Understanding the breakdown of robust pattern formation. *Phys. Rev. E*, 84:046216, 2011.
- [55] A. J. McKane A. J. Black. Stochastic formulation of ecological models and their applications. *Trends in Ecology and Evolution*, 27(6):337–345, 2012.
- [56] T. Galla T. Biancalani and A. McKane. Quasi-waves in a brusselator model with nonlocal interaction. *Phys. Rev. E.*, 84:026201, 2011.
- [57] T.H. Solomon M. S. Paoletti, C. R. Nugent. Synchronization of oscillating reactions in an extended fluid system. *Phys. Rev. Lett.*, 96:124101, 2006.
- [58] A. J. McKane, T. Biancalani, and T. Rogers. Stochastic formulation of ecological models and their applications. *Bull. Math. Bio*, 2013.
- [59] R. E. Baker L. J. Shumacher, T. E. Woolley. Noise-induced temporal dynamics in turing systems. *Phys. Rev. E*, 87(3):042719, 2013.
- [60] J. Schnakenberg. Simple chemical reaction systems with limit cycle behaviour. *J. Theor. Biol.*, 81(3):389–400, 1979.
- [61] S. Levin. The problem of pattern and scale in ecology. *Ecology*, 73:1943, 1992.
- [62] R. Lefever I. Prigogine. Symmetry breaking instabilities in dissipative systems. *J Chem. Phys.*, 48:1695, 1968.
- [63] M. Asslani, F. Di Patti, and D. Fanelli. Stochastic turing patterns on a network. *Phys. Rev. E*, 86:046105, 2012.
- [64] R. E. Baker, E. A. Gaffney, and P. K. Maini. Partial differential equations for self-organization in cellular and developmental biology. *Nonlinearity*, 21:R251–11R290, 2008.
- [65] D. E. Strier and S. Ponce Dawson. Turing patterns inside cells. *PLoS ONE*, 2:e1053, 2007.
- [66] S. R. de Groot and P. Mazur. *Non-Equilibrium Thermodynamics*. 1984 New York.
- [67] J. M. Chung and E. Peacock-López. Bifurcation diagrams and turing patterns in a chemical self-replicating reaction-diffusion system with cross diffusion. *J Chem Phys*, 127:174903, 2007.
- [68] M. Iida, M. Mimura, and H. Ninomiya. Diffusion, cross-diffusion and competitive interaction. *J Math Biol*, 53:617641, 2006.
- [69] N. Kumar and W. Horsthemke. Effects of cross diffusion on turing bifurcations in two-species reaction-transport systems. *Phys Rev E*, 83:036105, 2011.

- 
- [70] D. Fanelli and A. J. McKane. Diffusion in a crowded environment. *Phys Rev E*, 82:021113, 2010.
- [71] A. Campa, T. Dauxois, and S. Ruffo. Statistical mechanics and dynamics of solvable models with long-range interactions. *Physics Reports*, 480:57–159, 2009.
- [72] A. Antoniazzi, D. Fanelli, S. Ruffo, and Y. Yamaguchi. Non equilibrium tricritical point in a system with long-range interactions. *Phys. Rev. Lett.*, 99:040601, 2007.
- [73] T. Rogers and A. J. McKane. Jamming and pattern formation in models of segregation. *Phys. Rev. E*, 85:041136, 2012.
- [74] E. M. Nicola, M. Baer, and H. Egel. Multispecies reaction diffusion models and the turing instability revisited. *Phys. Rev. E*, 73:066225, 2006.
- [75] E. M. Nicola. Ph. d. thesis. Master’s thesis, University of Dresden, 2001.
- [76] J. D. Murray. *Mathematical Biology II: Spatial Models and Biomedical Applications*. Springer–Verlag, third edition, 2003.
- [77] L. Cantini, C. Cianci, D. Fanelli, E. Massi, and L. Barletti. Stochastic model for calcium oscillation. *Submitted to Journal of Theoretical Biology*.



# Ringraziamenti

Desidero ringraziare tutti coloro che mi hanno aiutato nella realizzazione della mia Tesi.

Il primo ringraziamento va indubbiamente al Prof. Fanelli grazie al quale ho intrapreso e portato a termine questo stimolante percorso.

Vorrei anche ringraziare:

Francesca Di Patti per l'aiuto e il supporto ricevuto nei momenti difficili che ho dovuto affrontare in questi tre anni di Dottorato;

Timoteo Carletti che mi ha permesso di lavorare con lui in Belgio;

Il Prof. Stefano Ruffo coordinatore del Dottorato per averci accompagnato in questo percorso e avendo dimostrato molta comprensione.

Joe (il mio ufficiale correttore d'inglese), Leo (il mio personale tecnico del pc), e Giovanna (la mia confidente-psicologa).

Vorrei anche ringraziare tutti gli abitanti delle stanze 210 e 211 del Dipartimento di Fisica per aver reso piene le nostre giornate! (Non so come ve la caverete con ordine e pulizia delle scrivanie in mia assenza...)

Infine desidero dedicare la tesi alla mia famiglia e a mio marito Lorenzo, perché hanno sempre appoggiato le mie scelte e continuano a farlo in maniera incondizionata.